REACTOR CORE MATERIALS

A Quarterly Technical Progress Review

Prepared for DIVISION of TECHNICAL INFORMATION,
U. S. ATOMIC ENERGY COMMISSION, by BATTELLE MEMORIAL INSTITUTE

November 1961

● VOLUME 4

● NUMBER 4

TECHNICAL PROGRESS REVIEWS

To meet the needs of industry for concise summaries of current atomic developments, the Atomic Energy Commission is publishing this series, Technical Progress Reviews. Issued quarterly, each of the reviews digests and evaluates the latest findings in a specific area of nuclear technology and science.

The four journals published in this series are:

Nuclear Safety, W. B. Cottrell and associates, Oak Ridge National Laboratory

Power Reactor Technology, Walter H. Zinn and associates, General Nuclear Engineering Corporation

Reactor Core Materials (covering solid material developments), R. W. Dayton, E. M. Simons, and associates, Battelle Memorial Institute

Reactor Fuel Processing, Stephen Lawroski and associates, Chemical Engineering Division, Argonne National Laboratory

Each journal may be purchased ($2.00 per year for subscription and individual issues $0.55) from the Superintendent of Documents, U. S. Government Printing Office, Washington 25, D. C. See back cover for remittance instructions and foreign postage requirements.

The views expressed in this publication do not necessarily represent those of the United States Atomic Energy Commission, its divisions or offices, or of any Commission advisory committee or contractor.

Availability of Reports Cited in This Review

Unclassified AEC reports are available for inspection at AEC depository libraries and are sold by the Office of Technical Services, Department of Commerce, Washington 25, D. C. Some of the reports cited are not available owing to their preliminary nature; however, the information contained in them will eventually be made available in formal progress or topical reports.

Unclassified reports issued by other Government agencies or private organizations should be requested from the originator.

Unclassified British and Canadian reports may be inspected at AEC depository libraries. British reports are sold by the British Information Service, 45 Rockefeller Plaza, New York, N. Y.; Canadian reports (AECL series) are sold by the Scientific Document Distribution Office, Atomic Energy of Canada, Ltd., Chalk River, Ontario, Canada.

Classified U. S. and foreign reports identified in this journal as Classified may be purchased by properly cleared Access Permit Holders from the Division of Technical Information Extension, U. S. Atomic Energy Commission, P. O. Box 1001, Oak Ridge, Tenn. Such reports may be inspected at classified AEC depository libraries.

REACTOR CORE MATERIALS

A REVIEW OF RECENT DEVELOPMENTS

Prepared for DIVISION of TECHNICAL INFORMATION,
U. S. ATOMIC ENERGY COMMISSION,
by BATTELLE MEMORIAL INSTITUTE

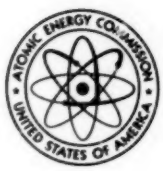

● NOV. 1961

● VOLUME 4

● NUMBER 4

foreword

Reactor Core Materials, one of a series of four quarterly reviews broadly covering the field of nuclear science and technology, is prepared by Battelle personnel from worldwide literature and covers materials and fabrication processes applicable to a nuclear reactor core. The coverage of this subject, however, is limited to materials that are solid at reactor operating temperatures. Pure chemistry, physics, core instrumentation, fuel processing, and source materials are not covered by this Review.

The authors and editors of *Reactor Core Materials* attempt to incorporate new developments and significant findings. This Review can serve as a useful summary of current research for both management and the technical specialist. For the latter group of readers, it is intended that the extensive referencing will aid in locating sources of more detailed information.

R. W. DAYTON
E. M. SIMONS
R. W. ENDEBROCK
Battelle Memorial Institute

DEPOSITED BY THE
TED STATES OF AMERICA

contents

Foreword

1 I FUEL AND FERTILE MATERIALS

1 Unalloyed Uranium
2 Alpha-Phase Uranium Alloys
2 Gamma-Phase Uranium Alloys
3 Dilute Uranium Alloys
3 Plutonium
4 Thorium
5 Dispersion Fuels
6 Coated-Particle Fuel Materials
9 Refractory Fuel and Fertile Materials
16 Mechanism of Corrosion of Fuel Alloys
16 Basic Studies of Radiation Effects in Fuel Materials
18 References

21 II MODERATOR MATERIALS

21 Graphite
22 Beryllium Metal and Alloys
27 Beryllium Compounds
27 Solid Hydrides
28 References

31 III NUCLEAR POISONS

31 Metallic Poison Materials
31 Dispersion Control Materials
31 References

33 IV CLADDING AND STRUCTURAL MATERIALS

33 Corrosion
36 Metal-Water Reactions
36 Radiation Effects in Nonfuel Materials
43 Selected Mechanical Properties of Cladding and Structural Materials
43 Selected Metallurgical Aspects of Cladding and Structural Materials
47 References

51 V SPECIAL FABRICATION TECHNIQUES

51 Melting, Hot and Cold Working
52 Cladding
55 Welding and Brazing
56 Explosive Forming
58 Nondestructive Testing
60 References

63 INDEX, VOLUME 4

Issued quarterly by the U. S. Atomic Energy Commission. Use of funds for printing this publication approved by the Director of the Bureau of the Budget on November 1, 1960.

Section I

FUEL AND FERTILE MATERIALS

Unalloyed Uranium

Papers presented and discussed at the X-Ray Preferred Orientation Meeting at Argonne National Laboratory (ANL) have been compiled.[1] These cover various facets of the physical metallurgy of uranium, such as preferred orientation in recrystallized material, diffraction intensities, and uranium-atom position as a function of temperature. Included are presentations on methods for, and results of, growth-index calculations and predictions.

British investigators[2] have shown that, contrary to previous evidence, the rates of anisotropic growth in single crystals and polycrystalline alpha uranium are found to be identical and are much higher for irradiations at −196°C than at +75°C. Values are $G = 11{,}500$ at −196°C and $G = 1200$ at +75°C, where G is the fractional extension divided by the fraction of all atoms fissioned. This rate is not affected by plastic deformation prior to irradiation. Possible explanations for this behavior are discussed in the article entitled "Radiation Effects in Nonfuel Materials," page 36 of this issue, in connection with anisotropic-growth observations in other metals. Along these lines a paper dealing with the growth of alpha uranium as the result of correlative collisions has been published in German and translated into English.[3]

At Hanford[4] the mechanisms and kinetics of uranium corrosion and fuel-element ruptures were investigated in water and steam at 170 to 500°C and at pressures from 100 to 2800 psig. The fuel-element samples, coextruded Zircaloy-clad uranium-core rods and tubes, were defected prior to exposure. Uranium corrosion was found to be the sum of two processes: direct oxidation by water and oxidation of uranium hydride intermediate. Fuel-element ruptures occur in two stages: an initial induction period is followed by accelerated corrosion of the core, causing the cladding to blister, swell, and fracture. Uranium corrosion and fuel-element ruptures were examined with respect to temperature, pressure, heat-treatment, carbon content of uranium, zirconium content of uranium, cladding thickness, fuel geometry, angular spacings, defect geometry and size, coolant flow, hydriding of Zircaloy components, and exposures to steam, water, and irradiation.

The defect-test behavior of unirradiated coextruded Zircaloy-2-clad uranium fuel as influenced by cladding thickness was also studied.[5] In the range of 0.010 to 0.030 in., the cladding thickness has little influence on the over-all defect-test behavior. There is a vague relation between cladding thickness and defect incubation period in that one increases with the other. There is a similar relation between cladding thickness and initial corrosion rate. The size of the initial blister developed at the site of the defect is proportional to the cladding thickness. The size of the blister required to rupture the cladding largely governs the incubation period and the initial fuel corrosion rate. Dimensional distortion of the fuel produced by cladding blistering increases with cladding thickness. Factors other than the failure behavior must be considered when selecting the proper cladding thickness for fuel elements. Some of these considerations are the feasibility of fabrication and closure, the maintenance of fuel-element dimensions by cladding restraint of the fuel material, and the avoidance of fuel-element failure resulting from plastic instability at thin or nonuniform sections.

Experiments at Atomics International[6] have shown that the corrosion of uranium by Santowax R at 350°F can be slowed down by having a CO_2 atmosphere above the bath. However, me-

chanical mixing of the bath is necessary for the atmosphere to be effective.

The occurrence, extraction, and preparation of uranium are reviewed in a recently published book.[7] Physical and mechanical properties are treated in detail. The topics of fabrication, compatibility, and irradiation resistance are also covered. A bibliography of corrosion and oxidation of uranium covering literature published from 1948 to 1960 has been compiled by the Israel Atomic Energy Commission.[8]

(M. S. Farkas)

Alpha-Phase Uranium Alloys

The constitution of uranium-molybdenum-niobium alloys has been investigated[9] at 1100, 1200, and 1300°C. The results are presented in Figs. I-1 to I-3.* (M. S. Farkas)

Gamma-Phase Uranium Alloys

Uranium-Molybdenum

The potential feasibility of casting high-quality 36-in.-long plates of the uranium–10 wt.% molybdenum alloy is reported by Atomics International.[10] Two heats were cast into plates $\frac{1}{10}$ in. thick and 36 in. long. Some metal was lost by leakage from the first casting, but the second casting yielded plates with no shrinkage and only slight surface porosity. Radiographs of the castings are being obtained.

A French paper[11] contains the results of a study of the effect of annealing at low temperatures on the fracture behavior of a gamma-quenched uranium–6.3 wt.% molybdenum alloy. At low temperatures, pearlitic type transformation products are not observed, but, rather, submicroscopic uranium particles precipitate. Fracture occurs by cleavage in the presence of this precipitate. After coalescence of the precipitate, fracture occurs intergranularly.

Uranium-Niobium

The uranium-niobium tetragonal gamma-prime phase reported by American investigators was studied by the British.[12] X-ray dif-

*Figures I-1 to I-3 are reprinted here by permission from the United Kingdom Atomic Energy Authority.[9]

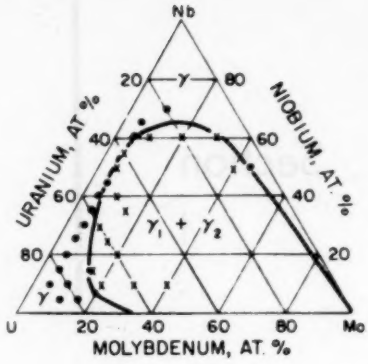

Fig. I-1 Isothermal section of the uranium-molybdenum-niobium system[9] at 1100°C. ●, single body-centered cubic phase. ×, two body-centered cubic phases.

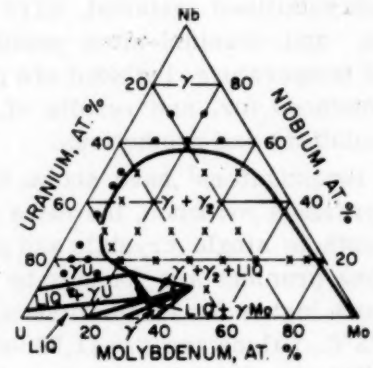

Fig. I-2 Isothermal section of the uranium-molybdenum-niobium system[9] at 1200°C. ●, single body-centered cubic phase. ×, two body-centered cubic phases. ▲, two body-centered cubic phases plus liquid. ▼, single body-centered cubic phase plus liquid.

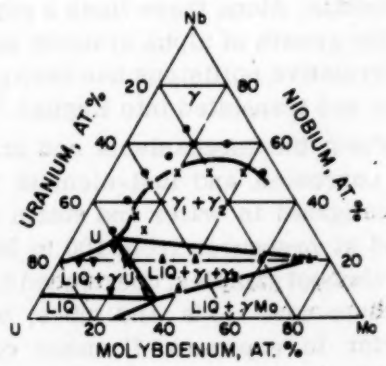

Fig. I-3 Isothermal section of the uranium-molybdenum-niobium system[9] at 1300°C. ●, single body-centered cubic phase. ×, two body-centered cubic phases. ▲, two body-centered cubic phases plus liquid. ▼, single body-centered cubic phase plus liquid.

fractometer results indicate that the phase is metastable and forms on quenching from the gamma field. On the basis of cursory examination of diffraction patterns, the structure was found to form infrequently, suggesting that critical cooling rates are required for formation.

(A. A. Bauer)

Dilute Uranium Alloys

Aluminum-Uranium Alloys

The use of aluminum-uranium alloys by Chalk River as stand-ins for aluminum-plutonium alloys provides an additional source of valuable data for the system. The sensitivity of the alloys to freezing rate was confirmed,[13] as well as the fact that malleability is closely associated with uranium content (i. e., the higher the uranium content the lower the workability of the alloy). In addition, the data show that anomalous work-hardening properties exist in the hypereutectic alloys. Initially, cold work causes hardening, but additional work causes softening. This is not a natural characteristic of aluminum.

It is postulated that this anomaly is connected in some way with the intermetallic phase. The simplest explanation would be direct breakup of the intermetallics. Although this may be contributory, there is doubt that it is the principal reason for softening. More than likely, softening occurs as the result of a recovery process in the aluminum matrix. The hard compound could cause localized deformation of the aluminum, which would initiate recovery. Support for this reasoning is offered by the turbulent flow pattern of the matrix caused by working which provides great deformation that may be sufficient to promote local recovery.

Castleman[14] studied interdiffusion of the aluminum–uranium alloy system over the 400 to 600°C temperature range at pressures ranging from $1\frac{1}{4}$ to 10 tsi. He reports that pressure increases the thickness of the UAl_3 layer formed. Other data that he obtained led him to the general conclusion that the growth of UAl_2 and UAl_4 phases, in incremental couples, is much slower than the growth of UAl_3.

Castleman proposes that the effect of pressure on UAl_3-layer growth is primarily mechanical, in that higher pressures repress the tendency for macroscopic voids to form, thus increasing the cross-sectional area available for interdiffusion.

General Atomic[15] reports recent results of studies on the ternary uranium-aluminum-oxygen system. A simple diagram exists. There were no phases observed which did not occur in the three related boundaries, and there was no evidence of solid solution between Al_2O_3 and the uranium oxides.

Uranium Alloy as Cladding

Darwin and Worley of Great Britain[16] have recently issued a patent on improving the strength of uranium fuel rods by using uranium alloy cladding. The application is stated to be "as cladding for gas-cooled graphite-moderated reactors." Alloys of the following compositions are listed: uranium–5 to 7 wt.% molybdenum, uranium–6 to 10 wt.% niobium, uranium with up to 30 wt.% zirconium, uranium with up to 4.8 wt.% carbon, and ternary alloys of uranium-niobium-zirconium and uranium-niobium-molybdenum. Although such cladding would probably provide for increased reactivity, it would be a source of a high-level fission-product release. In addition, there would be some doubt as to the corrosion resistance of the material to the coolant gas. (R. F. Dickerson)

Plutonium

The viscosity of molten plutonium has been determined at Mound Laboratory[17] at temperatures from 648 to 950°C. Results are plotted in Fig. I-4.

Two plutonium–1 wt.% aluminum alloy rods have been irradiated by Argonne[18] to estimated burnups of 0.1 at.% at central fuel temperatures near 385°C. The 8.5-in.-long, 0.200-in.-diameter rods were NaK-bonded to Zircaloy-2 tubes. On examination, one rod was found to have shortened 0.001 in. and the other, 0.004 in. No measurable changes in diameter occurred. One rod was bowed 0.018 in. over its length.

A homogenizing heat-treatment at 450 to 500°C was found to improve the load capacity of a plutonium–1.25 wt.% aluminum alloy.[19] No decrease in length was noted for homogenized alloys supporting static loads to 7.2 and 20.3 psi at temperatures up to 475°C. Similarly loaded as-cast specimens were found to exhibit decreases in length at temperatures as low as 400°C.

The results of an investigation to determine compatibility of the uranium–20 wt.%

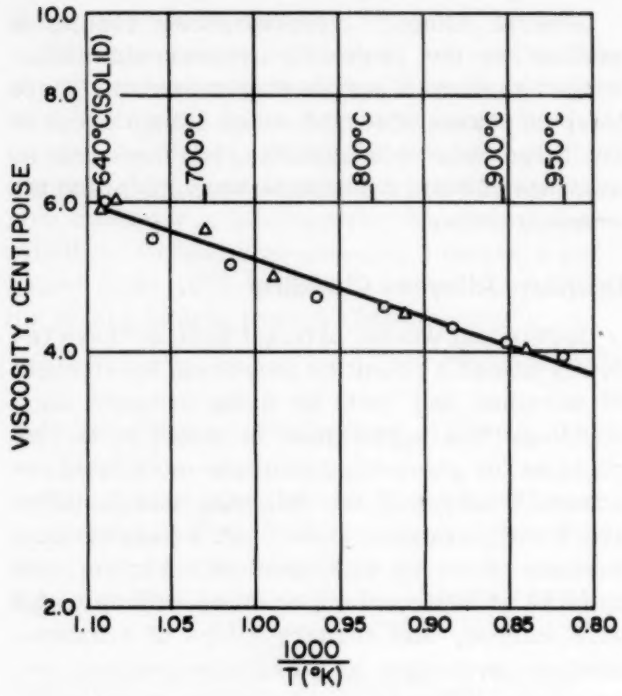

Fig. I-4 Viscosity of plutonium as a function of absolute temperature.[17]

plutonium–10 wt.% fissium alloy with potential jacket materials have been reported.[20] Diffusion penetration data, summarized in Table I-1, indicate that, of the materials tested, only the stainless steels are useless as jacket materials for the alloy at reactor operating temperatures. The niobium–5.3 wt.% vanadium alloy, zirconium, and Zircaloy-2 show enough penetration to make their use questionable, whereas the other materials all appear to be adequate.

Los Alamos[21] reports that a 5 at.% silicon addition to molten plutonium-iron alloy fuel is more effective than carbon additions for reducing the corrosion of tantalum container capsules. Plutonium-cerium-cobalt, copper, manganese, and nickel alloys are being investigated for use as dilute molten fuels. Preliminary results indicate that nickel and cobalt additions reduce the rate of attack on standard tantalum capsule material as compared with the plutonium-iron alloy. (V. W. Storhok)

Thorium

The constitution of the thorium alloy systems with the platinum metals is being studied by Thomson.[22] Initial investigations of the thorium-rich end of these systems have disclosed hexagonal compounds of the Th_7Fe_3 type in five of six systems. A eutectic exists between the first compound and thorium in each of these systems, as follows:

Eutectic phases	Eutectic composition, at.% alloy element	Eutectic temp., °C
Th + Th_7Ru_3	16	1260
Th + Th_7Rh_3	20	1240
Th + Th_2Pd	22	1110
Th + Th_7Os_3	14	1290
Th + Th_7Ir_3	15	1300
Th + Th_7Pt_3	17.5	1240

Oak Ridge has surveyed a series of thorium alloys for hot-hardness and recrystallization

Table I-1 DIFFUSION PENETRATION OF POTENTIAL CLADDING MATERIALS BY URANIUM–20 WT.% PLUTONIUM–10 WT.% FISSIUM[20]

U–20 wt.% Pu–10 wt.% Fs vs.	Time, days							
	800°C		700°C		600°C		550°C	
	1 mil	9 mils	1 mil	9 mils	1 mil	9 mils	1 mil	9 mils
Titanium	1.9	151	25.8	>1000	612	>1000		
Molybdenum	3.1	251	21.6	>1000	52.2	>1000		
Vanadium	1.2	96.7	17.6	>1000	56.5	>1000		
Tantalum	<1	30.8	†	†	†	†		
Niobium	<1	44.1	4.4	360	136	>1000		
Yttrium	<1	60.5	6.0	484	31.0	>1000		
Zircaloy-2	<1	10.1	14.2	>1000	19.8	>1000		
Zirconium	<1	4.9	6.8	555	14.3	>1000		
Nb–5.3 wt.% V	<1	3.0	<1	72.5	15.8	>1000		
Type 430 S.S.	*	*	*	*	*	*	10.0	806
Type 347 S.S.	*	*	*	*	*	*	9.2	748

*Molten.
†No detectable penetration.

characteristics.[23] At 600°C a thorium–4 wt.% indium alloy was four times harder than thorium and a thorium–5 wt.% zirconium alloy was three times harder than thorium. Softening during recrystallization occurs at about 600°C in thorium-indium alloys and at about 530°C in thorium-zirconium alloys.

A study of the effect of hydrogen upon the ductility of thorium has been completed by Peterson.[24] Less than 100 ppm hydrogen did not significantly affect the ductility of calcium-reduced thorium in tensile or impact tests at room temperature. Larger amounts of hydrogen did decrease ductility.

The properties of compounds of thorium are being investigated at Battelle.[25,26] The room-temperature hardness of a number of compounds is given in the following tabulation:

Compound	Hardness, DPH	Compound	Hardness, DPH
Th_2Al	360	$(Th_9U)_2Al$	330
ThB_4	960	$(Th_9U)B_4$	1150
$ThBe_{13}$	690	$(Th_9U)Be_{13}$	710
Th_3Si_2	470	$(Th_9U)_3Si_2$	410
ThSi	430		

After exposure to NaK containing traces of oxygen for one month at 1200°F, the $ThBe_{13}$ compound showed a weight loss of 0.0013 mg/(cm^2)(day). The other thorium compounds showed greater weight changes, either gains or losses, up to 0.045 mg/(cm^2)(day).

Argonne[20] irradiated forty-four cast specimens of various thorium-uranium alloys. All alloys contained 10 wt.% U^{235} except the 28 wt.% uranium alloy, which contained 26 wt.% U^{235}. The irradiation conditions and results are given in Table I-2. In addition, cast specimens of a thorium–5 wt.% plutonium alloy and of a thorium–10 wt.% plutonium alloy were irradiated at 450°C to burnups of 1.4 and 2.3 at.%, respectively. The dimensional and surface stabilities of these specimens were excellent and were comparable to the stabilities of thorium-uranium alloys. Higher temperature irradiations of thorium-plutonium alloys are planned. (W. Chubb)

Table I-2 IRRADIATION OF THORIUM-URANIUM ALLOYS[20]

Alloy composition (balance Th), wt.%	Estimated burnup, at.%	Estimated temp., °C	Volume change, % per at.% burnup	Appearance
10 U	2.8	680	2.8	Excellent
15 U	2.9	680	4.0	Excellent
20 U	2.9	680	4.7	Excellent
25 U	2.8	670	6.8	Roughened, slightly warped
28 U	4.5	820	19.3	Roughened, distorted

Dispersion Fuels

A report from Oak Ridge[27] describes the development of a dispersion fuel for the Enrico Fermi fast-breeder reactor. The element developed consists of 35 wt.% spherical UO_2 dispersed in a type 347B stainless-steel core and clad with type 347 stainless steel. Methods for achieving a uniform distribution of spherical UO_2 in the matrix powder are described. The degree of UO_2 fragmentation and stringering was found to be mainly a function of the degree of cold work and the quality of the UO_2 powder.

Two reports from Battelle[28,29] deal with the development of a dispersion fuel element for a proposed SM-2 reactor. An improved fuel plate containing 26 wt.% UO_2 dispersed with ZrB_2 in a low cobalt, low tantalum, type 347 stainless-steel matrix was developed as a reference design for the SM-2 reactor.[28] Design conditions include a maximum centerline temperature of 684°F, an average heat flux of 1.65×10^5 Btu/(hr)(sq ft), and an average U^{235} burnup of 39 per cent.

The improvement achieved over previously used UO_2–stainless steel dispersions may be attributed principally to the use of spherical UO_2 and the use of ZrB_2 as a burnable poison. The spherical UO_2 produces stronger cores with a more uniform dispersion and less stringering and fracturing of the UO_2 particles than does hydrothermal UO_2. The use of ZrB_2, combined with vacuum sintering at 2150°F and controlled hot rolling at 2200°F to about an 8-to-1 reduction in evacuated picture-frame packs, has allowed the control of boron content to within ± 5 per cent.

Irradiation and examination have been completed on four capsules of specimens prepared in the SM-2 Core Materials Development Program.[29] Each capsule contained five to eight flat-plate dispersion specimens roll clad with type 347 stainless steel. Six capsules containing

36 specimens are still under irradiation in the Engineering Test Reactor (ETR). Variables being studied include use of (1) fuel concentrations of nominal 26 and 40 wt.% UO_2 and 34 wt.% UN, (2) hydrothermal UO_2, spherical UO_2, and UN fuels, (3) B_4C, NbB_2, and ZrB_2 dispersion poisons and no poison loading, (4) a half loading of reference ZrB_2 dispersion poison, (5) a boron–10 wt.% stainless-steel picture frame, and (6) sintering or green pressing alone for core preparation.

The specimens in the first four capsules underwent burnups of 20 to 40 at.% of the U^{235} at surface temperatures near 700°F. It was found that the burnable poisons, both dispersed in the fuel and alloyed in the cladding, performed satisfactorily. No specimens containing a nominal 40 wt.% UO_2 or equivalent UN concentration were included in the first four capsules, but, at the 26 wt.% loading, both the hydrothermal and spherical UO_2 performed well. Encouraging results were obtained for the nonsintered core.

(D. L. Keller)

Coated-Particle Fuel Materials

Current interest in coated-particle fuel materials stems from a number of developments during the past four or five years. One such development was the demonstration that most chemical-vapor-deposition reactions can be carried out in beds of suspended particles which produce high yields of uniform products at economically attractive rates. Another development was the proof that these coatings are nonporous. Alumina coatings, 20 μ in thickness, protected 125-μ UO_2 particles from oxidation in air at temperatures up to 1300°C. Significantly, these coatings were found to have very low permeability for fission products, at least in the unirradiated condition. Finally, it was shown that the coatings can be prepared in a state of very high purity and that some control over the crystal structure can be maintained.

Thus a wide variety of core and coating combinations is possible for metallic, ceramic, and cermet fuel systems. The applications for coated-particle fuels are numerous, and the potential advantages are substantial. The coated particles might serve as the fuel element, such as in a suspension or fluidized system, or they can be fabricated with other materials into more conventionally shaped elements. Improvements in fission-product retention, oxidation and abrasion resistance of the particles, conductivity, strength and uniformity of dispersions, and prevention of reaction between fuel and other system components have already been demonstrated.

As a result of the widespread interest in coated-particle fuels, this new section in *Reactor Core Materials* has been established for reporting current progress.

Preparation and Fabrication

Nuclear Materials[30] reported on the operation of vibrating-tray chemical-vapor deposition equipment to produce niobium, chromium, molybdenum, vanadium, niobium-vanadium alloys, and silicon coatings on UO_2 and other techniques and procedures for nickel, chromium, and beryllium coatings. The direct chemical fabrication of metal-matrix fuel elements is also described. The reactions employed have been summarized in a monograph[31] on the subject, and most of these metallic coatings, as well as others, have also been prepared in fluidized-bed equipment.[32]

Both dense and porous Al_2O_3 coatings are being deposited at Battelle on uranium dioxide powder by hydrolysis of the chloride at temperatures of 1000 and 700°C, respectively.[25] The porous material, when overcoated with dense Al_2O_3 at 1000°C, results in coating rupture at 1240°C. If the porous coating is first heat-treated at 1240°C for 48 hr and then overcoated with dense Al_2O_3, a structure that is stable at 1240°C is obtained. Nonporous BeO coatings have been deposited from the basic acetate, but so far they have been contaminated with carbon. Research on the hydrolysis of the chloride to deposit BeO is also continuing.[26] The effect of impurities in the oxide coatings on the surface roughness is thought to be significant. Oxide coatings on UO_2 and UO_2-ThO_2 particles are also being produced by Nuclear Materials.[33,34]

National Carbon and Battelle have fabricated graphite-matrix elements containing Al_2O_3-coated UO_2 particles.[25,34] Some damage to the coated particles was encountered during initial fabrication studies at Battelle, but good results are now being obtained. A study of the direct chemical fabrication of graphite-matrix elements has been initiated[35] by pyrolysis of hydrocarbons in a packed bed of coated fuel parti-

cles. Pressure bonding of Al_2O_3-coated UO_2 particles is being attempted[26,36–38] for the purpose of developing dense oxidation-resistant fuel bodies. Owing to limitations on the loading, coating thicknesses are restricted to 5 to 10 μ. It has not yet been demonstrated that these thin coatings can provide adequate protection for all particles owing to the distribution of film thicknesses in a given lot of material. Methods of calculating the thermal conductivities of matrix elements containing coated particles on the basis of the thermal conductivities of the three phases have been reported by Knolls.[39]

Carbide-Base Materials. General Atomic[40,41] revealed that it had initiated coating programs both at Battelle[42] and in its own laboratories to coat $(U,Th)C_2$ particles with pyrolytic carbon, NbC, and ZrC films. Carbon films, 30 μ in thickness on 300-μ particles, provided good resistance to moisture attack of the dicarbides, and multiple thermal-shock treatments to 2600°C were necessary to release all the contained xenon gas after neutron activation. Data on the kinetics of carbon deposition from CH_4 were correlated by the expression:

$$W = \frac{2.25 \times 10^9}{T} P_{CH_4}^{1.30} S^{1.39} e^{-90,390/RT}$$

and, from C_2H_2, by

$$W = \frac{1.57 \times 10^6}{T} P_{C_2H_2}^{1.46} S^{0.92} e^{-51,000/RT}$$

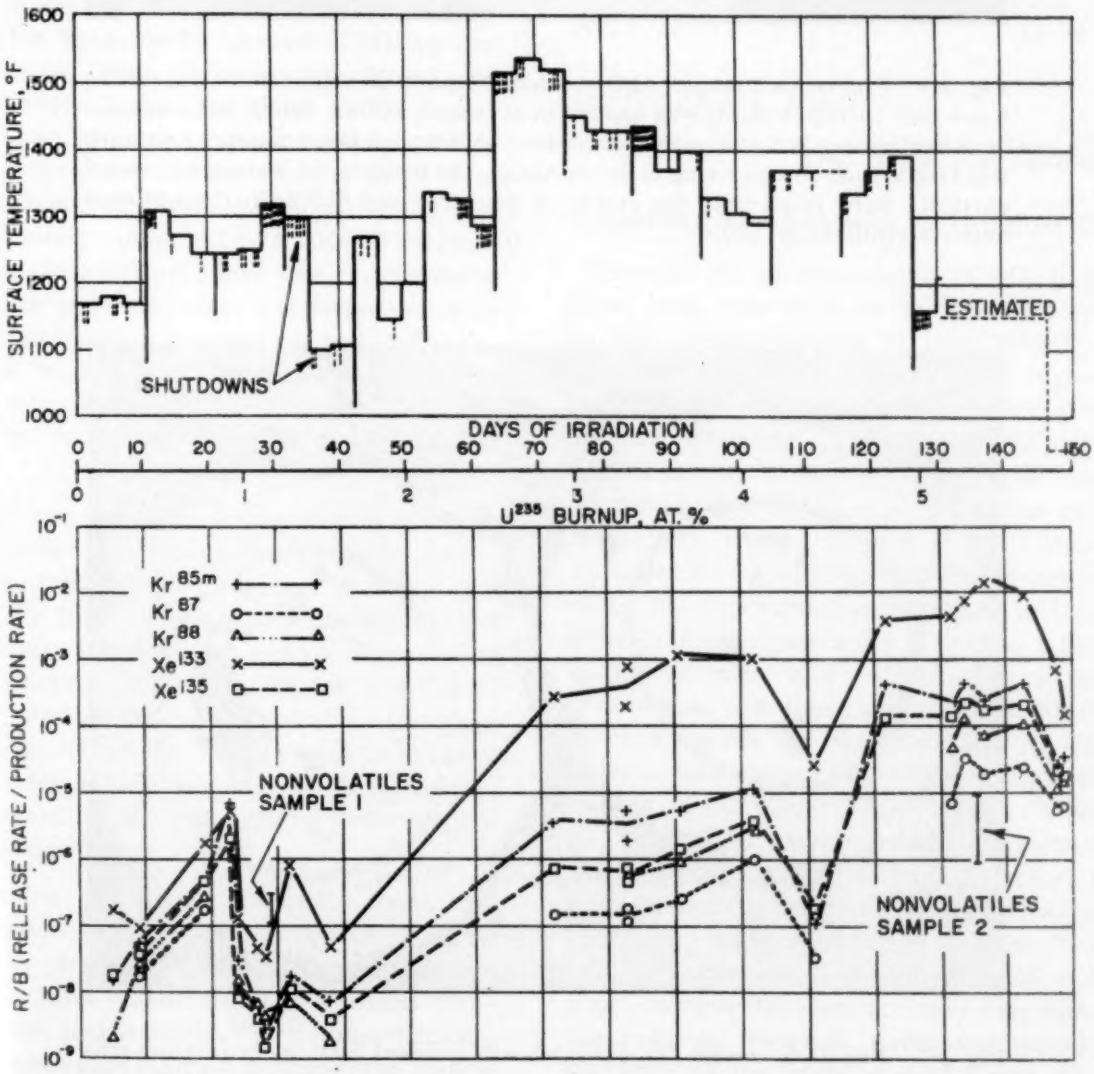

Fig. I-5 Performance of graphite ball[34] containing Al_2O_3-coated UO_2 particles in sweep capsule SP-5.

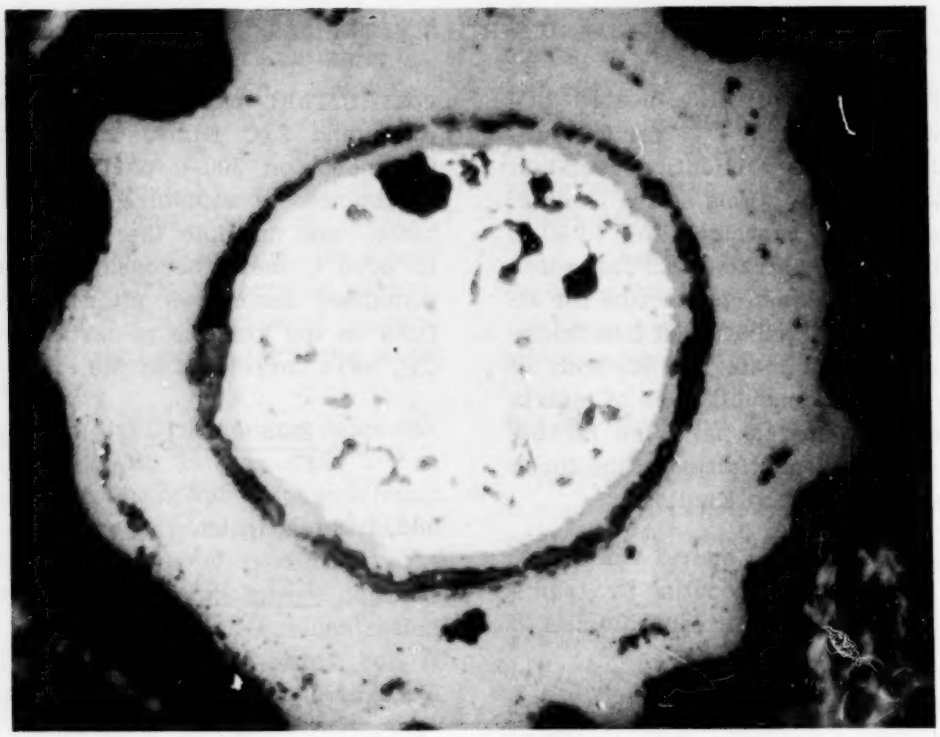

Fig. I-6 Typical undamaged Al_2O_3-coated UO_2 particle after irradiation to 4 to 5 per cent burnup. Coating was applied in six steps, and the fourth layer was inadvertently deposited in a porous condition. This porous layer appears as a dark 6-μ ring around an inner ring of dense Al_2O_3. The majority of undamaged coated particles were found near the center of the irradiated S&P ball. (Unpublished data.) Magnification, 500×.

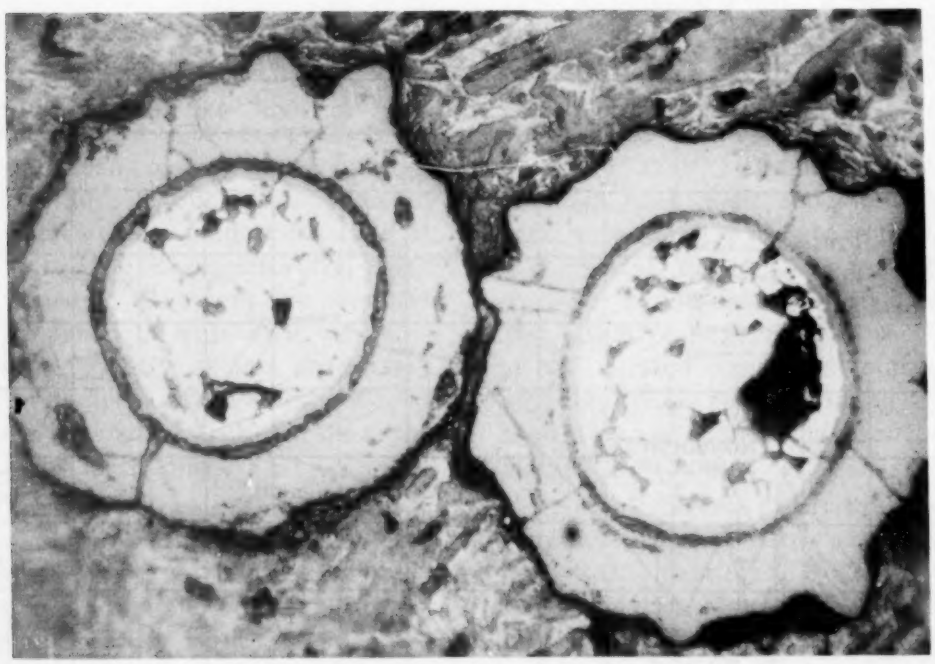

Fig. I-7 Two Al_2O_3-coated UO_2 particles with cracked coatings in graphite matrix after irradiation to 5 to 6 per cent burnup. The majority of particles with damaged coatings were found near the surface of the irradiated S&P ball. (Unpublished data.) Magnification, 250×.

where W = rate of carbon deposition, 0.03 to 24.6 g/hr
T = deposition temperature, 1123 to 1398°K
P = hydrocarbon partial pressure, 77 to 750 mm Hg
S = surface area of particles, 2690 to 11,900 cm^2
R = gas constant, 1.987 cal/(g-mole)(°K)

At a bed temperature of 1000°C, a hydrocarbon partial pressure of 760 mm Hg, and a bed surface area of 7000 cm^2, the rate of carbon deposition from C_2H_2 is 182 times that from CH_4. However, at 1600°C, the rates of carbon deposition from CH_4 and C_2H_2 should become equal under these same conditions. Efforts to prepare carbides were only partially successful.

Pyrolytic carbon-coated UC_2 particles were supplied to Sanderson and Porter for its Pebble-Bed Reactor Program by Minnesota Mining and Manufacturing, High Temperature Materials, National Carbon, American Metal Products, and Battelle. Acid leaching of these coated particles resulted in uranium losses ranging from 3 to 320 ppm. However, some of the products had been previously subjected to a 2000°C thermal cycle, and, in addition, there was considerable variation in particle size and shape, coating thickness, processing conditions, and preleaching before receipt by Sanderson and Porter. In general, nonporous carbon coatings can now probably be produced by any of these laboratories.[34]

At least two types of carbon structures have been identified as a result of processing conditions. Predominantly columnar coatings are prepared by High Temperature Materials, and predominantly laminar coatings are prepared by National Carbon, Minnesota Mining and Manufacturing, and initially by Battelle. Coatings prepared by American Metal Products seem to be of an intermediate structure.[34] Both deposition temperature and rate affect the structure of the coatings.[25]

Fabrication of matrix elements containing carbon-coated carbide fuel particles is being carried out at General Atomic, Speer, Minnesota Mining and Manufacturing, National Carbon, Armour, and Battelle.[25,34,43] Some difficulties have been experienced in preparing matrix specimens without damaging the carbon-coated particles.

Irradiation and Evaluation

Oxide-Base Material. Final results on the Sanderson and Porter SP-5 experiment in the Battelle Research Reactor involving a 1½-in.-diameter graphite ball containing Al_2O_3-coated UO_2 particles were reported.[25] The coated fuel was prepared at Battelle and consisted of 40-μ Al_2O_3 films on 125-μ-diameter UO_2 particles. National Carbon fabricated the fueled graphite ball. The results of radiochemical analysis of a sweep gas stream passing over the ball are shown in Fig. I-5. Postirradiation examination showed that 3.6 per cent of the particles had cracked coatings after 6 per cent burnup at temperatures between 510 and 730°C. The microhardness of the coatings[38] had decreased from 2200 to 1400 KHN as a result of irradiation. Photomicrographs of the uncracked and cracked particles are shown in Figs. I-6 and I-7. (J. H. Oxley)

Refractory Fuel and Fertile Materials

Properties and Behavior of Uranium Oxides

Results of investigations of UO_2 properties have been reported by several laboratories. In-pile measurements at Oak Ridge[44] showed that the electrical resistivity of high-density UO_2 did not change with irradiation up to about 10^{18} nvt, thermal, at which point the resistivity decreased by a factor of 3. These measurements are presented in Fig. I-8. The electrical resistivity ranged from 8.75×10^3 ohm-cm at 21°C before irradiation to 0.4 ohm-cm at 773°C after an exposure greater than 10^{18} nvt. The activation energy was 0.5 ev during irradiation, compared with 0.65 ev before irradiation. In conjunction with these experiments, the thermoelectric power for the platinum-UO_2-platinum system was determined. The thermal electromotive force ranged from 130 μv/°C at 162°C to 29 μv/°C at 900°C. During irradiation the UO_2 behaved like an n type conductor. Postirradiation measurements of electrical conductivity have been reported by Hanford.[45] Sintered UO_2 irradiated to a burnup of 0.005 at.% had a room-temperature conductivity one-fifth that of unirradiated material. Room-temperature conductivity of the irradiated UO_2 was about one-third that of unirradiated UO_2 after both materials had been heated to 800 to 900°C and then

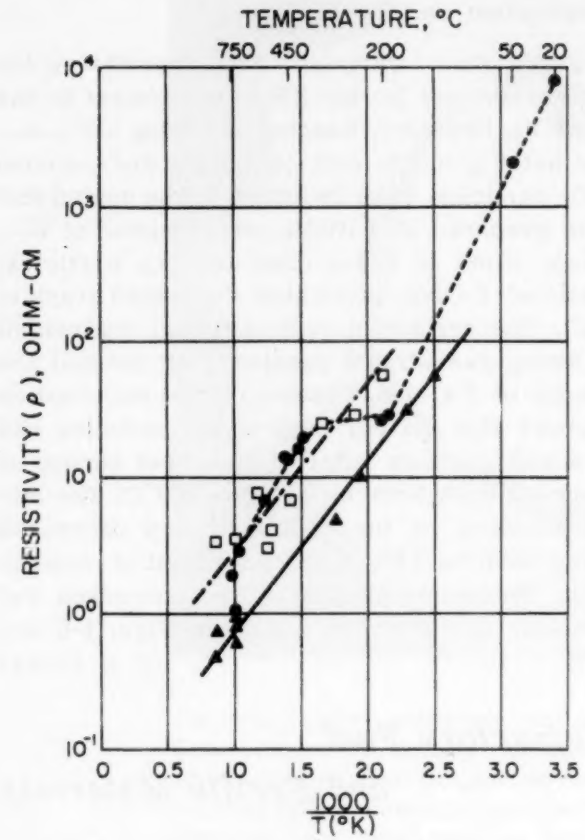

Fig. I-8 Electrical resistivity of UO_2 as a function of temperature.[44] In-pile: —·— □, nvt < 10^{18}. —— ▲, nvt > 10^{18}. ●---, before irradiation.

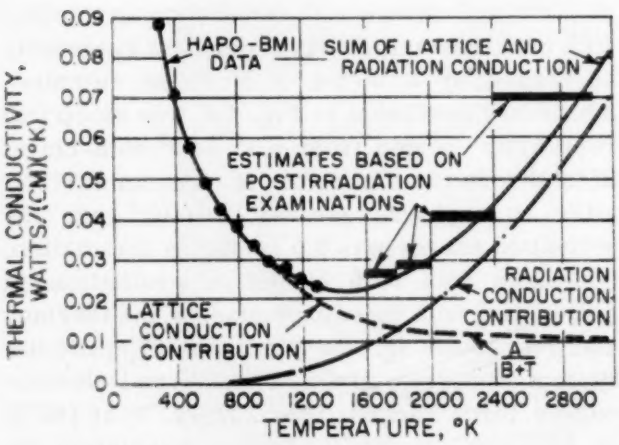

Fig. I-9 Thermal conductivity[46] of UO_2.

cooled. The electrical conductivities were about the same for both irradiated and unirradiated material above 600°C.

Experimental evidence[46] suggests that above 1400°C the thermal conductivity of UO_2 improves significantly with increasing temperature instead of decreasing, as would be expected from extrapolation of lower temperature data. The increase appears to be due to the relatively high transparency of UO_2 to infrared radiation at wavelengths of maximum emissive power. Figure I-9 shows the contributions of lattice and radiation to heat conduction at high temperatures in UO_2.

Observation that irradiation increases the melting point of UO_2 has led Hanford investigators[47] to suggest that UO_2 dissociates to a stable substoichiometric oxide before the melting point is reached. Thus melting points currently quoted for UO_2 may actually be the temperature at which a stable UO_{2-x} melts.

Thermal-expansion coefficients for UO_2, UO_2-ThO_2, ThO_2, and UN between the temperatures of 26°C and T°C are given below (per degree centigrade):

$$\bar{\alpha}\,(UO_2) = 8.3067 \times 10^{-6} + 2.211 \times 10^{-9}\,T$$

$$\bar{\alpha}\,(UO_2\text{-}ThO_2) = 8.8553 \times 10^{-6} + 1.329 \times 10^{-9}\,T$$

$$\bar{\alpha}\,(ThO_2) = 8.1950 \times 10^{-6} + 1.121 \times 10^{-9}\,T$$

$$\bar{\alpha}\,(UN) = 7.5074 \times 10^{-6} + 1.099 \times 10^{-9}\,T$$

Auskern and Belle[48,49] have published diffusion coefficients for oxygen and uranium self-diffusion in stoichiometric UO_2. Uranium diffusion between 1450 and 1785°C follows the expression

$$D = 4.3 \times 10^{-4} \exp(-88{,}000/RT) \quad cm^2/sec$$

whereas oxygen-ion diffusion in the temperature range of 550 to 780°C can be represented by the equation

$$D = 1.2 \times 10^{3} \exp(-65{,}300/RT) \quad cm^2/sec$$

Oxygen-diffusion rates in nonstoichiometric UO_2 are increased, and the activation energy is decreased by more than half.

In-pile and postirradiation fission-gas-release studies are continuing at Oak Ridge.[50] Measurements of in-pile release for UO_2 of 97 per cent theoretical density are in progress. Preliminary diffusion coefficients calculated for Xe^{133} and Xe^{135} in combination with their iodine precursors ranged from 1.3×10^{-14} cm^2/sec at 720°C to 5.8×10^{-10} cm^2/sec at 1100°C. From 710 to 1100°C, Kr^{85m} and Kr^{88} diffusion coefficients varied from 8.7×10^{-16} to 5×10^{-11}

cm^2/sec, respectively. The activation energy in both cases is about 40 kcal/g-mole up to about 1000°C. In other work, fission-product release from Pressurized-Water Reactor (PWR) type UO_2 pellets was measured during postirradiation heating in air and purified helium at temperatures up to the melting point.[51] Diffusion measurements for periods up to 5 hr in high-purity helium yielded the release data for principal fission products shown in Fig. I-10. Rates at which release occurred were characterized by an initial rapid release followed by a slower release rate that was linear with the square

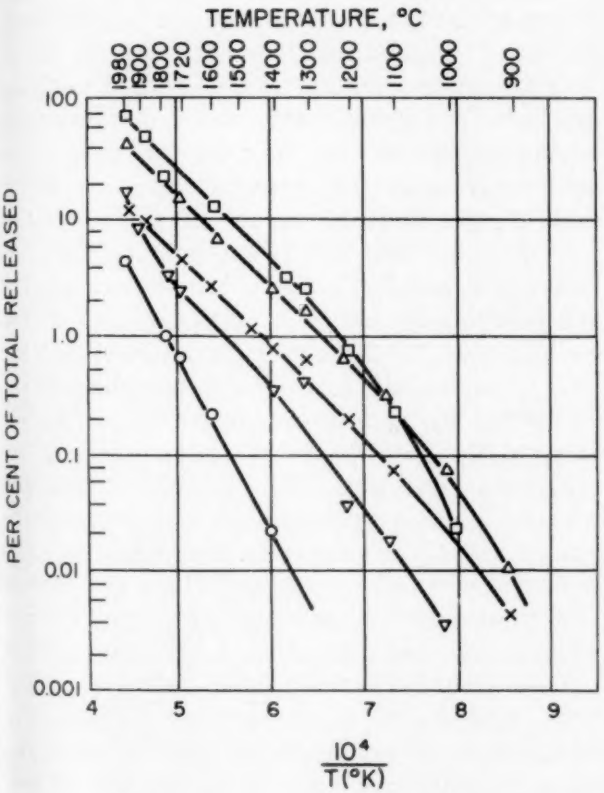

Fig. I-10 Release by diffusion of fission products from sintered UO_2 heated in purified flowing helium (heating time ~5 hr).[51] Δ, iodine. □, tellurium. ▽, cesium. ○, strontium. ×, gases (Xe-Kr).

root of heating time. Apparent diffusion coefficients $D' = D/a^2$ calculated from the linear portion of the release data for krypton and xenon are presented in Fig. I-11. Under oxidizing conditions and at the melting point, fission-product release was enhanced considerably.

Tests of the compatibility of UO_2 with various cladding materials have been performed.[52] UO_2 appears to be compatible with tungsten up to the melting point of UO_2. Molten UO_2 was found to

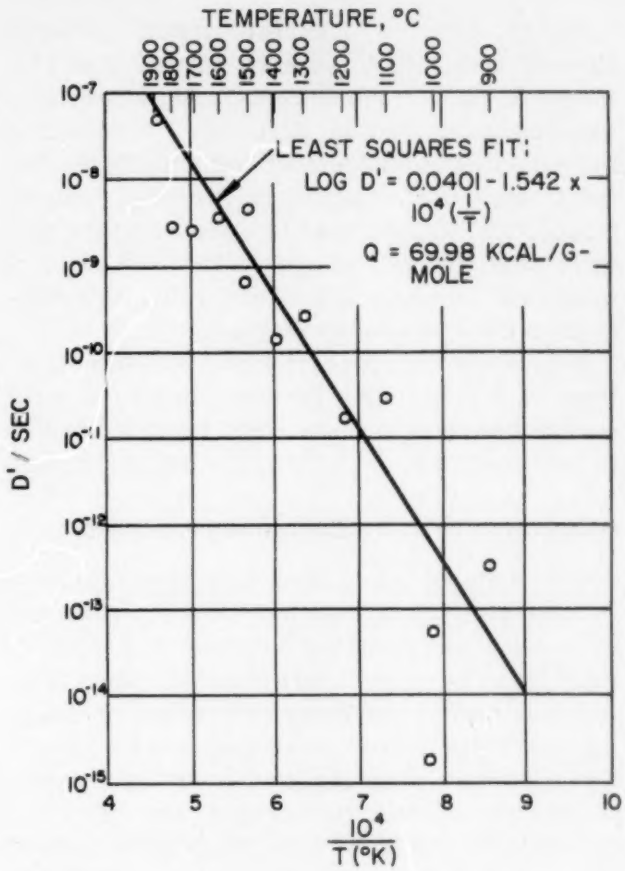

Fig. I-11 Rare-gas diffusion from PWR UO_2 in helium.[51]

react rapidly with tantalum, but, at temperatures less than 2800°C, the two appear to be compatible. Molybdenum does not react appreciably with UO_2 at temperatures to 2275°C. At 100°C below the melting points of Zircaloy-2, Fansteel-80, and Fansteel-82, reactions with UO_2 were observed. Weight changes of various alloys after 10 min of contact with UO_2 at 1000 and 1500°C are given in Sec. IV.

Short-time irradiations at Chalk River[53] of $UO_{2.12}$ having a density of 10.55 g/cm^3 indicate that this material exhibits more melting and grain growth than similar specimens of stoichiometric UO_2 under the same conditions. This suggests that during irradiation the mean thermal conductivity of $UO_{2.12}$ is about 20 per cent lower than that of UO_2 between 350 and 2800°C. The diametral expansion of $UO_{2.12}$ specimens was greater than that for $UO_{2.0}$ at the same heat fluxes. Metallographic examination of the $UO_{2.12}$ showed that oxygen had migrated from the molten core to a lower temperature region of the specimen.

Sheath failures occurred during Savannah River[54] irradiation tests of tubular fuel elements of vibratory-compacted and swaged fused uranium oxide within Zircaloy-2 tubes. It is believed that moisture contamination in the UO_2 led to local hydriding in the Zircaloy-2 during irradiation. Normal tensile stresses in the element were then sufficient to initiate cracks that propagated through the sheath wall with subsequent failure of the fuel element.

A recent Polish paper[55] discusses phase relations of the $BaO-UO_2$ system. Another report[56] covers phase studies of solid solutions of UO_2 in ZrO_2 and CeO_2. (R. H. Barnes)

Fabrication of UO_2-Containing Ceramics

The costs of fabricating fuel elements for a reactor core using pelletized and granular fuel have been compared by Combustion Engineering.[57] It is concluded that elements made from granular fuel by vibratory compaction or swaging are considerably less expensive than pellet type elements made by cold-pressing and sintering the pellets. In essence, the savings claimed are realized because granular, fused UO_2 is considerably less expensive than UO_2 pellets and because scrap losses in vibratory compaction or swaging are lower.

There are several factors affecting relative costs which do not appear to have been taken into account in the analysis. These are

1. *Possible differences in permissible burnup and reliability of elements.* Slight increases in density of sintered pellets, which appear to be technically possible, could have an appreciable favorable effect on element life. The problem of adsorbed gases on granular fuel has not been resolved.

2. *Criticality limitations.* Because of volatility of UO_2 at high temperature and the nature of the process, electric-arc fusion of UO_2 can be accomplished economically only with large batches. Other methods of obtaining suitable granular materials have not been proved, and their costs are less certain.

3. *Scrap considerations.* It should be possible to reduce both the amount of scrap generated in pelletizing and the cost of reprocessing it below the levels used in the analysis.

With these factors considered, it would appear that differences in costs between pelletized and granular fuel may, in the long term, prove to be minor.

The fabrication of $ZrO_2-CaO-UO_2$ fuel to be used in spike elements for the Experimental Boiling-Water Reactor (EBWR) has been described.[58] Mixtures of UO_2, $CaCO_3$, and U_3O_8 were pressed at about 15,000 psi and sintered in air at $1675 \pm 25°C$ to form cubic solid-solution fuel having a density of about 4 g/cm^3. Porosity and oxygen content of the fuel are not given. (H. D. Sheets)

Properties of Refractory Fuels Other Than Uranium Oxides

The properties of the uranium carbides are being investigated in a number of laboratories. Murson[59] studied the thermal behavior of UC and UC-plus-uranium bodies with 5 per cent porosity and found them to be dimensionally stable through 500 and 1000 thermal cycles, respectively, over the temperature range 200 to 1000°C. The thermal conductivity of these bodies varied from 0.028 to 0.04 cal/(cm)(sec)(°C) between 100 and 700°C. Between 20 and 1500°C the thermal-expansion coefficient was found to be $11.6 \times 10^{-6}/°C$. Lattice-parameter data for $UC_{0.83}$ was found[60] to vary with temperature (20 to 690°C) by the following equation: $a_0 = 4.9592 [1 + (10.98 \pm 0.08) 10^{-6} t]$ A. In the case of the dicarbide structure, the lattice parameters for $UC_{1.83}$ material expanded with temperature (20 to 935°C) according to the equations: $a_t = 3.5256 [1 + (16.56 \pm 0.23) 10^{-6} t]$ and $c_t = 6.0014 [1 + 10.43 \times 10^{-6} t]$. In comparison, Los Alamos reports thermal-expansion coefficients for UN to be $7.5074 \times 10^{-6} + 1.099 \times 10^{-9} t$ and, for ThO_2, $8.1950 \times 10^{-6} + 1.121 \times 10^{-9} t$. Electrical-resistivity and hot-hardness data[26,61] for uranium carbides are given in Tables I-3 and I-4. High-temperature deformation studies[62] show that UC deforms at 1200°C, UN at 1600°C, and U_2Si_3 at 800°C. Grain growth of UC between 950 and 1700°C is reported[63] to occur in two successive stages.

Reaction was observed[64] between UC and tantalum during irradiation of capsules (burnups of 4000, 8000, and 11,000 Mwd/ton) at central temperatures of 2000 to 2500°F. Fission gas released from the UC at the lower burnup amounted to 1.7 per cent of the Kr^{85} generated. UC_2-ThC_2 fueled graphite bodies examined[40,41] after irradiation, giving 16 to 18 per cent U^{235} burnup (48,000 to 51,000 Mwd/ton), showed good dimensional stability with no evidence of cracking or spalling. However, migration of the fuel

Table I-3 ELECTRICAL-RESISTIVITY VALUES FOR THREE URANIUM-CARBON SPECIMENS[61]

Temp., °F	Electrical resistivity, μohm-cm		
	U–4.8 wt.% C	U–7.0 wt.% C	U–9.0 wt.% C
200	51	69	128
400	65	83	147
600	80	97	166
800	94	111	183
1000	108	125	193
1200	122	139	197
1400	136	153	198
1600	149	167	199
1800	161	181	208
2000	174	195	223
2200	185	209	238
2400	196	223	253
2600	207	237	268
2800	216	251*	
2900	221*		

*Extrapolated.

Table I-4 HOT HARDNESS OF URANIUM–9 WT.% CARBON ALLOY[26]

Temp., °C	Hardness, DPH
1000	185
1100	105
1200	66
1300	51
1400	40
1500	21

appears to concentrate the uranium and thorium at different locations in the body. Vapor-pressure studies of UC_2 and ThC_2 are in progress. Preliminary experimental data fit the following thermodynamic equations as well as would be expected:

For UC_2,

$$\log p = \frac{-144{,}300 + 6(T - 1400)}{4.575\,T} + \frac{27.5}{4.575}$$

and for ThC_2,

$$\log p = \frac{-160{,}700}{4.575\,T} + \frac{28.8}{4.575}$$

Vapor-pressure data[65] for ThO_2 are given in Table I-5.

Battelle[26,66] has obtained data on the vapor pressure of PuO_2. These results are presented in Table I-6. (D. A. Vaughan)

Fabrication of Ceramic Fuels Other Than Uranium Oxides

The third in a series of informal meetings to coordinate the efforts of the various laboratories engaged in research on uranium carbide fuels under AEC contract was held at the Oak Ridge National Laboratory on Dec. 1 and 2, 1960. Summaries of the status of work at that time at each of the participating organizations have been compiled[67] by the AEC Division of Technical Information.

Oak Ridge investigators[50] have developed techniques for arc-melting and casting crack-free high-purity UC cylinders, 0.25 to 0.5 in. in diameter and 3 in. long. Small shrinkage cavities that occur in the top 20 per cent of the casting cannot be eliminated. A cavity forms because molten alloy "drops" into the mold and simultaneously freezes in the outer regions of the casting. A solidification pattern results that allows very little molten alloy to act as a feeding head.

The variability of carbon content of skull-melted castings of UC has been shown to be due to: (1) carbon pickup from the graphite electrode which is eroded by spatterings caused by volatile impurities in the charge and (2) segregation of carbon and uranium in the skull because of the refractory nature of graphite in the elemental charge and the inconsistent position of the molten pool in the skull. Battelle[35] melters

Table I-5 THORIA-VAPOR-PRESSURE DATA*

Run	Temp., °K	Evaporation, g/(cm²)(sec)	Log pressure, atm
Th-C-1	2109	3.04×10^{-8}	−8.713
Th-C-2	2115	2.94×10^{-8}	−8.728
Th-G-1	2308	2.95×10^{-7}	−7.706
Th-G-2	2364	9.1×10^{-7}	−7.211

*Based on data taken from reference 65.

Table I-6 VAPOR PRESSURE OF PLUTONIUM OXIDE[26]

Transpiring gas	Temp., °C	Pressure, atm
Oxygen	1540	1.1×10^{-5}
Oxygen	1640	3.6×10^{-5}
Argon	1000	2.5×10^{-5}
Argon	1750	3.3×10^{-4}
Air	1600	3.1×10^{-4}
Air	1730	1.2×10^{-4}

indicate that the carbon addition due to electrode erosion can be predicted to be about 0.5 wt.% carbon with a confidence limit of about ±0.1 wt.% carbon but that carbon variation due to uncontrolled segregation in the skull is less predictable because the haphazard movement of the molten pool may cause carbon-rich and uranium-rich segregates in the skull. After melting four charges (one prealloyed UC shot of 4.6 wt.% carbon yielding a casting about 5.0 wt.% carbon and three charges of vacuum-outgassed TSF graphite and uranium metal of 4.2 wt.% carbon yielding castings of about 7 wt.% carbon), Battelle workers examined the skulls and found that segregation of uranium metal to the bottom of the charges was responsible for the high carbon content of the castings.

To produce UC from mixtures of UO_2 and carbon, Argonne[20] has added carbon as a soluble carbonaceous material in the mixing operation to coat each UO_2 particle, and thus obtain high carbon and UO_2 surface areas. They prefire at 900°C in argon to carburize the petroleum pitch dissolved in alcohol. The product of a 1-hr soak at 1400°C and 1-hr firing in flowing argon at 1700°C was UC with not more than 10 per cent UO_2. By prefiring in flowing argon for 1 hr at 1450°C, then evacuating to 10^{-4} mm Hg and firing 1 hr at 1700°C, Argonne obtained a product that showed no UO_2 by X-ray diffraction.

Russian investigators[59] lined a graphite extrusion die with molybdenum foil and placed this assembly in a hermetically sealed metal vacuum chamber (~10 mm Hg) to study the effects of extrusion pressure, temperature, and holding time on the density of UC. The powder was produced from the reaction of UO_2 and carbon black. Temperatures above 1850°C caused a lowering of the density, as shown in Fig. I-12.

High-density pellets of ZrC-UC solid solutions were hot pressed by a process wherein ZrC, UO_2, and graphite powders were mixed, loaded into a graphite die, allowed to react at about 2000°C in a vacuum or argon, and then pressed. Stephas and Hoyt[68] call this "reactive hot pressing," although the reaction occurs prior to the pressing. The method bypasses handling of pyrophoric UC powders, but it requires a long time (up to 8 hr) to produce a pellet. Addition of 1 wt.% nickel enhanced grain growth.

Argonne[20] produced US powder by decomposing hydrided uranium turnings to fine powder and reacting this powder with a measured

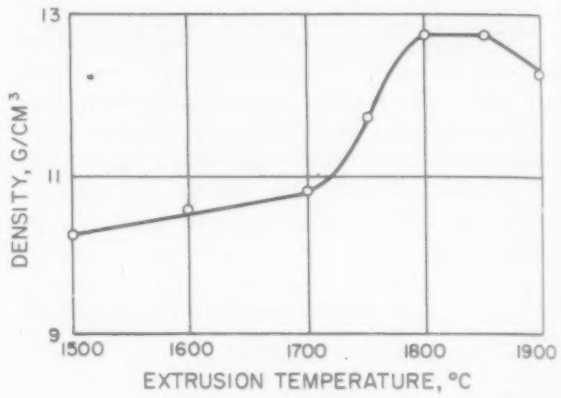

Fig. I-12 Relation between density of hot-extruded specimens of UC and extrusion temperature (p = 300 kg/cm²; t = 5 min).[59]

amount of H_2S at 550°C. The resulting mixture of US_2, alpha uranium, and UH_3 was homogenized to US at higher temperatures, crushed, pelletized, and finally sintered. The best temperature for homogenization is 1800 to 1900°C. Above this temperature, weight loss becomes considerable, and the material is also difficult to crush. In the sintering study, pellets isostatically pressed at 55,000 psi and fired in vacuum reached a maximum fired density at either 1800 or 1900°C. The density dropped slightly at 2000°C. The material of highest density (85.8 per cent of the theoretical density) analyzed 99 per cent $US_{0.98}$ and 1 per cent (U + UOS), which represents about 0.05 per cent oxygen contamination. Weight loss increased considerably at sintering temperatures over 1800°C. Homogenization and sintering in argon produced US of 91.5 per cent of the theoretical density, compared with 84.6 per cent for vacuum-treated material at 1800°C. Of the 7 per cent density gain, 3 per cent is attributed to the argon homogenization and 4 per cent to the argon sintering.

In trying to produce UN by arc-melting techniques, it had been found that the reaction was virtually complete after 10 min of arc-melting uranium in nitrogen at 3-atm pressure. Investigation of the effect of pressure had shown that the nitrogen content varied from 3.15 wt.% in a button produced at ¼ atm to 4.82 wt.% in one produced at 3 atm. Although extrapolation of this data indicates that stoichiometric material should be produced by direct arc-melting procedures at nitrogen pressures of less than 1

atm, Battelle[35] has found that other melting conditions, such as arc voltage and arc length, are equally important in the control of the nitrogen content, homogeneity, and purity of buttons. Exploratory tests in the 10- to 24-atm pressure range made at the same power conditions as the 3-atm or less pressure resulted in substoichiometric UN containing about 5 wt.% nitrogen. As the pressure was raised, the arc length was shortened, the melting area was diminished, losses of the tungsten electrode increased, and the composition and amount of UN_x smoke produced during melting was changed. At an arc current of 200 amp and a potential of 100 volts, a button was produced under 10 atm of nitrogen which appears metallographically to be very nearly stoichiometric UN, although chemical analysis indicates only 5.26 wt.% nitrogen and about 1.0 wt.% tungsten pickup.

The sinterability of thoria compacts prepared from powders with different properties was determined[23] as a function of starting particle size, crystallite size, surface area, immersion density, and particle size after a 3-min treatment in a Waring Blendor. The sinterability, as indicated by density after firing at 1800°C for 2 hr, decreased gradually with increasing particle size, but the scatter of points far exceeded the experimental error. For surface area, crystallite size, and immersion density, there was a rough correlation with sinterability for powders in which the precipitation technique varied. However, for sinterability of powders with properties changed by higher calcination temperatures, there was an abrupt departure from the correlation. The best correlation of sinterability with powder properties was with particle size after Waring Blendor treatment, which represents a measure of particle integrity. The larger the resultant particle size after blending, the lower the sinterability of the powder from which the sample was taken.

Material[5] analyzing 96.5 per cent ThS (remainder ThO_2), vacuum homogenized at 1700 or 1900°C, was vacuum sintered to about 85 per cent of the theoretical density at 1900°C for 1 hr and densified to about 98 per cent of the theoretical density at 2000 and 2100°C.

Dry-pressing and sintering studies were conducted on a pure PuO_2 preparation.[69] Die-binding difficulties due to fines wedging between the punches and die body were overcome by preliminary dry slugging at 6500 psi in a 0.467-in. die followed by hand granulation through a 20-mesh screen. The green strength of pellets pressed in the range 10 to 90 tsi was excellent. The pellets were 0.19 in. in diameter and had a diameter-to-length ratio varying from 1 to 2.4. For a given pressing pressure, the green density is virtually independent of the length-to-diameter ratio. Green pellet densities (4.5 to 7.0 g/cm^3) increased linearly with pressing pressure in the 10- to 90-tsi range. Sintering trials were conducted at 1400 and 1600°C in a 5 per cent hydrogen–95 per cent nitrogen environment. Heatup and cooldown steps were held to a temperature change rate not greater than 10°C/min, with a 4-hr hold at temperature. Densities determined by a weight-in-air–weight-in-water method ranged from 10.2 to 11.0 g/cm^3 (88.9 to 95.9 per cent of the theoretical density). The sintered density of PuO_2 pellets is relatively independent of green density above 5.6 to 6.0 g/cm^3 (corresponding to a pressing pressure of 50 tsi) for pellets sintered at 1400 to 1600°C. The only apparent advantage of dry pressing above 50 tsi is to reduce the amount of shrinkage during sintering.

A cooperative experiment in the fabrication of plutonium-bearing glass fibers is being carried out by Rensselaer Polytechnic Institute, Owens-Corning Fiberglas Corporation, and Mound Laboratory. An experimental glass composition containing 56 wt.% SiO_2, 24 wt.% Na_2O, and 20 wt.% PuO_2 was successfully homogenized and fabricated into fibers.[17] It was homogenized after extensive thermal treatment at about 1650°C. The limit of PuO_2 which can be dissolved in this composition and successfully drawn into fibers without devitrification appears to be near 20 wt.%. The liquidus temperature of equilibrium crystallization of PuO_2 for the composition appears to be a little under 1375°C, which is the holding temperature for the molten glass during fiber drawing.

It appears that the rate of dissolution of PuO_2 from glass fibers by a leaching solution is not related to the PuO_2 concentration in the glass but is dependent on the concentration of alkali metal oxides in the glass.[70]

Arc melting of PuC using spectrographically pure carbon and high-purity plutonium in an interchangeable-hearth (deep hearth) arc furnace has been investigated at Argonne.[20] Buttons (30 g) made with a graphite electrode gained 0.2 to about 0.5 wt.% carbon after six melts of about

30-sec duration. The buttons were assumed heterogeneous. The composition was held to within ±0.1 wt.% carbon using a tungsten tip, and the tungsten contamination was kept below 50 ppm. Homogeneous buttons had oxygen contents of about 100 ppm. Alloys of 45 to 53 at.% carbon were difficult to cast into pins and had to be cooled very slowly to prevent cracking. Alloys just above 50 at.% carbon were not as susceptible to cracking. Arc-melted buttons near the Pu_2C_3 composition must be cooled very slowly to prevent shattering.

Hanford[71] studied the $PuO_2 + 2C \rightarrow PuC + 2CO$ reaction and found that it begins with a slight evolution of gas at 850°C. The rate of gas release increases parabolically with temperature and is extremely rapid at 1500°C. The formation of stoichiometric PuC from the oxide appears to be very difficult, and any carbide found is usually accompanied by a lower plutonium oxide. The quantity of residual oxide is time and temperature dependent. Preliminary results indicate that the reduction of the oxide and conversion to carbide, based on 45 at.% carbon in PuC, occurs as follows:

$$PuO_2 + C \rightarrow \alpha Pu_2O_3 \rightarrow \beta Pu_2O_3 \rightarrow PuC + Pu_2C_3$$

The PuC quantity increases with temperature; however, there always remains residual Pu_2C_3.

(E. O. Speidel)

Mechanism of Corrosion of Fuel Alloys

Investigations have been conducted at Harwell[72] on the oxidation of uranium and uranium-molybdenum alloys in the temperature range of 300 to 800°C. Specimens were first heated to the desired temperature in argon and then air was admitted to the reaction vessel. No signs of ignition were observed, although self-heating occurred (specimen temperature rose above the furnace temperature) at all temperatures investigated.

The Harwell workers propose that the nature of the oxide film that forms on the specimen surface accounts for the behavior observed. The following is believed to occur on unalloyed uranium:

1. At 300°C the oxide is sufficiently adherent to serve as a thermal barrier to prevent the loss of heat from the specimen, but it is not protective enough to cause the oxidation rates to fall with time. At this temperature, neither the film thickness nor the self-heating attain very high values.

2. At 400 to 450°C the oxide film is thicker but is more of a barrier to heat flow than to oxidation, thus causing large temperature rises. Oscillations in the self-heating temperature are attributed to spalling of the oxide which then allows the specimen to cool somewhat. Subsequent buildup of the oxide film again restricts the loss of heat, and the specimen temperature rises again.

3. At 450 to 650°C the oxide begins to "sinter," but is nonadherent. No oscillations in temperature occur, but relatively high self-heating is observed at the higher temperatures.

4. At 650 to 800°C the sintering is more advanced, and a relatively adherent oxide film apparently prevents oscillations in the temperature. However, self-heating is low, being similar to that observed at 400°C. This is attributed to the oxide film being a less effective heat barrier than those films formed at lower temperatures, despite the oxidation rates being almost twice as great.

Oxidation rates and self-heating of the uranium-molybdenum alloys were found to be low at all temperatures. This was attributed to the plastic nature of the film, which appeared to be "protective" in the sense that self-heating, and presumably the oxidation rates, fell with time.

(W. E. Berry)

Basic Studies of Radiation Effects in Fuel Materials

Metallic Fuels

Articles appearing in the literature for this three-month period include those devoted to establishing mechanisms of anisotropic fission damage in alpha uranium, the nature of damage produced by fission events in thin films and in bulk metal, and mechanisms of swelling in fissionable fuels.

The relation of structural changes to thermal expansion in uranium, neptunium, and plutonium has been analyzed by the Russians.[73] In all examined structures, thermal-expansion anisotropy results from the weakening of four covalent

bonds and irregular distributions in interatomic distances in crystalline lattices. The established regularities describe certain specific properties of uranium, neptunium, and plutonium.

Experiments by the French[74] dealing with the growth of uranium, effects of radiation on single crystals and polycrystal samples, and surface deformation have been analyzed and treated theoretically in terms of thermal-spike and point-defect theories. A detailed translation was not available.

An experiment has been conducted at Harwell[75] to clarify the role of point defects in the radiation growth of alpha uranium. The experiment was conducted to relate the strain induced in the [0 1 0] direction to the concentration of point defects produced by alpha-particle bombardment (alpha particles will not produce fission). The strain thus induced per unit point defect was an order of magnitude smaller than that for experiments where fission occurred. Therefore it is reasoned that theories of fission growth which attribute the growth to anisotropic-defect accumulation by anisotropic migration of point defects or by processes of atomic displacement which are dissimilar in different crystal directions are invalid. The author believes that a choice between the alternative theories must await further information. The alternative theories are those which ascribe the anisotropic growth to irreversible deformation produced by stresses in the heated region surrounding the fission track and those which relate anisotropic condensation of point defects to local thermal stresses.

At Brookhaven[76] a study of fission-product damage in thin films of various metals by electron transmission has indicated some interesting results. In films of about 100 A or more, it was concluded that the matrix was vaporized along the fission-product track causing loss of metal. In thicker films, melting and recrystallization occurred along the fission-product track causing larger crystallites. In films exceeding 250 A in thickness, no effect was observed. In the latter case, however, observation of dislocations and vacancy clusters was not possible. Single-crystal films are being sought.

Recent experiments at Hanford[46] have shown a surprising correspondence of uranium swelling as a function of temperature when it is produced, on the one hand, by in-pile irradiation and, on the other hand, by irradiation and long-time postirradiation heating.

Those following the research being conducted on swelling in fissionable fuels may find a series of discussions in the *Journal of the Institute of Metals*[77] to be provocative. This discussion presents different points of view on the swelling problem, along with a variety of original information, and comprises the response to a paper by G. W. Greenwood, *J. Inst. Metals*, 88: 31 (1959-1960).

Studies at General Atomic[78] have been made of the vapor transport of fission products from recoil-impregnated surfaces of nickel foils *in vacuo*. Significant transport occurs as low as 1200°F. (F. A. Rough)

Radiation Effects in Ceramic Fuels

Current fundamental studies of ceramic fuels include those on techniques for observing dislocations in UO_2 by optical microscopy, on fission-fragment trajectories in thin-film UO_2, and on the restoration of the crystal parameter by heating irradiated UO_2.

Techniques have been developed at Saclay[79] to permit direct observation of the arrangement of dislocations in sintered uranium dioxide by optical microscopy.

In research at Hanford[80] the fission-fragment trajectories in thin-film UO_2 (100 A thickness) have been studied by transmission electron microscopy and diffraction after neutron exposures at temperatures of 60°C or less in air. After exposures of 1 to 2×10^{16} nvt, typical fission-fragment paths are observed; after 3.9×10^{17} nvt, the trajectories are still discernible, but localized regions have become opaque, these regions becoming larger at exposures of 1.6×10^{18} and 4.4×10^{19} nvt. These opaque regions were shown by shadowing techniques to be flocculent outgrowths on the carbon substrate. After an exposure of 3×10^{19} nvt, no sharp diffraction pattern could be obtained; but, at 4.4×10^{19} nvt, crystallinity had been restored. It is not certain whether this was an effect of irradiation destroying crystallinity or a loss of crystallinity associated with changes occurring perhaps by vaporization and condensation. This latter effect was not observed when the films were irradiated in vacuum instead of air, and the tendency to form flocculent aggregates was reduced.

The restoration of crystalline parameters by isochronous annealing was investigated[81] in a

UO_2 sample for which the relative parameter variation had reached a maximum of 8.6×10^{-4}. The irradiation was done at 2.5×10^{12} nv for seven days to achieve an integrated flux of 1.48×10^{18} nvt, at a temperature below 62°C. The results show that restoration took place in two principal stages: one beginning at 200°C and the other at 500°C. The explanation for the variation of the parameters is the formation of point defects by irradiation which disappear upon annealing. (F. A. Rough)

References

1. M. H. Mueller (Ed.), Papers and Discussion from the X-Ray Preferred Orientation Meeting Held at Argonne National Laboratory, December 15–16, 1960, USAEC Report ANL-6359, Argonne National Laboratory, May 1961.
2. S. N. Buckley, Irradiation Growth, British Report AERE-R-3674, March 1961.
3. U. Gonser, Growth of Alpha Uranium as the Result of Correlative Collisions, USAEC Translation AEC-tr-4522 [translated from *J. Nuclear Materials*, 2: 43–50 (1960)].
4. V. H. Troutner, Mechanisms and Kinetics of Uranium Corrosion and Uranium Core Fuel-Element Ruptures in Water and Steam, USAEC Report HW-67370, Hanford Atomic Products Operation, July 21, 1961.
5. J. W. Goffard, Influence of Cladding Thickness on Defect-Test Behavior of Coextruded Zircaloy-2-Clad Uranium, USAEC Report HW-68390, Hanford Atomic Products Operation, February 1961. (Classified)
6. H. C. Field, Effect of CO_2 and N_2 Atmospheres in Reducing the "Corrosion" Rate of Uranium in Santowax R, USAEC Report NAA-SR-Memo-2264, Atomics International, Nov. 11, 1957.
7. A. B. McIntosh and T. H. Heal, *Materials for Nuclear Engineers*, pp. 8–63, Interscience Publishers, Inc., New York, 1960.
8. S. Scapa and M. Gazith (Comps.), Bibliography on Corrosion and Oxidation of Uranium, Israeli Report LS-75, December 1960.
9. G. H. Bannister and J. R. Murray, Some Observations on Uranium-Molybdenum-Niobium Alloys, British Report AERE-R-3380, June 1960.
10. Atomics International, April 1961. (Unpublished)
11. H. Mikailoff, Micrographic Fracture Study of the Precipitate Formed by Annealing at 300°C of the Gamma Phase in Uranium–Molybdenum Alloys, *Mém. sci. rev. mét.*, 58(3): 171–175 (March 1961).
12. J. D. Browne and G. K. Williamson, The Stability of a Tetragonal-Phase Gamma Prime in Uranium-Niobium Alloys, *J. Inst. Metals.*, 89: 246–247 (March 1961).
13. T. I. Jones et al., Some Properties of Aluminum-Uranium Alloys in the Cast, Rolled, and Annealed Conditions, Canadian Report FD-43(AECL-1215), June 1960.
14. L. S. Castleman, Layer Growth During Interdiffusion in the Aluminum-Uranium Alloy System, *J. Nuclear Materials*, 3: 1–15 (January 1961).
15. L. J. Dykstra, Maritime Gas-Cooled Reactor Program, X-Ray Study of the Ternary System Uranium-Aluminum-Oxygen, USAEC Report GA-1479, General Atomic Division, General Dynamics Corp., Sept. 17, 1960.
16. G. E. Darwin and N. G. Worley, Improvements in or Relating to Nuclear Reactors, British Patent 857,009, Dec. 29, 1960.
17. J. F. Eichelberger, Mound Laboratory Monthly Progress Report for February 1961, USAEC Report MLM-1112, Mound Laboratory, Feb. 28, 1961.
18. Argonne National Laboratory, Reactor Development Program Progress Report for April 1961, USAEC Report ANL-6355.
19. Argonne National Laboratory, Reactor Development Program Progress Report for May 1961, USAEC Report ANL-6374, June 15, 1961.
20. Argonne National Laboratory, Metallurgy Division Annual Report for 1960, USAEC Report ANL-6330.
21. Los Alamos Scientific Laboratory, Quarterly Status Report on LAMPRE Program for Period Ending February 20, 1961, USAEC Report LAMS-2531, March 1961.
22. J. R. Thomson, Some New Intermetallic Compounds of Thorium of the Type Th_7X_3, *Nature*, 189: 217 (Jan. 21, 1961).
23. Oak Ridge National Laboratory, June 7, 1961. (Unpublished)
24. D. T. Peterson, Effect of Hydrogen on Tensile and Impact Properties of Thorium, *Reactive Metals*, Vol. 2, pp. 477–485, Interscience Publishers, Inc., New York, 1959.
25. R. W. Dayton and C. R. Tipton, Jr., Progress Relating to Civilian Applications During March 1961, USAEC Report BMI-1509, Battelle Memorial Institute, Apr. 1, 1961.
26. R. W. Dayton and C. R. Tipton, Jr., Progress Relating to Civilian Applications During April 1961, USAEC Report BMI-1514, Battelle Memorial Institute, May 1, 1961. (Classified)
27. J. H. Cherubini et al., Fabrication Development of UO_2–Stainless Steel Composite Fuel Plates for Core B of the Enrico Fermi Fast-Breeder Reactor, USAEC Report ORNL-3077, Oak Ridge National Laboratory, Apr. 18, 1961.
28. S. J. Paprocki et al., Incorporation of a Boron Burnable Poison and Spherical UO_2 in SM-2 Stainless-Matrix Fuel Plates, USAEC Report BMI-1527, Battelle Memorial Institute, July 6, 1961.

29. S. J. Paprocki et al., Fabrication and Irradiation of SM-2 Core Materials, USAEC Report BMI-1528, Battelle Memorial Institute, July 12, 1961.
30. Nuclear Materials and Equipment Corp., Final Report on Corrosion and Radiation-Damage-Resistant Fuel Material, November 15, 1959, Through November 14, 1960, USAEC Report NYO-9187.
31. C. F. Powell et al., *Vapor Plating*, John Wiley & Sons, Inc., New York, 1955.
32. J. M. Blocher, Jr., et al., Fluidized-Bed Coating on UO_2 Powder with Niobium and Other Elements, USAEC Report BMI-1440, Battelle Memorial Institute, May 25, 1960.
33. Sanderson and Porter, Fuel Element Development Program for the Pebble Bed Reactor, Quarterly Progress Report, November 1, 1960, to January 31, 1961, USAEC Report NYO-9063.
34. Sanderson and Porter, Apr. 30, 1961. (Unpublished)
35. R. W. Dayton and C. R. Tipton, Jr., Progress Relating to Civilian Applications During May 1961, USAEC Report BMI-1518, June 1, 1961. (Classified)
36. Aerojet-General Nucleonics, Army Gas-Cooled Reactor Systems Program, Monthly Progress Report for November 1960, USAEC Report IDO-28566, Dec. 30, 1960.
37. Aerojet-General Nucleonics, Army Gas-Cooled Reactor Systems Program, A Preliminary Study of a 1000-Kw(e) Mobile Nuclear Power System, USAEC Report AGN-TM-390, December 1960.
38. Aerojet-General Nucleonics, Army Gas-Cooled Reactor Systems Program, Monthly Progress Report for January 1961, USAEC Report IDO-28568, Feb. 28, 1961.
39. A. E. Powers, Conductivity in Aggregates, USAEC Report KAPL-2145, Knolls Atomic Power Laboratory, Mar. 6, 1961.
40. General Atomic Division, General Dynamics Corp., 40-Mw(e) Prototype High-Temperature Gas-Cooled Reactor Research and Development Program, Quarterly Progress Report for the Period Ending June 30, 1960, USAEC Report GA-1640, April 1961.
41. General Atomic Division, General Dynamics Corp., 40-Mw(e) Prototype High-Temperature Gas-Cooled Reactor Research and Development Program, Quarterly Progress Report for the Period Ending September 30, 1960, USAEC Report GA-1774, April 1961.
42. J. H. Oxley et al., Coating and Preparation of Uranium and Thorium Carbide Powders, USAEC Report BMI-X-160, Aug. 2, 1960.
43. C. W. Boquist and S. W. Bradstreet, Modified Graphite Technology, USAEC Report LAR-49, Illinois Institute of Technology, Armour Research Foundation, Jan. 5, 1961.
44. M. D. Karkhanavala and R. M. Carroll, In-Pile Measurements of the Electrical Resistivity and Thermoelectric Power of Sintered UO_2, USAEC Report ORNL-3093, Oak Ridge National Laboratory, May 2, 1961.
45. F. W. Albaugh, Reactor and Fuels Research and Development Operation Monthly Report for April 1961, USAEC Report HW-69408-A, Hanford Atomic Products Operation, May 15, 1961. (Classified)
46. J. M. Atwood and W. A. Snyder (Eds.), Plutonium Recycle Program Annual Report for Fiscal Year 1960, USAEC Report HW-67000, Hanford Atomic Products Operation, Aug. 15, 1960.
47. F. W. Albaugh, Reactor and Fuels Research and Development Operation Monthly Report for May 1961, USAEC Report HW-69822-A, Hanford Atomic Products Operation, June 15, 1961. (Classified)
48. A. B. Auskern and J. Belle, Oxygen Ion Self-Diffusion in Uranium Dioxide, *J. Nuclear Materials*, 3(3): 267–276 (March-April 1961).
49. A. B. Auskern and J. Belle, Uranium Ion Self-Diffusion in Uranium Dioxide, *J. Nuclear Materials*, 3(3): 311–319 (March-April 1961).
50. Oak Ridge National Laboratory, Gas-Cooled Reactor Project Quarterly Progress Report for Period Ending March 31, 1961, USAEC Report ORNL-3102, May 26, 1961.
51. G. W. Parker et al., Fission-Product Release from UO_2 by High-Temperature Diffusion and Melting in Helium and Air, USAEC Report CF-60-12-14, Oak Ridge National Laboratory, Feb. 14, 1961.
52. F. W. Albaugh, Reactor and Fuels Research and Development Operation Monthly Report for March 1961, USAEC Report HW-6902-A, Hanford Atomic Products Operation, Apr. 15, 1961. (Classified)
53. A. Ridal et al., Irradiation of Nonstoichiometric Uranium Oxide for Short Durations, Canadian Report CRFD-994 (AECL-1199), February 1961.
54. R. R. Hood and L. Isakoff (Comps.), Heavy-Water-Moderated Power Reactors, Progress Report for April 1961, USAEC Report DP-615, E. I. du Pont de Nemours & Company, Inc., June 1961.
55. Wlodzimierz Frzebiatowski and Andrzej Jablonski, Some Phase Relations of the $BaO-UO_2-O_2$ System, *Nukleonika*, 5: 587–596 (1960).
56. G. Zuromsky, The Development and Testing of Homogeneous Ceramic Fuels, Progress Report for the Period May 15–August 31, 1959, USAEC Report TID-11294, Combustion Engineering, Inc., Nuclear Division.
57. Combustion Engineering, Inc., Nuclear Division, The Development and Testing of the UO_2 Fuel-Element System, Quarterly Report for September 1, to November 30, 1960, USAEC Report CEND-112, December 1960.
58. R. C. Lied et al., The $ZrO_2-CaO-UO_2$ Ceramic Fuel Fabrication for the EBWR Spike Core Elements, USAEC Report ANL-6168, Argonne National Laboratory, May 1961.

59. G. Murson et al., Uranium Monocarbide, *At. Energ.*, 9: 387–391 (November 1960).
60. I. F. Ferguson et al., High-Temperature X-Ray Diffraction Studies. Part II: Uranium Monocarbide and Uranium Dicarbide, British Report AERE-M-819, January 1961.
61. R. W. Dayton and C. R. Tipton, Jr., Progress Relating to Civilian Applications During June 1961, USAEC Report BMI-1524, Battelle Memorial Institute, July 1, 1961. (Classified)
62. Carborundum Co., May 1961. (Unpublished)
63. A. Accary and R. Lucas, Influence of the Heat-Treatment on Uranium Monocarbide and Sintered U-UC, *Rev. mét.*, 58(5): 383–387 (May 1961).
64. J. A. Coffman et al., Carbonization of Plastics and Refractory Materials Research, Report WADD-TR-60-646(Pt. I), General Electric Co., Flight Propulsion Laboratory Dept., Oct. 15, 1960.
65. Westinghouse Electric Corp., Bettis Atomic Power Laboratory, Materials Dept., Technical Progress Report for the Period December 26, 1960, to March 25, 1961, USAEC Report WAPD-MRK-9. (Classified)
66. S. J. Paprocki et al., Properties of PuO_2 and PuO_2-ThO_2 Ceramics, USAEC Report BMI-X-170, Battelle Memorial Institute, June 30, 1961. (Classified)
67. Proceedings of the Uranium Carbide Meeting Held at Oak Ridge National Laboratory, Oak Ridge, Tennessee, December 1–2, 1960, USAEC Report TID-7603.
68. P. Stephas and E. W. Hoyt, Reactive Hot Pressing of ZrC-UC Solid Solution, *Am. Ceram. Soc. Bull.*, 40(5): 320–323 (May 15, 1961).
69. Nuclear Materials and Equipment Corp., Development of Plutonium-Bearing Fuel Materials, Progress Report for the Period January 1 Through March 31, 1961, USAEC Report NUMEC-P-60, Apr. 21, 1961.
70. J. F. Eichelberger, Mound Laboratory Monthly Progress Report for March 1961, USAEC Report MLM-1113, Mound Laboratory, Mar. 30, 1961.
71. O. J. Wick, Plutonium Metallurgy Operation Quarterly Progress Report for April, May, and June 1960, USAEC Report HW-66081, Hanford Atomic Products Operation, July 15, 1960. (Classified; however, the data taken from page 3.41 is unclassified.)
72. J. W. Isaacs and J. N. Wanklyn, The Reaction of Uranium with Air at High Temperatures, British Report AERE-R-3559, December 1960.
73. N. T. Chebatarev, The Relation of Structure to Anisotropy in the Thermal Expansion for Uranium, Neptunium, and Plutonium, *At. Energ.*, 10: 43–49 (January 1961).
74. P. Bussy, Effects of Irradiation in Reactors on Metallic Uranium (in French), *Métaux (Corrosion-Inds.)*, 413: 24–39 (January 1960).
75. M. W. Thompson, An Experiment to Clarify the Role of Point Defects in the Radiation Growth of Alpha Uranium, *J. Nuclear Materials*, 3(3): 354–356 (March-April 1961).
76. Brookhaven National Laboratory, Nuclear Engineering Dept., Progress Report for May 1–August 31, 1960, USAEC Report BNL-646.
77. Discussion: Volume Increases in Fissile Materials on Neutron Irradiation, *J. Inst. Metals*, 89(8): 308–316 (April 1961).
78. General Atomic Division, General Dynamics Corp., Maritime Gas-Cooled Reactor Program Quarterly Progress Report for the Period Ending March 31, 1960, USAEC Report GA-1259.
79. A. Portnoff and R. Caillat, Direct Observation of Dislocations in Sintered Uranium Dioxide, French Report CEA-1563, 1960.
80. T. K. Bierlein and B. Mastel, Damage in UO_2 Films and Particles During Reactor Irradiation, *J. Appl. Phys.*, 31(12): 2314–2315 (December 1960).
81. J. Bloch, Thermal Restoration of Parameters of Weakly Irradiated UO_2, *J. Nuclear Materials*, 3: 237–238 (February 1961).

Section II

MODERATOR MATERIALS

Graphite

A British patent[1] described the following method for decreasing the permeability of graphite. The pores of the graphite sample were either evacuated or filled with water vapor. The sample was immersed in molten sugar or a concentrated aqueous sugar solution under pressure to force the sugar into the pores. The sample was then drained, cooled, and placed in a pressure vessel. The temperature was raised to 250°C under a pressure great enough to prevent the water vapor formed by the sugar decomposition from forcing the carbon residue out of the pores. The sample was then heated slowly to 1000°C to expel the remaining volatile decomposition products. With this method, the permeability of a graphite specimen was reduced by a factor of 50 in a single impregnation and by a factor of 1000 in two or three impregnations.

Oak Ridge researchers[2] irradiated two capsules containing UC_2-graphite fuel pellets in graphite cans in the Materials Testing Reactor (MTR). Irradiation conditions and fuel loadings are shown in Table II-1. Dimensional data for the two pellets in one of the capsules are summarized in Table II-2. A significant decrease in diameter and an increase in length were observed in both cases.

Numerous metals and alloys[3] were screened at General Atomic for application as a cladding

Table II-1 IRRADIATION CONDITIONS OF CAPSULES CONTAINING UC_2–GRAPHITE FUEL PELLETS[2]

	Capsule MTR-48-1		Capsule MTR-48-2	
	Pellet A	Pellet B	Pellet A	Pellet B
Time at power, hr	1440	1440	2700	2700
Average temp., °F:				
Graphite can wall	1570	1310	1500	1500
Center line of pellet (calc.)	3350	3600	2500	2500
Estimated U^{235} burnup, at.%	13	6	20	20
Average fission power density, g/cm³	270	300	140	140
Fuel loading, wt.% UC_2	10.52	19.33	5.59	8.00
U^{235} enrichment, at.%	93.12	93.12	93.12	93.12

Table II-2 EFFECTS OF IRRADIATION ON UC_2–GRAPHITE FUEL (CAPSULE MTR-48-1)[2]

	Pre-irradiation	Post-irradiation	Per cent change
Element A			
Diameter, in.:			
Average	0.997		
Top		0.966	−3.1
Middle		0.962	−3.4
Bottom		0.954	−4.2
Length, in.:			
Average	1.469		
Edge		1.508	+2.7
Center		1.544	+5.2
Element B			
Diameter, in.:			
Average	0.997		
Top		0.973	−2.4
Bottom		0.946	−5.1
Length, in.:			
Average	1.468	1.521	+3.5

material on graphite to operate in helium at temperatures up to 1000°C. It was found that the heat-resistant nickel-base alloys, the stainless steels, and molybdenum all carburized rapidly above 816°C. Of the alloys tested, nickel-copper alloys appeared to be the most promising for use as a high-temperature graphite cladding. Aging data indicated that Monel is more resistant to graphitization than nickel.

(J. Koretzky)

Beryllium Metal and Alloys

Beryllium Purification, Casting, and Alloy Development

There is still much interest in the production of superpure beryllium metal. Thus far, efforts to make beryllium metal by the iodide decomposition method have resulted in no pure beryllium being deposited. When deposition was attempted on molybdenum or tungsten filaments, no beryllium was deposited, and on a platinum filament a platinum-beryllium alloy was formed.

Efforts to make pure beryllium by distillation of Pechiney flake from a beryllia crucible and collection of the distillate on tantalum were more successful, as may be seen in Table II-3.

Table II-3 ANALYSIS OF DISTILLED BERYLLIUM[4]

	Impurities, ppm				
	Fe*	Ni†	Mn*	Cr*	C‡
Starting materials:					
Pechiney flake	142	45	15	6	
Melted Pechiney flake (starting material for run 4)	280	116	25	12	20
Best product:					
Run 4	5	0	5	0	
Run 5	0	0	0	0	30

*±5 ppm or 2 per cent, whichever is greater.
†±2 ppm or 2 per cent, whichever is greater.
‡±10 ppm.

However, the BeO crucibles did introduce iron and nickel as impurities.[4]

The zone-refining work at Franklin Institute[5,6] continues to show encouraging results. It was reported that the extent of basal glide during tensile testing of zone-refined single crystals shows that the movement is not necessarily limited to very small values. A single-crystal specimen from material subjected to eight zone passes exhibited 156 per cent glide strain on the basal plane, equivalent to 92 per cent elongation. Another specimen showed 140 per cent elongation in a single crystal, with the basal plane initially at 45° to the tensile axis. It is planned to try to determine the particular impurities that are responsible for brittleness in ordinary beryllium.

The final report[7] on an Air Force project to develop a reliable technique for producing fine-grained, sound beryllium cast ingots indicate that accelerated cooling through mold design was the most effective approach to this objective. Small additions of germanium, zirconium, and lanthanum appeared to have a grain-refining effect on cast beryllium, whereas additions of titanium and silicon in amounts of 0.1 per cent each improved the fluidity of the molten metal. Low-frequency mechanical vibration broke up the cast structure of beryllium into a structure more favorable for hot-working operations. The fine-grained cast ingots could be successfully hot extruded. At the temperature used for extrusion (1850°F), the microstructure was partially recrystallized into an equiaxed structure. Fine-grained equiaxed sheet was produced from cast beryllium using an intermediate extrusion step.

Dense alloys of magnesium and beryllium have been prepared[8] by infiltration of beryllium skeletons with molten magnesium and also by sintering compacts of magnesium and beryllium powders. These alloys contain a compound believed to be $MgBe_{13}$, which is usually present as a continuous intergranular phase.

Fabrication of Beryllium

The second interim technical report[9] of the Beryllium Corporation's project for development of techniques for producing beryllium structural shapes notes that preliminary work has produced exceptionally high yields of usable materials suitable for further evaluation. It appears probable that it will be desirable to use extruded working billets as starting stock for the development of rolled high-strength squares and rounds. Meanwhile, the Northrop Corporation reported[10] that continued efforts to extrude a bare beryllium channel section on the high-speed press of Wolverine Tube Company were discouraging. Therefore they expect that future effort on this program will be directed toward extrusion of canned billets.

Sprayed coatings of −300-mesh beryllium powder can be applied satisfactorily to steel or beryllium by the plasma arc, using argon as a carrier gas. The following results have been reported:[11]

Spraying distance, in.	Bond strength, psi	Density, %
1	3005*	89.6
2	2420	
3	1791	

Various factors were studied[12] in an effort to produce randomly oriented wrought beryllium sheet. During rolling, the crystallographic basal-plane population parallel to the plane of the sheet increased with the reduction in area. When the sheet was subjected to annealing temperatures in excess of 950°C, the third-dimensional ductility was increased from 0.2 per cent (in the stress-relieved condition) to 1.75 per cent.

A British paper[13] discusses the requirements for uniform densification during hot pressing. It is concluded that a double-pressing method is essential if thin-walled hemispherical shapes are required.

In an attempt to produce porous beryllium bodies with a density of 0.10 g/cm^3 and a compressive strength of 2000 psi, five methods were investigated.[14] Although the project was discontinued before the experimental work was completed, it appeared that a product consisting of random-packed hollow spheres had the best chance of success. This material can be fabricated by a combination of slip casting and the lost-wax process.

Specialized techniques for deep-hole drilling of beryllium include the use of cutting fluids under pressures of up to 3000 psi and special oil-hole drills or rifle drills.[15] For very deep, small-diameter holes, oil pumps as large as 50 hp may be required. The standard drill design is a two-flute, oil-hole drill, carbide tipped, with its point ground to a 90° included angle. Single-flute carbide-tipped gun drills are used also. The shank of this type is a seamless steel tube with one side depressed to form a V-groove that extends the entire length of the shank to the point of the drill. This groove permits the outflow of chip-laden coolant (supplied through the hollow shank) from the cutting site.

Significant advances have been reported[16] in the development of finned beryllium tubing. Tubing fabricated by hot extrusion, using either the filled-die or ribbed-billet technique, has been fabricated in 3-ft lengths. Preliminary room-temperature rupture tests of the finned tubing gave breaking strengths in the 95,000-psi range, which indicate mechanical strengths exceeding that of smooth-walled tubing produced by the same methods.

Beryllium Joining

It has been reported[4] that, in ultrasonic welding of beryllium, all the energy must be delivered to the beryllium in 0.5 sec or less to avoid cracking the metal. With a standard 3-in. tip radius, a clamping force of about 500 lb, and power to the transducers of about 2400 watts, a weld interval of about 0.5 sec or less is required to weld 0.010- to 0.012-in. beryllium sheet having a Vickers hardness of 254. The energy required varies with the tip radius and the material hardness and thickness. Astroloy (a G.E. alloy), a relatively new nickel alloy, made suitable tips. The process is regarded as a promising method of joining beryllium.

Results of testing butt-brazed tensile specimens were reported[17] on Lockheed's program on the collection of design data for beryllium. These results led to the decision to braze the beryllium cylinders and sandwiches with a 94.8 wt.% silver−5 wt.% aluminum−0.2 wt.% manganese brazing alloy, using a ½-min brazing cycle (at 1675°F) to minimize the effects of recrystallization. Oak Ridge reports[2] that initial experiments with the electron-beam-fusion welding process have indicated it to be very promising for the sealing of beryllium fuel tube elements. Joining by pressure bonding was investigated at Battelle. Good bonds could be obtained when the mating surfaces were first pickled to produce a bright shiny surface and then abraded. Grain growth across the interface was observed in specimens bonded at 1600°F for 2 hr at 10,000 psi and in sheet specimens bonded at 1525 and 1650°F for 4 hr at 10,000 psi. Metallographic examination of beryllium-to-UO_2 bonds made at 1650 and 1750°F for 4 hr at 10,000 psi revealed reaction zones at the interfaces on the order of 0.0001 in. or less. Similar reaction zones were observed by

* Adhesive failure; bond did not fail.

Knapton and West[18] in beryllium-UO_2 compatibility tests.

Physical Metallurgy of Beryllium

The preparation and thermal analysis of binary and ternary beryllium alloys were continued at Nuclear Metals. Copper appears to be an effective beta stabilizer. A tentative beryllium-copper phase diagram shows a eutectoid at a copper content of approximately 13.5 at.% copper at a temperature[19] of about 1117°C. Gas-quenching experiments on a nominal beryllium–8 at.% nickel alloy were begun in a modified Greninger apparatus. Samples have been cooled by helium gas with initial cooling rates ranging from 210°C to over 12,000°C/sec. To date, 100 per cent beta retention has not been achieved.[20]

Single crystals of BeB_2 and BeB_6 were prepared by sintering powder mixtures in a BeO crucible under argon. The authors reported[21] chemical analyses and X-ray powder patterns for these compounds.

A Russian report[22] on rhenium-beryllium alloys noted that the maximum hardness of 2221 kg/cm^2 was attained in alloys containing 1 at.% (17.4 wt.%) rhenium. The limits of solubility for alloys containing 66.7 at.% beryllium were determined at 1600°C. Peritectic transformations were found in the $ReBe_2$-beryllium system.

In general, investigation of the niobium–beryllium binary system at Denver Research Institute[23] confirmed the work of previous investigators. The following intermetallic compounds were observed:

Compound	Composition, wt.%	Structure
$NbBe_{12}$	46 Nb	Bc tetragonal $a_0 = 7.344$ $c_0 = 4.234$
Nb_2Be_{17}	55 Nb	Rhombohedral $a_0 = 7.40$ $c_0 = 10.76$ (hex.)
$NbBe_3$	77 Nb	Rhombohedral $a_0 = 4.56$ $c_0 = 20.97$ (hex.)
$NbBe_2$	84 Nb	Fc cubic $a_0 = 6.524$
Nb_3Be_2		Tetragonal $a_0 = 6.52$ $c_0 = 3.35$

Compositions between 55 and 77 wt.% niobium revealed two-phase structures (Nb_2Be_{17} and $NbBe_3$),* and the microstructures indicated a eutectic transformation. The experimental temperature of the solidus was 1675°C, and the composition of the eutectic point was 67 wt.% niobium. The occurrence of a possible phase transformation in the $NbBe_{12}$ was noted in the region between 800 and 1500°F, which may explain the brittleness found in that temperature range.

Studies of beryllium by transmission electron microscopy[4] indicate that impurities in the samples prepared from Pechiney flake seem to precipitate in the annealing process preferentially along subgrain boundaries and dislocations. It is also indicated that strong pinning forces are effective which tend to fix dislocations. The anchoring may be caused by small impurity clusters or super jogs or both.

As-received beryllium hot-pressed (machined on both sides) sheet showed cracks to depths of 0.005 in. and twins to depths of 0.01 in. Annealing for 2 hr at 800°C would remove these twins with no observable grain growth. The cracks can be removed by etching or carefully grinding 0.006 in. from each side. Annealing at 800°C does not remove twins from hot-rolled sheet. Some are removed by annealing for 30 min at 850°C, but recrystallization occurs in many places, and twins still remain.

At temperatures above 500°C, strength and ductility of wrought beryllium increase with aging time, leveling out after one week at 700 or 800°C at about 95,000 psi and 14 per cent elongation.[4] These values are similar to the as-extruded value (98,000 psi, 16.6 per cent elongation). At lower temperatures, both strength and ductility are decreased. The solution treatment preceding aging did not affect the texture.

After initial rolling of beryllium at 1950°C, low-temperature finishing passes appeared to be ineffective in improving its mechanical properties. When preceded by rolling at lower temperatures, however, finishing at 1000°F (580°C) produced significant increases in yield and ultimate strengths at the cost of some loss in ductility.

The progress of diffusion of carbon in thin films of beryllium was observed by diffraction and electron-microscope techniques.[24] Under

pressure of 10^{-5} mm Hg, the beryllium started to oxidize at 200°C. At 550°C the beryllium film was completely oxidized. When carbon was present at 600°C, the appearance was essentially the same as that of the oxidized specimens, but carbide was present. At 900°C the rings of Be_2C disappeared from the diffraction pattern and BeO alone remained. Under these conditions of vacuum and temperature, it is possible that the Be_2C decomposed and oxidized, and the residual carbon was left in an amorphous state.

A British study[25] notes that low-load indentation hardness measurements on beryllium are markedly dependent on orientation and surface condition. Machining produces a uniform surface layer with a hardness of 300 DPN on both single and polycrystalline beryllium. Removal by etching of 0.02 cm (0.008 in.) of surface reveals the marked crystallographic dependence: 230 DPN on the basal plane and 7 DPN on the prism plane for a single crystal and 300 to 170 DPN, depending on the angle of testing, for a highly oriented sheet. In all cases the maximum hardness corresponds to the greatest concentration of basal planes.

Results of hot-hardness testing[26] showed that beryllium from magnesium-reduced pebble exhibits both strain and precipitation aging mechanisms that are removed by precipitation annealing between 600 and 800°C, with consequent improvement in high-temperature annealing characteristics. No such phenomena were detected in beryllium from electrolytic flake. The optimum parameters to induce maximum precipitation appear to be about 700 to 750°C for 100 hr.

Physical and Mechanical Properties of Beryllium

The temperature dependence of electrical resistivity (R) of 400- to 2500-A-thick beryllium films, vacuum deposited at liquid-helium temperature, was determined in the 3 to 360°K range. All specimens became superconductive at 7 to 9°K, but irreversible loss of superconductivity occurred on heating to more than 60°K, from which the existence of a superconductive modification stable below 30°K was inferred. A decrease in R observed at 200°K was attributed either to the existence of another modification of beryllium or to its recrystallization.[27]

From Lockheed it is reported[28] that notch-sensitivity tests show that the notch sensitivity of beryllium decreases with increasing temperatures up to 800°F (430°C) and then tends to increase again at 1000°F (540°C). In general, the data indicate that beryllium is not prohibitively notch sensitive, even at room temperature.

In another study[29] the effect of various surface finishes was investigated. Beryllium specimens that were etched to remove surface defects caused by machining were found to have the best mechanical properties. The fatigue endurance limit was equivalent to the static tensile strength and was improved by etching.

An important summary of the effect of strain rate and heat-treatment on the tensile properties of extruded beryllium rods was reported by Brown et al.[30] The fracture mode was found to depend on the temperature and the strain rate. The rate of tensile straining affected properties at all temperatures, but particularly in the range of 300 to 600°C where strain aging and intergranular failure are operative. Three modes of failure were encountered in ingot extrusion between 25 and 600°C:

1. Transverse cleavage of prism planes
2. Longitudinal slitting of basal planes
3. Failures originating at grain boundaries

Multiple yielding was observed in the range of 400 to 500°C. This effect is dependent on strain rate, purity, grain size, and possibly on the geometry of the test piece. It is also sensitive to heat-treatments involving long-term annealing followed by slow cooling from 780°C. Multiple yielding is coincident with the plateau in the strength-versus-temperature curves.

Beryllium responds to heat-treatment in the range of 600 to 800°C. The results of heat-treatment are a reduction of strength in the temperature range above 300°C (formerly associated with solution hardening) and the removal of multiple yielding. An outstanding increase in ductility of pebble-ingot extrusions was obtained by heat-treatment, but this improvement did not occur in extrusion of purer flake beryllium.[30]

The tensile properties[30] of flake-ingot bar between room temperature and 600°C were not affected markedly by variations in extrusion temperature between 1000 and 1050°C.

The mechanism of fracture in a heat-treated pebble-ingot extrusion was altered at 600°C

from a brittle intergranular mode to a mode that allows extensive ductile elongation of grains. The alteration of properties after annealing has been ascribed to purification of the matrix by precipitation of impurity. It has not been possible so far to identify either the impurities responsible for strain aging or those responsible for grain-boundary strengthening. Possibly the two effects may be caused by a redistribution after heat-treatment of the same element.[30]

Results of an extensive program of testing the mechanical properties of cross-rolled beryllium sheet were reported by Curtiss-Wright Corporation.[31] The results of extensive tensile testing of QMV beryllium from 20 to 870°C were reported by Lockheed.[32] Mechanical properties were correlated with BeO content and with microstructure. Fracture, which was transcrystalline to 480°C, was initiated by stress concentration at twin intersections, intersections of twins at grain boundaries, at $\{\bar{1}012\}$ twin-matrix interfaces, and at impurity particles, particularly carbides. Intercrystalline fractures, starting at 480°C, were characterized by void formation at grain boundaries normal to the stress axes. Voids were observed to have nucleated at carbide particles in grain boundaries and presumably at other smaller unidentified impurity particles. Boundaries of large-grain clusters free of impurities showed no intercrystalline voids, whereas the surrounding fine-grain materials that did contain impurity particles in the grain boundaries had numerous cracks and voids.

Corrosion and Irradiation Behavior of Beryllium

Beryllium tensile specimens irradiated at 350°C to fission neutron doses up to $\sim 2 \times 10^{20}$ nvt and at 600°C to fission neutron doses up to $\sim 7 \times 10^{20}$ nvt showed no changes in transverse mechanical properties. No changes in longitudinal properties of specimens irradiated at 600°C were noted. The specimens irradiated to $> 2 \times 10^{18}$ nvt at 350°C and tested below this temperature showed an increase in yield strength and some loss of ductility. Some of this damage could be annealed out by heating above 500°C before testing.[33]

The use of beryllium in a reactor may introduce two types of problems: (1) corrosion and (2) irradiation effects. The corrosion of beryllium in sodium or NaK becomes significant above 750°F. Beryllium is expected to be compatible with organic coolants of interest and most dry gas coolants up to 1100°F.

The effect of irradiation on the properties of beryllium does not become apparent until doses are in excess of 10^{20} fast neutrons/cm^2. Thereafter the main effect is the reduction of the ductility if the irradiation temperatures are low; at these temperatures the volume change is negligible. If the irradiation temperature is 600°C, doses of up to 3×10^{20} fast neutrons/cm^2 have little effect.[34]

Oak Ridge found[35] that the effect of irradiation on stress rupture of beryllium tube-burst specimens at 700°C is about the same as that observed at 600°C. For tube machined from hot-pressed block, the reduction in 100-hr rupture strength at a dose of 1.8×10^{19} fast neutrons/cm^2 (>1 Mev) is approximately 23 per cent in terms of stress.

Gregg et al.[36,37] reported on the high-temperature oxidation of beryllium in various media. The oxidation product formed in CO_2 is protective up to nearly 750°C. In CO the oxidation product is nonprotective above 550°C, the rate of oxidation being considerably greater than in CO_2. In water vapor and moist oxygen, the rate continually decreases with time to reach a very small value after about 100 hr up to nearly 650°C; above this temperature the oxidation product is no longer protective.

In a test to determine the compatibility of beryllium and uranium dioxide, UO_2 pellets were clamped to hot-rolled beryllium sheet. Although the reaction appeared to be restricted to small areas, it showed considerable penetration of the sheet even at 600°C. Further work will be required to confirm this trend and to establish what it means in terms of beryllium cans under reactor conditions.[18]

Corrosion resistance of beryllium in the British AGR reactor is reported to be satisfactory at 600°C and below but unacceptable at 650 to 700°C. For some reason not understood, the corrosion seems to be much worse on commercially produced tubes than on experimental tubes.[16]

Chemical and X-ray analysis of the products of the reaction of beryllium with CO_2 showed that these are BeO and Be_2C. The weight gains of two types of beryllium tubing and beryllium powder exposed to dry CO_2 are given in the following tabulation.[2]

Specimen	Weight gain, $\mu g/cm^2$ 50 hr	500 hr
Hot-pressed tubing at 700°C	24.6	104
Hot-extruded tubing at 700°C	23.5	131
Powder (−200 + 230) at 720°C	27	88

The reaction of various types of beryllium with approximately 4 per cent water vapor in flowing helium at 550 to 600°C is shown in Fig. II-1.

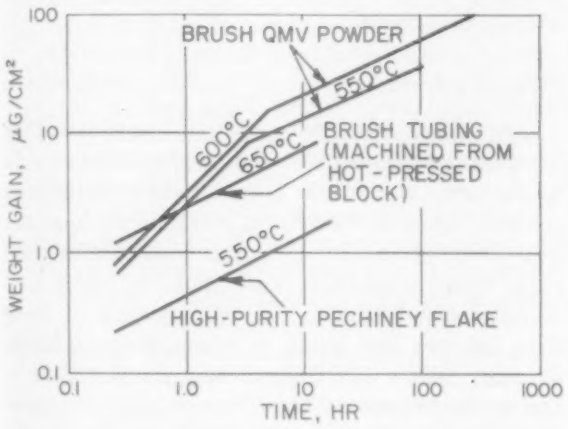

Fig. II-1 Rate curves for the reactions of various types of beryllium with ~4 per cent H_2O vapor in flowing helium.[2]

Oak Ridge reported[38] that beryllium specimens, whether from Pechiney flake or thermally reduced powder, were resistant to dry CO_2 at all temperatures between 500 and 1000°C for times up to 5000 hr, there being little difference between the samples except that the specimens made from thermally reduced powder were slightly more resistant than those from flake. Both types developed protective films. With the addition of 3 to 4 vol.% water vapor to the gas at 700°C, the product was no longer protective, and the rate of attack depended markedly upon the method used to fabricate the sample. Samples made from powder behaved similarly in either CO_2 or oxygen at 700°C. The behavior of the flake samples was different, the oxide films being no longer protective in oxygen after 500 hr.

Beryllium Bibliographies

Kinney[39] prepared a bibliography containing 491 references which provides a general survey of the unclassified literature on beryllium published between 1945 and 1960. Gex[40] furnished an annotated bibliography on electroplating on magnesium and beryllium with 109 references to the subject. (W. Hodge)

Beryllium Compounds

General Atomic researchers[41] irradiated fuel pellets composed of 19 vol.% UO_2 dispersed in a BeO matrix to an exposure of approximately 2×10^{20} fissions/cm³ at an estimated pellet temperature of 2200 to 2300°F. The UO_2 was present in the form of irregularly shaped grains of approximately 125-μ average diameter. No significant change in the dimensions of the pellets or in the lattice parameters of the BeO matrix was observed. The crushing strength of the pellets and their resistance to abrasion were reduced as a result of the irradiation.

(J. Koretzky)

Solid Hydrides

Zirconium Hydride

The heat capacities of ZrH_2 and ZrD_2 in the temperature range of 5 to 350°K were measured at Argonne.[42] Figure II-2 shows the change in heat capacity with temperature for the two materials. The heat capacity of ZrH_2 in the range of 20 to 100°K, although it is not shown on the plot, actually was about 1 per cent higher than that of ZrD_2, an amount believed to be appreciably larger than the experimental

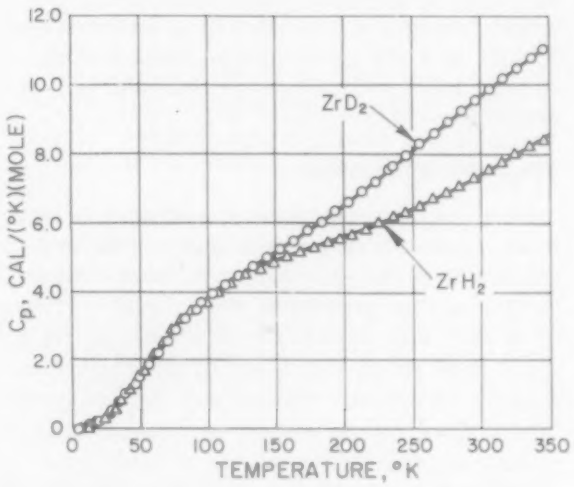

Fig. II-2 Heat capacities[42] of ZrH_2 and ZrD_2.

from a brittle intergranular mode to a mode that allows extensive ductile elongation of grains. The alteration of properties after annealing has been ascribed to purification of the matrix by precipitation of impurity. It has not been possible so far to identify either the impurities responsible for strain aging or those responsible for grain-boundary strengthening. Possibly the two effects may be caused by a redistribution after heat-treatment of the same element.[30]

Results of an extensive program of testing the mechanical properties of cross-rolled beryllium sheet were reported by Curtiss-Wright Corporation.[31] The results of extensive tensile testing of QMV beryllium from 20 to 870°C were reported by Lockheed.[32] Mechanical properties were correlated with BeO content and with microstructure. Fracture, which was transcrystalline to 480°C, was initiated by stress concentration at twin intersections, intersections of twins at grain boundaries, at $\{\bar{1}012\}$ twin-matrix interfaces, and at impurity particles, particularly carbides. Intercrystalline fractures, starting at 480°C, were characterized by void formation at grain boundaries normal to the stress axes. Voids were observed to have nucleated at carbide particles in grain boundaries and presumably at other smaller unidentified impurity particles. Boundaries of large-grain clusters free of impurities showed no intercrystalline voids, whereas the surrounding fine-grain materials that did contain impurity particles in the grain boundaries had numerous cracks and voids.

Corrosion and Irradiation Behavior of Beryllium

Beryllium tensile specimens irradiated at 350°C to fission neutron doses up to $\sim 2 \times 10^{20}$ nvt and at 600°C to fission neutron doses up to $\sim 7 \times 10^{20}$ nvt showed no changes in transverse mechanical properties. No changes in longitudinal properties of specimens irradiated at 600°C were noted. The specimens irradiated to $> 3 \times 10^{18}$ nvt at 350°C and tested below this temperature showed an increase in yield strength and some loss of ductility. Some of this damage could be annealed out by heating above 500°C before testing.[33]

The use of beryllium in a reactor may introduce two types of problems: (1) corrosion and (2) irradiation effects. The corrosion of beryllium in sodium or NaK becomes significant above 750°F. Beryllium is expected to be compatible with organic coolants of interest and most dry gas coolants up to 1100°F.

The effect of irradiation on the properties of beryllium does not become apparent until doses are in excess of 10^{20} fast neutrons/cm^2. Thereafter the main effect is the reduction of the ductility if the irradiation temperatures are low; at these temperatures the volume change is negligible. If the irradiation temperature is 600°C, doses of up to 3×10^{20} fast neutrons/cm^2 have little effect.[34]

Oak Ridge found[35] that the effect of irradiation on stress rupture of beryllium tube-burst specimens at 700°C is about the same as that observed at 600°C. For tube machined from hot-pressed block, the reduction in 100-hr rupture strength at a dose of 1.8×10^{19} fast neutrons/cm^2 (>1 Mev) is approximately 23 per cent in terms of stress.

Gregg et al.[36,37] reported on the high-temperature oxidation of beryllium in various media. The oxidation product formed in CO_2 is protective up to nearly 750°C. In CO the oxidation product is nonprotective above 550°C, the rate of oxidation being considerably greater than in CO_2. In water vapor and moist oxygen, the rate continually decreases with time to reach a very small value after about 100 hr up to nearly 650°C; above this temperature the oxidation product is no longer protective.

In a test to determine the compatibility of beryllium and uranium dioxide, UO_2 pellets were clamped to hot-rolled beryllium sheet. Although the reaction appeared to be restricted to small areas, it showed considerable penetration of the sheet even at 600°C. Further work will be required to confirm this trend and to establish what it means in terms of beryllium cans under reactor conditions.[18]

Corrosion resistance of beryllium in the British AGR reactor is reported to be satisfactory at 600°C and below but unacceptable at 650 to 700°C. For some reason not understood, the corrosion seems to be much worse on commercially produced tubes than on experimental tubes.[16]

Chemical and X-ray analysis of the products of the reaction of beryllium with CO_2 showed that these are BeO and Be_2C. The weight gains of two types of beryllium tubing and beryllium powder exposed to dry CO_2 are given in the following tabulation.[2]

Specimen	Weight gain, $\mu g/cm^2$ 50 hr	500 hr
Hot-pressed tubing at 700°C	24.6	104
Hot-extruded tubing at 700°C	23.5	131
Powder (−200 + 230) at 720°C	27	88

The reaction of various types of beryllium with approximately 4 per cent water vapor in flowing helium at 550 to 600°C is shown in Fig. II-1.

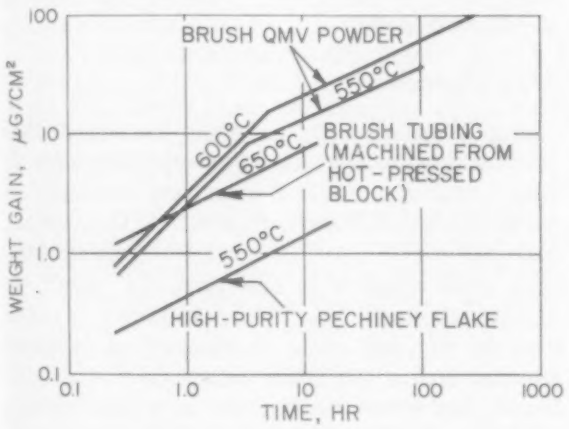

Fig. II-1 Rate curves for the reactions of various types of beryllium with ~4 per cent H_2O vapor in flowing helium.[2]

Oak Ridge reported[38] that beryllium specimens, whether from Pechiney flake or thermally reduced powder, were resistant to dry CO_2 at all temperatures between 500 and 1000°C for times up to 5000 hr, there being little difference between the samples except that the specimens made from thermally reduced powder were slightly more resistant than those from flake. Both types developed protective films. With the addition of 3 to 4 vol.% water vapor to the gas at 700°C, the product was no longer protective, and the rate of attack depended markedly upon the method used to fabricate the sample. Samples made from powder behaved similarly in either CO_2 or oxygen at 700°C. The behavior of the flake samples was different, the oxide films being no longer protective in oxygen after 500 hr.

Beryllium Bibliographies

Kinney[39] prepared a bibliography containing 491 references which provides a general survey of the unclassified literature on beryllium published between 1945 and 1960. Gex[40] furnished an annotated bibliography on electroplating on magnesium and beryllium with 109 references to the subject. (W. Hodge)

Beryllium Compounds

General Atomic researchers[41] irradiated fuel pellets composed of 19 vol.% UO_2 dispersed in a BeO matrix to an exposure of approximately 2×10^{20} fissions/cm³ at an estimated pellet temperature of 2200 to 2300°F. The UO_2 was present in the form of irregularly shaped grains of approximately 125-μ average diameter. No significant change in the dimensions of the pellets or in the lattice parameters of the BeO matrix was observed. The crushing strength of the pellets and their resistance to abrasion were reduced as a result of the irradiation. (J. Koretzky)

Solid Hydrides

Zirconium Hydride

The heat capacities of ZrH_2 and ZrD_2 in the temperature range of 5 to 350°K were measured at Argonne.[42] Figure II-2 shows the change in heat capacity with temperature for the two materials. The heat capacity of ZrH_2 in the range of 20 to 100°K, although it is not shown on the plot, actually was about 1 per cent higher than that of ZrD_2, an amount believed to be appreciably larger than the experimental

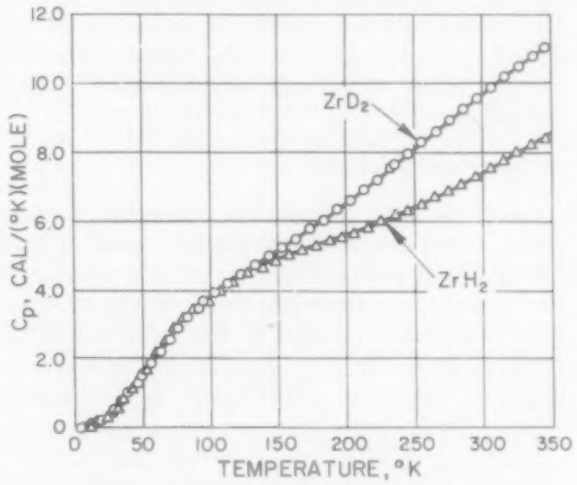

Fig. II-2 Heat capacities[42] of ZrH_2 and ZrD_2.

error. From the experimental data, thermodynamic functions were calculated, and S° was found to be 8.374 and 9.168 cal/(°K)(mole) for ZrH_2 and ZrD_2, respectively. Corresponding free energies of formation at 298°K were −30.9 and −31.2 kcal/mole, in good agreement with values reported by other authors.

Lithium Hydride

In studies performed at General Electric,[43] molten LiH was found to have negligible corrosive effect on austenitic stainless steels. Exposures lasted 65 hr at 1325°F and 100 hr at 1425°F on 19-9DL alloy sheet (Universal Cyclops), and preliminary data on the 300-series stainless steels show the same behavior. A slight decrease in ultimate tensile strength was attributed to the extended heating of the alloy because it occurred with the control samples also.

Scandium Hydride

Efforts to prepare hydrides of scandium at Los Alamos[44] have resulted in a product of the composition $ScH_{2.027}$ by reaction of the metal with hydrogen at 450°C and slightly less than 1 atm of hydrogen pressure. The dissociation pressures observed were represented by the relations:

$$\log p = 2.788 - 1137/T \text{ in the range 300 to 650°C}$$

$$\log p = 5.484 - 3632/T \text{ in the range 650 to 900°C}$$

X-ray diffraction data revealed that the material has a face-centered cubic structure, with a lattice constant $a_0 = 4.78315$ A, and a theoretical density of 2.581 g/cm^3. Under these conditions an N_H value of 7.3 can be obtained with this material.

Magnesium Hydride

Data on the magnesium-hydrogen system were reported in a joint publication of Los Alamos and the University of New Mexico.[45] Decomposition pressures were found to range from 2.31 atm at 314°C to 280.7 atm at 576°C. Table II-4* shows the values of several thermodynamic functions determined in this work.

Table II-4 THERMODYNAMIC PROPERTIES OF MAGNESIUM HYDRIDE[45]

Temp., °K	$\Delta F°$, cal/mole	$\Delta S°$, cal/mole	$\Delta H°$, cal/mole
298	−8170	−32.3	−17,790
600	+1580	−32.2	−17,830
800	+8000	−31.5	−18,350

Only the heat of formation at 298°K has been reported previously, and it is in fair agreement at −16 kcal/mole.

Alloy Hydrides

The kinetics of the eutectoid transformation of a zirconium-uranium-hydrogen alloy with an atom ratio of 1:0.03:1 have been examined at General Atomic.[46] During quenching through the eutectoid temperature, the transformation of the beta solid solution to metastable α' occurred rapidly above 450°C, being initiated in less than 10 sec and going to completion in about 30 min. Below 450°C the decomposition rate of the α' decreased rapidly. The reverse reaction of alpha zirconium and the hydride to form beta phase at 600°C was very rapid, being initiated in less than 10 sec and being 50 per cent complete in 100 sec.

The hydriding characteristics of a number of intermetallic compounds have been investigated at Denver Research Institute.[47] Three compounds (ZrV_2, HfV_2, and $ZrCr_2$) were found to have poor thermal stability, but they are particularly interesting from a theoretical standpoint because they absorb more hydrogen than does the sum of their individual components. This phenomenon is being studied further in hopes of uncovering stable materials for nuclear applications. (H. H. Krause)

References

1. D. A. Boyland and J. W. Brightwell, Improvements in or Relating to Processes for Production of Low Permeability Carbon, British Patent 857,157, Dec. 12, 1960.
2. Oak Ridge National Laboratory, Gas-Cooled Reactor Project, Quarterly Progress Report for Period Ending March 31, 1961, USAEC Report ORNL-3102, May 26, 1961.
3. J. C. Bokros, Graphite-Metal Compatibility at Elevated Temperatures, *J. Nuclear Materials*, 3(1): 89–100 (January 1961).

* Table II-4 is adapted from data published in the *Journal of the American Chemical Society*.[45]

4. S. H. Gelles, Beryllium Research and Development Program, Quarterly Progress Report for Period October 1–December 31, 1960, Report NMI-9509, Nuclear Metals, Inc., Mar. 1, 1961.
5. G. E. Spangler and M. Herman, Preparation and Evaluation of High-Purity Beryllium, Bimonthly Progress Report for January 2–March 1, 1961, Report P-A2476-2, Franklin Institute, 1961.
6. G. E. Spangler and M. Herman, Preparation and Evaluation of High-Purity Beryllium, Bimonthly Progress Report for March 2–May 1, 1961, Report P-A2476-3, Franklin Institute, 1961.
7. K. C. Taber and R. C. Harris, Beryllium Casting — Phase II, Final Report Covering Period September 19, 1958–December 15, 1960, Report NP-9958, Beryllium Corp., 1961.
8. J. W. S. Jones and J. Williams, The Preparation of Beryllium-Magnesium Alloys by Powder Metallurgical Methods, British Report AERE-M-828, January 1961.
9. K. C. Taber and E. E. Weismantel, Development of Techniques for Producing Beryllium Structural Shapes, Phase II, Second Interim Technical Report for Period October 29, 1960–January 28, 1961, Report NP-9911, Beryllium Corp., 1961.
10. Northrop Corporation, Norair Division, Development of Extruded Beryllium Shapes, Interim Engineering Report No. 11 for Period December 1, 1960, Through February 28, 1961, Report NOR-61-66, 1961.
11. A. R. Stetson and C. A. Hauck, Plasma Techniques for Spraying Toxic and Oxidizable Materials, paper presented at AIME Symposium on Plasma Arc Applications to Metallurgy, The Western Metal Conference, Mar. 23, 1961.
12. F. M. Yans et al., Development of Randomly Oriented Wrought Beryllium Sheet, Report WADD-TR-60-403, Nuclear Metals, Inc., Sept. 8, 1960.
13. A. J. Martin et al., The Forming of Hollow Shapes in Beryllium by Loose Sintering and Hollow Pressing, *Powder Met.*, No. 7: 268–282 (1961).
14. E. B. Lympany et al., Investigation and Development of Methods for Producing High-Porosity Beryllium Bodies, Final Technical Report No. 164, Report SCR-302, Brush Beryllium Co., January 1960.
15. Drilling and Reaming Beryllium, *Metalworking Production*, 105: 52–53(Apr. 5, 1961).
16. General Nuclear Engineering Corp., Gas-Cooled Reactor Project, Progress Report No. 8 for the Period September 1, 1960, to February 28, 1961, Report GNEC-164 (Del.), Mar. 15, 1961.
17. Lockheed Aircraft Corp., Structural Design Data for Beryllium, Progress Report for February 1961, Report LMSD-312201-13, Mar. 1, 1961.
18. A. G. Knapton and K. B. C. West, The Compatibility of Beryllium and Uranium Dioxide, *J. Nuclear Materials*, 3(2): 239–240 (1961).
19. Nuclear Metals, Inc., Fundamental and Applied Research and Development in Metallurgy, Progress Report for October 1960, USAEC Report NMI-2090, Nov. 21, 1960.
20. Nuclear Metals, Inc., Fundamental and Applied Research and Development in Metallurgy, Progress Report for December 1960, USAEC Report NMI-2092, Feb. 7, 1961.
21. D. E. Sands et al., The Beryllium-Boron System, *Acta Cryst.*, 14: 309–310 (Mar. 10, 1961).
22. V. N. Bulanov and I. N. Frantsevich, Investigations of Rhenium-Beryllium Alloys (in Russian), *Voprosy Poroshkovoi Met. i Prochnosti Materialov, Akad. Nauk Ukr. S.S.R.*, 6: 32–35 (1958).
23. Denver Research Institute, Study of Ceramic and Intermetallic Materials, Progress Report No. 11, USAEC Report XDC-61-2-2 (also TID-11847), Nov. 1, 1960. (Classified)
24. J. J. Trillat et al., Oxidation and Carburization of Thin Aluminum and Beryllium Films (in French), *Mém. sci. rev. mét.*, 57: 845–851 (November 1960).
25. N. A. Hill and J. W. S. Jones, The Crystallographic Dependence of Low Load Indentation Hardness in Beryllium, *J. Nuclear Materials*, 3(1): 138–155 (February 1961).
26. R. Thomson et al., Hot Hardness Testing Applied to the Aging and Heat-Treatment of Beryllium, *J. Less-Common Metals*, 3(2): 170–178 (April 1961).
27. G. C. Lazarev et al., Superconductivity [of Thin Films] of Beryllium and Its Low Temperature Polymorphism (a letter, in Russian), *Zhur. Eksp. i Teoret. Fiz.*, 37(5): 1461–1463(1959).
28. Lockheed Aircraft Corp., Structural Design Data for Beryllium, Progress Report for January 1961, Report LMSD-312201-12, Feb. 1, 1961.
29. M. V. Ward et al., Effect of Surface Finish on the Properties of Beryllium Sheet, *Trans. Am. Soc. Metals*, 54: 84–95 (March 1961).
30. A. B. Brown et al., The Effect of Strain Rate and Heat-Treatment on the Tensile Properties of Extruded Beryllium Rods Between 25 and 600°C, *J. Less-Common Metals*, 3(1): 62–68 (February 1961).
31. Curtiss-Wright Corporation, The Tensile, Notched Tensile, and Tensile Impact Properties of Cross-Rolled–100 Mesh QMV Beryllium Sheet, Progress Report No. 1, Report MEDA-D-848, Sept. 13, 1960.
32. M. I. Jacobson and F. M. Almeter, Tensile Properties of QMV Beryllium from Room Temperature to 870°C, Report LMSD-895083, Lockheed Aircraft Corp., March 1961.
33. J. B. Rich and G. P. Walters, The Mechanical Properties of Beryllium Irradiated at Various Temperatures, British Report AERE-R-3684, March 1961.
34. R. S. Barnes, The Effect of Neutron Irradiation on Beryllium, *Nuclear Eng.*, 6: 149–150 (April 1961).
35. Oak Ridge National Laboratory, May 4, 1961. (Unpublished)

36. S. J. Gregg et al., The High-Temperature Oxidation of Beryllium. Part III. In Carbon Dioxide, Carbon Monoxide, and Carbon Monoxide-Carbon Dioxide Mixtures, *J. Nuclear Materials*, 3(2): 175–189 (1961).
37. D. W. Aylmore et al., The High-Temperature Oxidation of Beryllium. Part IV. In Water Vapor and in Moist Oxygen, *J. Nuclear Materials*, 3(2): 190–200 (1961).
38. Oak Ridge National Laboratory, Proceedings of the U.S./U.K. Meeting on the Compatibility Problems of Gas-Cooled Reactors, held at Oak Ridge National Laboratory on February 24–26, 1960, USAEC Report TID-7597(Bk. 2), Mar. 3, 1961.
39. M. Kinney, A Selected Guide to Beryllium Literature, ASTIA Report AD-253352, Autonetics Division of North American Aviation, Inc., Mar. 16, 1961.
40. R. C. Gex (Comp.), Electroplating on Magnesium and Beryllium—An Annotated Bibliography, Special Bibliography SB-61-4, Report NP-9987, Lockheed Aircraft Corp., February 1961.
41. D. E. Johnson, Stability of BeO-UO_2 Reactor Fuel Material During Irradiation; Maritime Gas-Cooled Reactor Program, USAEC Report GA-2065, General Atomic Div., General Dynamics Corp., Mar. 31, 1961.
42. H. E. Flotow and D. W. Osborne, Heat Capacities and Thermodynamic Functions of ZrH_2 and ZrD_2 from 5 to 350°K, and the Hydrogen Vibration Frequency in ZrH_2, *J. Chem. Phys.*, 34: 1418–1425 (April 1961).
43. F. H. Welch, Properties of Lithium Hydride II: Lithium Hydride Corrosion Studies, 19-9DL Alloy, USAEC Report APEX-586, General Electric Co., Aircraft Nuclear Propulsion Dept., Apr. 10, 1961.
44. J. C. McGuire and C. P. Kempter, Preparation and Properties of Scandium Dihydride, *J. Chem. Phys.*, 33: 1584–1585 (November 1960).
45. J. F. Stampfer et al., The Magnesium-Hydrogen System, *J. Am. Chem. Soc.*, 82(14): 3504–3508 (1960).
46. J. C. Bokros, Transformation Kinetics of a Zirconium-Hydrogen Alloy, *J. Nuclear Materials*, 3(3): 320–326 (March–April 1961).
47. R. L. Beck, Investigation of Hydriding Characteristics of Intermetallic Compounds, USAEC Report LAR-52, Denver Research Institute, Feb. 14, 1961.

Section III

NUCLEAR POISONS

Metallic Poison Materials

Rare Earths

Results of fabrication studies at Knolls[1] indicate that erbium, gadolinium, and samarium could be hot worked using standard techniques for the fabrication of reactive metals. It was possible to cold-work these metals about 10 per cent before cracking began. Europium was found to be amenable to an unlimited degree of cold work, whereas dysprosium could be cold worked 38 per cent before annealing became necessary.

Boron

Data obtained by Armour[2] in an investigation of the boron-carbon system indicate that a boron carbide exists over a solubility range of approximately 10 to 20 at.% carbon at 1500 to 2000°C. A carbide-graphite eutectic was found to occur at 30 at.% carbon in the temperature range of 2325 to 2350°C. Solubility of carbon in boron was found to be very small.

(V. W. Storhok)

Dispersion Control Materials

General Electric[3] has issued a report that summarizes data from various laboratories engaged in work for the AEC on boron carbide as a control and poison material. Data on physical and mechanical properties, compatibility, and irradiation are included. Most of the data were published previously, but the report provides a compilation of much of the latest data on boron carbide. One problem has been noted which is not generally reported, namely, large amounts of hydrogen can be released during irradiation. In most cases this hydrogen stems from the sorption of hydrogen by boron carbide at some stage of the processing.

The same laboratory has studied the metallography of the borides,[4] and it is reported that most borides can be prepared by grinding with diamond wheels and polishing with a fine diamond compound. Etching of most borides can be accomplished with a mixture of 20 ml of water, 15 ml of HF, and 10 ml of HNO_3.

The effects of radiation upon the structure of hafnium diboride powders have been studied at Battelle.[5] One sample contained an enriched boron of about 55.6 wt.% B^{10}, and the second sample was made with natural boron (18.3 wt.% B^{10}). Both specimens showed a complete loss of crystallinity after irradiation. The enriched boride was irradiated to a 23.2 per cent B^{10} burnup, and the natural boride was irradiated to a 51.5 per cent B^{10} burnup as determined by lithium analysis. Irradiation temperatures varied from 400 to 625°F.

General Atomic[6] is investigating dispersions of boron carbide in graphite as a possible control material for the High-Temperature Gas-Cooled Reactor (HTGR). After an irradiation at 1200°F at about one-third the exposure lifetime of an HTGR control rod, it was reported that dimensional changes were no more than would be expected for graphite after a similar exposure.

(G. W. Cunningham)

References

1. G. I. Friedman, The Fabrication of Five Rare-Earth Metals. The Mechanical Conversion of Samarium, Europium, Gadolinium, Dysprosium, and Erbium to Sheet, USAEC Report KAPL-M-GIF-2, Knolls Atomic Power Laboratory, Dec. 15, 1960.
2. R. P. Elliott, The Boron-Carbon System, Quarterly Report No. 3 for November 1, 1960–January 31,

1961, USAEC Report ARF-2200-9, Armour Research Foundation, Feb. 6, 1961.
3. E. W. Hoyt, Information on the Use of Boron Carbide as a Nuclear Control and Poison Material, USAEC Report GEAP-3680, General Electric Co., Vallecitos Atomic Laboratory, Mar. 15, 1961.
4. D. R. Lewis, Metallography of the Borides, USAEC Report GEAP-3626, General Electric Co., Vallecitos Atomic Laboratory, Jan. 9, 1961.
5. R. A. Ewing and D. N. Sunderman, Effects of Radiation upon Boron Carbide, USAEC Report BMI-1521, Battelle Memorial Institute, June 14, 1961.
6. General Atomic Division, General Dynamics Corp., 40 Mw(e) Prototype High-Temperature Gas-Cooled Reactor Research and Development Program, Quarterly Progress Report for the Period Ending September 30, 1960, USAEC Report GA-1774, April 1961.

Section IV

CLADDING AND STRUCTURAL MATERIALS

Corrosion

Zirconium Corrosion

Hydrogen absorption by Zircaloy-2 and related alloys has been studied in the United Kingdom.[1] The data indicate that the mechanism of absorption changes during exposure to steam at 1-atm pressure and at 300 to 600°C. During the growth of the interference-color oxide film, as much as 50 per cent of the hydrogen released by corrosion is absorbed. It is postulated that, during this period, transport of OH ions through the oxide film, under the influence of an electric field, accounts for the entry of hydrogen.

From the time the interference colors disappear until transition, little hydrogen is absorbed. This is believed to be due to the release of hydrogen atoms at surface sites where they recombine to form molecular hydrogen faster than they can diffuse through the oxide film.

After transition, hydrogen absorption is again high, since it is released at the bottom of pores or breaks in the oxide film rather than on the outer surface, thus increasing the chance of diffusion into the metal before molecular hydrogen is formed and released.

Experiments are being conducted at Hanford Atomic Products Operation (HAPO)[2] to test the hypothesis that the oxygen content of the water may influence hydrogen pickup in Zircaloy-2 and -4. Studies conducted in water at 400°C revealed that hydrogen pickup is higher for deoxygenated water than for that containing 3 to 4 ppm oxygen. Zircaloy-2 picked up about twice as much hydrogen in refreshed deoxygenated water as it did in an oxygenated system.

(W. K. Boyd)

Aluminum Corrosion

The possible use of aluminum for the cladding of free-standing oxide pellet fuel in the Experimental Boiling-Water Reactor (EBWR) is being studied at Argonne National Laboratory (ANL).[3] Samples of Alcoa's impact-extruded tubing, made from A-288 (1 wt.% nickel–0.5 wt.% iron–0.10 wt.% titanium as atomized powder), have been corrosion tested for 120 days in 290 and 360°C water. Rates were 1.2 and 0.5 mils/year, respectively, which is equivalent to the rates for the wrought product. The powder products, however, show a tendency to blister during corrosion testing, especially at 260°C.

Metal growth during corrosion tests has been observed at Hanford[4] for aluminum alloys. Owing to compressive stresses developed in the oxide films formed in 360°C deionized water, it was found that X-8001 aluminum samples grow both in length and width. Studies to determine the magnitude of the stresses developed are being conducted for both aluminum- and zirconium-base materials.

Some of the factors that affect the corrosion rate of aluminum alloys have been studied in the United Kingdom.[5] The investigation covered (1) the relative corrosion behavior of various alloys, (2) couple tests with stainless steel, (3) placement in autoclave, (4) temperature change in the system, and (5) prefilming under static conditions before dynamic exposure. In general, the effect of most of the variables was small. However, prefilming in 325°C water was found to reduce corrosion rates by a factor of 3 to 4 in dynamic systems for at least 7 weeks of exposure.

In studies at Argonne,[6] the corrosion behavior of pure aluminum and some of its alloys in superheated steam (400 to 540°C, 150 to 600

psig) was found to depend markedly on the technique employed during startup of the corrosion test. For example, unalloyed aluminum specimens survived only those tests in which the system was brought rapidly to operating temperature and pressure. On the other hand, aluminum-nickel-iron alloys were resistant only if a slow startup procedure was employed; they blistered and disintegrated completely in a test using a rapid startup. (W. K. Boyd)

Corrosion of Stainless Steels

The corrosion behavior of types 304L and 347 stainless steel in neutralized zirconium–hydrofluoric acid waste and in aluminum nitrate waste neutralized with paraformaldehyde has been determined by Phillips Petroleum Co.[7] After 6 months' exposure at 60°C, corrosion rates of both materials ranged from 0.0002 to 0.005 mil/month in the aluminum waste neutralized with paraformaldehyde and 0.09 to 0.12 mil/month in the neutralized zirconium waste. These low rates and the absence of pitting attack suggest that either alloy would be a suitable storage-tank material.

At Hanford,[8] two-year tests in 360°C deionized water have shown type 446 stainless steel to be the best alloy for service in the water system for the Plutonium Recycle Test Reactor. Types 316, 347, and 304 stainless steels evinced corrosion rates about five times that noted for type 446. However, penetration for the worst alloys was only of the order of 0.01 mil in the two-year period, based on weight loss of stripped corrosion coupons.
(W. K. Boyd)

Niobium Oxidation

Studies at Oak Ridge National Laboratory (ORNL)[9] have shown that niobium alloys, which are quite oxidation resistant at atmospheric pressure, generally oxidize faster than unalloyed niobium at 5×10^{-4} mm oxygen pressure. However, the low-pressure oxidation resistance of niobium at 1000°C is improved by additions of 0.5 to 1 wt.% of elements forming highly stable oxides, such as aluminum and zirconium. Elements such as molybdenum or tungsten, with oxides that are less stable than Nb_2O_5, have little effect on the low-pressure oxidation behavior. Thus new niobium alloys may be required for long-time service in semiprotective atmospheres, such as argon containing traces of oxidizing gases.

Additional studies at Oak Ridge[10] indicate that internal oxidation of niobium becomes serious at very low pressures. At 850°C, under oxygen pressures of 5×10^{-5} to 5×10^{-4} mm, oxygen diffuses into niobium and forms Nb_2O along grain boundaries. These internal oxides grow and erupt at the surfaces, forming NbO and traces of Nb_2O_5. At 850°C, the oxidation rates of niobium in 1×10^{-4} mm oxygen and 760 mm air are about 0.3 and 40 mg/(cm^2)(hr), respectively.

Protective coatings for niobium are under development at Boeing Airplane Co., Chance Vought Aircraft, Inc., Pfaudler Co., and Thompson Ramo Wooldridge Inc., according to recent information from the Defense Metals Information Center.[11] These are primarily silicide-base coatings modified with additions including aluminum, chromium, boron, and titanium. The protective life of these coatings is on the order of 10 hr at 2700°F (1480°C) and 1 hr at 3000°F (1650°C).

Molybdenum Coatings

Recent studies on molybdenum have been concerned with the development of protective coatings.[11] These coatings, like those for niobium, are primarily silicide base. The coatings also exhibit the same order of protectiveness to molybdenum as quoted above for niobium.

Superior protection for molybdenum is afforded by a coating developed by American Machine and Foundry.[12] This coating, which contains silicon and is applied by the pack-cementation method, protects molybdenum for 8 hr at 3200°F (1760°C) and 45 min at 4200°F (2320°C). The coating also is partly self-healing.
(W. D. Klopp)

Corrosion of Base-Metal Alloys (Iron, Nickel, Cobalt, Chromium)

Additional corrosion tests on Hastelloy X (regular and modified) and Inconel 702 as cladding materials for a gas-cooled reactor were continued at Aerojet-General.[13] Exposures to the 300-psi, 1750°F, nitrogen–0.5 wt.% oxygen reference environment were continued. Further observations of the loss of ductility after 2500 hr in the reference gas, nitrogen, nitrogen–0.1 wt.% CO, and air have been

made.[14,15] The results of heat-treatment studies suggest that metallurgical instability during service may be the chief contributor to the loss of ductility, rather than corrosion.[16] If so, the degradation in properties can probably be controlled.

The French report stress-corrosion cracking in Inconel in static 660°F water containing about 0.15 ml of dissolved oxygen per liter.[17] Exposure times were four to five days. Similar behavior was observed for 17-4-PH steel at Bettis after six days in static 600°F water containing 5 to 10 ppm oxygen. Static degassed water (< 0.06 ppm oxygen) did not promote stress-corrosion cracking in over 500 hr. Realistic environmental tests,[18] simulating Pressurized-Water Reactor (PWR) startup and operation, revealed no stress-corrosion cracking in 17-4-PH steel in 500 hr. It thus appears that both oxygenation and stagnation contribute (and perhaps are essential) to stress-corrosion cracking.

Continued work at ANL[19] showed that, for certain low-alloy steels, the dissolved oxygen required to attain desirably low oxidation rates in pressurized hot water can be decreased relative to that required for iron (see *Reactor Core Materials*, Vol. 4, No. 2, pages 33 and 34). Additional investigations were recommended.

Magnesium Corrosion

French work[20] has demonstrated that the temperature to which magnesium retains oxidation resistance in moist air can be raised from 660 to 915°F by promoting the formation of a fluoride film on the surface of the magnesium. This film can be formed by treatment in HNO_3-HF acid (4 and 2 vol.% of commercial acids, respectively, in water) prior to exposure, or by the addition of as little as 0.003 mg/liter (at 1-atm pressure) of HF to the corrosive environment. Inhibition is reported to be effective for several thousand hours. This finding is in general agreement with work done at ANL (*Reactor Core Materials*, Vol. 4, No. 1, page 44).

(E. S. Bartlett)

Corrosion by Liquid Metals and Fused Salts

In a program at Rocketdyne Division of North American Aviation, the compatibility of potentially useful containment materials with elevated-temperature potassium is being investigated. A variety of capsule corrosion experiments have been run, and large-scale flow-loop corrosion systems are in the design and construction stage.[21] Experiments with Hastelloy X capsules containing inserts of niobium and niobium–1 wt.% zirconium alloy, which were operated at temperatures up to 2000°F and for periods up to about 350 hr, demonstrated that, above 1450°F, the refractory-metal specimens lose weight and develop surface coatings of niobium carbide and nitride. The effects are pronounced enough to lead to a recommendation against potassium pumping loops incorporating a nickel alloy–refractory metal combination. All-refractory-metal (niobium-zirconium alloy) capsule experiments were also conducted. The observed specimen weight changes were quite low at a temperature as high as 2200°F for a period as long as 140 hr. No attempt was made in any of the experiments to purify the test potassium; the possibility was advanced that the minor corrosion effects observed in the all-refractory-metal cases could be attributed to trace amounts of oxygen.

Investigations at Atomics International resulted in information along the following lines:

1. Coatings and coating techniques were investigated as a means of preventing the decrepitation of graphite in high-temperature sodium.[22] The coatings examined included chromium, nickel, zirconium, zirconium carbide, tungsten carbide, silicon carbide, silicon nitride, and molybdenum disilicide. None gave satisfactory protection during 1000°F exposures. In all cases the failure stemmed from porosity or cracks in the coating materials.

2. In experiments designed to evaluate nitrogen as a cover-gas substitute for helium in sodium systems, it was found[23] that, at 1000°F, type 304 stainless steel will nitride rapidly, particularly in zones just below the sodium-nitrogen interface. The degree of nitriding observed will produce increased yield strength accompanied by decreased ultimate strength and decreased ductility.

Recent information reported by Oak Ridge in connection with the Molten Salt Reactor Program includes the following:

1. A pumping-loop experiment was conducted[24] to examine the compatibility of INOR-8 and graphite (low-permeation National Carbon grade CT-1-23-82, 82.4 per cent of the theoretical density) with molten fluoride (LiF-BeF_2-UF_4) salt circulating at a peak tempera-

Table IV-1 ATTACK AND CONCENTRATION DATA FOR TYPE 347 STAINLESS STEEL IN LITHIUM[26]

Element	Attack rate* (removal of source metal) in lithium, $\mu g/(cm^2)(month)$		
	825°C	625°C	425°C
Iron	1922	5.8	1.0
Nickel	70	6.0	0.07
Manganese	62	2.3	0.09
Cobalt	4.1	0.1	0.002
Tantalum	0.24	0.007	0.006
Zinc	0.24		
Silver	0.17	0.0028	7×10^{-4}
Tin	8×10^{-3}	6.0×10^{-4}	$<3 \times 10^{-5}$
	Equilibrium concentration in lithium, $\mu g/g$ of lithium		
Element	825°C	625°C	425°C
Iron	0.31	0.037	0.15
Nickel	20		0.071
Manganese	56	3.1	0.094
Cobalt	6.9×10^{-3}	1.5×10^{-4}	1.6×10^{-4}
Tantalum	0.61	5.8×10^{-3}	0.027
Zinc	0.99	6.0×10^{-4}	0.026
Silver	0.69	0.012	2.6×10^{-3}
Tin	0.017	1.2×10^{-3}	1.2×10^{-4}

* 30-day isothermal exposures; metal removal determined by radiotracers.

Table IV-2 SOLUBILITY DATA FOR NICKEL IN SODIUM[27]

Temp., °C	Solubility, 10^{-3} $\mu g/g$ of sodium	Sodium purity, wt.% oxygen
200	5	0.005
300	6	0.004
350	6	0.003
400	4	0.004
500	9	0.002
600	12	0.003

ture of 1200°F. After 8850 hr of operation, there was no evidence of appreciable corrosion or carburization of the INOR-8, and very little permeation of the graphite.

2. A variety of data are presented[25] from continuing studies of the chemistry of fluoride salts. These cover (*a*) phase equilibria for and solubilities of HF and BF_3 in several salt mixtures, (*b*) oxide behavior in selected mixtures, (*c*) density and viscosity characteristics and characteristics relating to the wetting of graphites, and (*d*) analytical chemistry procedures.

A continuing study of the attack of structural materials by liquid metals is in force at the Naval Research Laboratory. The concentration and transport of type 347 stainless steel in isothermal lithium were investigated[26] by use of radiotracer techniques. Data established from one-month exposures are presented in Table IV-1. The solubility of nickel in sodium has also been investigated.[27] Data are given in Table IV-2; equilibrium in this system appears to be established within 2 hr. (J. H. Stang)

Metal-Water Reactions

Vallecitos Atomic Laboratory[28] recently published some "speculations" regarding the fast, potentially hazardous, chemical reaction between a metal and water which might occur in a nuclear reactor. It is believed that this can occur only above the melting point of the metal, T_m. There is a critical temperature, $\theta > T_m$, at which the process changes over from the slow corrosionlike reaction to one that proceeds with explosive speed and violence. For the alkali metals, θ is only slightly greater than T_m. The critical temperature θ has been experimentally determined for three high-melting-point metals, aluminum, zirconium, and uranium; it is shown that θ is approximately equal to the temperature at which the metal vapor pressure is 0.15 mm for these cases. This relation suggests that the initiation of the violent metal-water reaction for refractory metals may be a vapor-phase phenomenon. On the basis of this hypothesis, and the empirical correlations developed, predictions of the value of θ are presented for a number of other metals for which experimental data are not presently available. Table IV-3 gives these predictions for many metals and compares them with experimental data where available.

A bibliography of literature concerned with various aspects of research performed for the Atomic Energy Commission on metal-water reactions has recently been published by Knolls Atomic Power Laboratory (KAPL).[29]

(A. W. Lemmon, Jr.)

Radiation Effects in Nonfuel Materials

Defects: Structure and Properties

Metals. Focusing collisions in platinum[30] are used to explain the preferential formation

of defects at coherent twin boundaries. Damage is produced from fission recoils with concentrations up to $2.5 \times 10^{10}/cm^2$ and observed in thin foils with transmission electron microscopy. Primary collisions on either side of the twin boundary will cause focusing in the $\langle 1\,1\,0 \rangle$ direction, for example. As the boundary is crossed, this direction becomes a $\langle 1\,1\,4 \rangle$, which is a nonfocusing direction; hence defects will be produced. The defects so produced can be annealed out of the foils at about 400 to 500°C. This recovery corresponds to a vacancy migra-

Table IV-3 CRITICAL METAL-WATER REACTION TEMPERATURES[28]

Metal	Melting point of metal (T_m), °K	1.03 T_m	Melting point of oxide, °K	Boiling point of metal at 0.15 mm, °K	Observed critical reaction temp. (θ), °K
Lithium	453.7	467		1089	473
Sodium	370.5	382		635	383
Potassium	336.4	346		539	342
Rubidium	312.1	321			
Cesium	301.8	311			
Freon	300	309			
Beryllium	1556	1603	2803	1649	
Magnesium	923	951	3073	812	
Calcium	1123	1157	2853	983	
Strontium	1043	1074	2703	917	
Barium	983	1012	2196	1019	
Aluminum	931.7	960	2288	1423	1443
Boron	2300	2369	723	1843	
Iron	1812	1866	1693	1890	
Chromium	2176	2241	2263	1833	
Nickel	1725	1777	2263	1912	
Cobalt	1768	1821	2073	2075	
Manganese	1512	1563	1923	1426	
Titanium	1940	1998	2103	2216	
Zirconium	2130	2194	2950	2983	2873
Hafnium	2495	2570	3083	2938	
Uranium	1406	1448	3033	2477	2473
Plutonium	912.7	940	2568	2017	
Thorium	1968	2017	3323	2969	
Zinc	692.7	713	2253	693	
Cadmium	594	612		603	
Indium	429.3	442		1380	
Gallium	303	312	2013	1519	
Tellurium	577	594		996	
Silicon	1685	1736	1983	1884	
Vanadium	2190	2256	1818	2344	
Cerium	1077	1109	1963	1887	
Ytterbium	1097	1130		988	
Europium	1099	1132	2323	1075	
Lanthanum	1193	1229		2324	
Praseodymium	1208	1244		1926	
Neodymium	1297	1336		1842	
Samarium	1325	1365	2573	1208	
Gadolinium	1623	1672	2603	1849	
Terbium	1723	1775		1762	
Dysprosium	1760	1813	2613	1581	
Erbium	1773	1826		1644	
Holmium	1773	1826		1708	
Thulium	1798	1852		1167	
Yttrium	1820	1875	2953	1942	
Lutetium	1973	2032		2036	

tion. Wehner et al.[31,32] have expanded their studies of surface bombardment by <1-kev ions. Preferred directions of ejection are observed for the atoms sputtered from the single-crystal surfaces. These preferred directions are the close-packed directions and serve as strong evidence to support the concept of a momentum transfer process in sputtering. The first of their reports[31] discussed Hg^+ bombardment of copper, nickel, gold, iron, and germanium, in which germanium was found to act more like the body-centered cubic (bcc) materials. The second paper[33] expanded the studies to include bombardment with Ne^+ and Ar^+ and added molybdenum, vanadium, tungsten, titanium, silicon, and α brass as targets. The bcc patterns show a fine structure characteristic of each material. Bombardment of germanium and silicon produces interstitials, which implies a transformation from the diamond to a more bcc structure. At these energies the phenomena observed are surface effects, and focusing chains are a few atoms long. Sputtering yields[33] are about 0.2 atom/ion. Another group has reported[34] the effects of obliquely incident ion bombardment.

Gold wires, 0.008 in. in diameter with 99.999 per cent purity, were irradiated[35] with electrons from a 2.5-Mev Van de Graaff at 10.5 and 13°K. Imperfection annealing was studied by measuring the electrical resistance at temperatures up to 260°K. Activation energies for the various processes range from 0.037 ev at the lower temperatures to 0.13 ev. First-order kinetics are assumed for these calculations. Differences between gold and copper annealing, in terms of absence of some stages of annealing, are explained by assuming that, in gold, clustering of interstitials predominates over recombination once the defects start to move. Resistivity increase per atomic per cent of Frenkel pairs in gold is reported to exceed 2.8×10^{-8} ohm-cm. Pervakov and Khotkevich[36] observed that the energy for the formation of vacancies in quenched gold was 19 kcal/g-atom. Calorimetric techniques were used during the vacancy annealing.

Anisotropic growth (elongation in the $\langle 11\bar{2}0 \rangle$ direction) produced by fission-fragment damage has been observed[37] in zinc, zirconium, titanium, and cadmium at −196°C and in zirconium and titanium at 75°C. No growth of anisotropy has been detected in beryllium, magnesium, or the cubic metals. Growth rates at −196°C decrease with decreasing atomic mass from $G \approx 70$ for cadmium to $G \approx 15$ for titanium. Previous theories of irradiation growth have been unable to explain these results. The dependence of growth rate on atomic mass suggests a mechanism depending on the generation of widely separated groups of vacancies and interstitials in displacement spikes. It is shown that the stresses available are sufficient to overcome the anisotropy of dislocation-loop energy and force vacancies and interstitials to condense on different planes, which results in an anisotropic shape change. Elongation due to interstitial clusters is in the direction of minimum thermal expansion, whereas the elongation due to vacancy clusters is in the direction of maximum expansion. It is also suggested that an observed disappearance of a temperature-dependent growth rate above self-diffusion temperatures is a manifestation of thermal annealing of the defect clusters.

Seeger et al.[38] reported on annealing experiments in polycrystalline nickel wires that were drawn at room temperature. By the use of techniques of internal friction and the variation of initial ferromagnetic susceptibility, they were able to conclude that stage III annealing in copper is due to monointerstitial migration, as opposed to a process involving diinterstitials. The same conclusions are drawn from the results of Kronmuller.[39] Increased dislocation densities due to neutron irradiation at 30°C have been observed by means of the change in thermal conductivity in superconducting niobium and vanadium crystals.[40] Increase in vacancy concentration is studied by electrical measurements in the normal state. Clarebrough et al.[41] have observed an impurity effect in the annealing of cold-worked nickel. The results indicate that recovery processes involving dislocations that operate in 99.6 per cent purity nickel at temperatures below recrystallization are completely inoperative and hence absent in the recovery of the 99.85 per cent purity material.

Changes in density, X-ray lattice parameter, and line breadth due to doses of 1.4×10^{20} neutrons/cm^2 (fast) at 50°C have been investigated in aluminum, copper, palladium, gold, platinum, iron, molybdenum, tungsten, and zirconium.[42] Only zirconium and molybdenum showed a measurable increase in lattice parameter, indicating interstitial formation. In zirconium, from the increases observed in the

a and c directions, the conclusion was drawn that the interstitials form platelets in the plane containing the c axis. The molybdenum increases are somewhat less than those reported by Gray and Cummings,[43] but they are explained in terms of impurity contents. Significant line broadening in copper, gold, and platinum indicates that stable interstitials or vacancy clusters have probably formed which produce isotropic strains. Relation of the observed data to other experiments is discussed in detail; however, it is presently impossible to isolate particular defect structures in any of these metals other than those specifically discussed. Nickel crystals have been irradiated with 3-Mev electrons from a Van de Graaff generator and studied with the Kossel line technique.[44] Lattice parameters and X-ray line widths are reported for doses of 10^{16}, 10^{17}, and 10^{18} electrons/cm^2 at liquid-nitrogen temperatures. All defects are annealed by heating to 400°C. At room temperature the defects are Frenkel pairs associated with impurities or other sinks. Lattice constants are reported in some cases to one part in 300,000.

Makin et al.[45] have used interstitial loops to explain their observations of dislocation-loop formation in copper irradiated at −195°C. Foils 0.001 in. thick were neutron-irradiated to 3.1×10^{17} fast neutrons/cm^2 and transferred cold to an electron microscope for observations at −50°C. The observed loops formed below this temperature must be due to interstitials since the vacancies are not mobile even at −50°C. This conclusion is also supported by other experimenters. Some of the temperature dependence of lattice hardening due to irradiation can be explained by the use of loops; however, the authors point out that loops are not the sole cause of the hardening. Loop size is also considered in terms of formation due to increase in dose and its effect on the hardening. Greenfield and Wilsdorf[46] have reported further on their extensive studies of neutron effects in the plastic deformation of copper. Plastic deformation has been observed[47] to greatly enhance the annealing of gold quenched from 700°C. Activation energies are 0.82 ev before deformation and 0.64 ± 0.03 ev after deformation. This change is explained by supposing that the vacancies prefer to exist as divacancies near dislocations.

Hanford reports further studies on fission damage in thin metal films.[48] They report that the damage as observed by transmission electron microscopy is a function of the distance between the fission-fragments path and the free surface of the metal film and is not subject to contrast effects produced by different thicknesses of the metals used. Platinum, palladium, and germanium show different effects and have different fission-fragment-scattering powers. Aluminum foils (1000 A) with larger grain sizes show tracks due to decrease in effective electron-scattering power in the grains. This is probably due to the uniform diffraction of electrons in the large grains, giving rise to considerably different contrast effects.

Hanford also reports lattice-constant measurements in high-purity aluminum foils.[48] Values of a_0 were obtained from d-spacing measurements for four high-angle lines (331, 420, 422, and 333).

Annealed preirradiation a_0 = 4.04860 A
Annealed irradiated 10^{18} nvt (fast) a_0 = 4.04900 A
Annealed irradiated 10^{19} nvt (fast) a_0 = 4.04900 A
Cold-worked, preirradiation a_0 = 4.04882 A
Cold-worked, irradiated 10^{19} nvt (foil) a_0 = 4.04902 A
All values to ± 0.00005 A

Line broadening was very slight.

Defects in Metal Alloys. The trapping of vacancies by solute atoms in a neutron-irradiated aluminum−5 wt.% magnesium alloy has been studied by Nilson.[49] Low-frequency internal-friction data were used in studying the shift of a damping peak (~150°C) to lower temperatures. This shift results from a reduction in relaxation time for the damping process as the vacancy concentration increases and trapping occurs.

Carbon precipitation in α-iron was studied by Hull and Mogford[50] by means of transmission-electron microscopy. At 100°C the carbon precipitates into platelets that grow in size to about 400 A (diameter) after 72 hr in a flux of 1.5×10^{11} neutrons/(cm^2)(sec) >1 Mev. The plates along {0 0 1} planes are described as a monatomic layer of carbon in the 0, 0, and ½ interstitial sites. Annealing experiments revealed that the plates were replaced by needle-shaped particles at about 250°C.

Helium is found to precipitate along dislocations in an aluminum−0.1 wt.% lithium alloy.[51] The helium was formed from the Li^6 transmutations during an irradiation of 220 hr at 10^{13} nv and at a temperature of 60°C. Etching indicated that the precipitates form continuous

or semicontinuous cylindrical cavities along the dislocations.

Batenin[52] has extended his work[53] on neutron damage in metals and alloys up to doses of 10^{21} neutrons/cm^2. X-ray line half-widths increased by 20 for copper and iron but showed little change for the iron alloys studied. This increased line width is explained in terms of reduction of the size of the region of coherent scattering and the increase in microstress. Dislocation pinning was also observed in the alloys by an increase in microhardness.

Defects in Other Materials. Nuclear magnetic resonance (NMR) and electron-spin paramagnetic resonance (ESPR) are being used[54] to study neutron damage in LiF. Three successive dose intervals have been observed; up to 10^{16} nvt, ESPR data indicate that the number of electron spins produced by the irradiation grows in proportion to the neutron flux; above this dose the spin concentration saturates. Above 10^{16} nvt, NMR data show that fluorine gas forms at a rate proportional to dose up to 10^{19} nvt, where this effect saturates. Above 10^{19} nvt, lithium metal ions collect in clusters to form colloids of substantial size. Similar studies in NaF show no observable gas or metal collections.

Lattice expansion[55] in LiH of 0.0020 ± 0.0007 A, due to beta irradiation from 5.56 at.% LiT in the LiH sample, was observed after exposures at 77 and 245°K. This is explained in terms of He^3 interstitials being formed in the LiH lattice. NaCl showed an increase of 0.0061 ± 0.0009 A, even though the beta particles with maximum energies cannot produce defect displacements in NaCl. Formation of Cl^- interstitials and vacancies (Frenkel defects) could explain this increase. Such Frenkel defect formation has already been proposed to explain *F*- and *H*-center formation in NaCl.

Collections of lattice defects formed by fission-fragment damage have been observed by diffraction contrast in the electron microscope.[56] The tracks were straight lines about 100 A wide, which supports the thermal spike concept of fission damage. A larger (100 to 2000 A) concentric fringe pattern is sometimes seen, which is explained in terms of local buckling between the hexagonal planes caused by atomic displacements. Bollmann[57] has used dark-field electron microscopy to observe defects produced by neutron irradiation of graphite down to dimensions of about 10 A. Brinkman displacement spikes are used to explain the results, taking the layer structure of graphite into account. Room-temperature irradiations result in holes in the graphite planes, with interstitials between the layers. The energy release at 200°C is due to closing of these holes. Incomplete closing causes dislocation dipoles, which then move by glide and cluster, explaining the release of energy from 200 to 1300°C. Above 1300°C, diffusion mechanisms allow climb, which results in the annihilation of the dislocations. A critical dose of 6×10^{20} neutrons/cm^2 is interpreted as the threshold for interaction of the holes, and thus the probability of the formation of dislocation dipoles increases rapidly. Blackman[58] also discusses some of the structures that he observed in irradiated graphite. Reynolds et al.[59] have reported on natural graphite crystals that were annealed after irradiations of 4.8×10^{20} neutrons/cm^2 at temperatures from 150 to 650°C. Complete recovery was observed at temperatures above 1700°C. The results are used to support the statement that highly stable defect complexes are formed by annealing of low-temperature damage. The buildup and thermal annealing of stored energy in graphite has been studied by Hetrick[60] at temperatures up to 700°C. A semiempirical description of the annealing, which is valid for exposures up to 500 Mwd/central ton, is obtained in terms of three six-order processes, each with a discrete activation energy. The rate constant is assumed to be independent of exposure when determining the dependence of these activation energies on dose. The processes with the higher activation energies are found to be increasingly important as the dose increases. Also, the activation energy of each process increases with exposure.

Neutron-irradiated quartz has been found to display an anisotropy in induced strain of three to one in going from the X- to the Z-cut crystals.[61] The doses received were of the order of 10^{19} to 10^{20} nvt. Primak et al.[62] have measured in detail the frequency factor associated with annealing of neutron-induced density changes in vitreous silica.

A dose of 2×10^{20} fast neutrons/cm^2 has been observed to transform crystalline quartz and vitreous silica into the same isotropic substance.[63] The transformation was observed by means of density changes, thermal expansion,

internal energy, and elastic and piezoelectric constants. Quartz crystals pass through a state with the symmetry of β-quartz before reaching this isotropic state. On reheating, depending on the neutron dose, the samples can be transformed back into vitreous silica, crystalline quartz, or another structure.

Dislocation loops[64] have been formed in thin cadmium crystals at $-90°C$. The vacancy loops are formed while the specimens are being observed by transmission-electron microscopy. The filament gives off negative ions of unknown origin that are accelerated and strike the specimens, forming the loops which expand upon further irradiation. (T. G. Knorr)

Theories of Radiation Effects

Lehmann and Leibfried[65] have added to their calculations on focusing collisions in face-centered cubic (fcc) lattices. This paper is specifically concerned with focusing in $\langle 110 \rangle$ direction, and the authors show that, for small angular deviations from this direction, exact treatment of subsequent collisions is possible. They compare their results with the machine calculations of Gibson et al.[66] and find practically complete agreement.

A Russian report[67] discusses a method for studying the processes of slowing down fission products in metals and alloys. Specific energy losses as a function of particle range are recorded in an ionization fission chamber. Results are reported for light and heavy fission fragments being stopped in gold and aluminum.

Point-defect annealing kinetics in metals are discussed in detail by Sosin.[68] Impurity content and binding effects are also considered to allow the determination of the recovery at various stages. (T. G. Knorr)

Surveys on Radiation-Induced Defects

Vineyard[70] commented, in a brief review of radiation effects, on the machine calculations of radiation-displacement events which are being conducted at Brookhaven and which have been reported previously.[66] Kishkin[71] reviews the irradiation effects produced in structural metals, based on the formation of Frenkel defects. In metals, Kishkin reports that melted zones are not formed if the self-diffusion activation energy is less than 92 kcal/mole. Uhlmann[72] surveys radiation effects in aluminum, magnesium, zirconium, and their alloys. His bibliography is annotated extensively and covers the period from 1952 to early 1961.

The proceedings of the European Regional Conference on Electron Microscopy, held at Delft in 1960, have been published.[73] Of particular interest are sections on lattice defects and transformations in metal lattices which appear in Vol. 1. Section IIIA (Nature and Behavior of Defects) of the recent compilation of the USAEC basic research programs in solid-state physics and metallurgy is of general interest.[74] Three other surveys are of interest: Linnenbom[75] reported on damage mechanisms in insulators, Weil[76] introduced the radiation damage at low temperatures, and Aqua and Allio[77] discussed radiation effects on recovery of mechanical properties in metals.

(T. G. Knorr)

Effects of Radiation on Mechanical Properties

Workers at Oak Ridge[9,78] have also investigated the effect of irradiation on the mechanical

Table IV-4 RESULTS OF STRESS-RUPTURE TESTS OF TYPE 304 STAINLESS-STEEL TUBING AT 1500 AND 1600°F IN AIR[9]

Test temp., °F	Specimen	Stress, psi	Irradiation dose at rupture, Mw-hr	Time to rupture, hr
1500	310	6,300		517*
	318	6,300		487*
	537	6,300		183
	319	5,800		691*
	239	5,250		1,025*
	73	5,250		1,134
	536	4,700		857
	240	4,200		2,450*
	72	4,200		1,670
	17-3	4,000	36,900	851†
	17-10	3,500	50,080	>1,600‡
	17-1	3,000	50,080	>1,600‡
	17-9	3,000	50,080	>1,600‡
1600	17-8	5,000	3,750	49
	360	3,700		265
	17-5	3,000	13,500	414
	17-6	2,600	27,100	870
	17-4	2,200	43,900	1,430
	17-7	2,200	47,400	>1,505‡

* Specimens 6 in. long; remaining specimens $2\frac{1}{2}$ in. long.

† Specimen received 11,500 Mw-hr of irradiation prior to stressing.

‡ Specimens did not rupture.

properties of structural materials. Stress-rupture tests have been made on AISI type 304 stainless steel in reactor fluxes of approximately 1×10^{13} neutrons/(cm^2)(sec) at 1300, 1500, and 1600°F. When compared with results from stainless steel tested without irradiation, the ductility at rupture decreased by a factor of 2 to 10. Strain at rupture was as low as 1 per cent at 1500 and 1600°F. Results are given in Table IV-4.

Investigators at the Naval Research Laboratory[79] have examined two pressure-vessel steels, ASTM A212 grade B and ASTM A302 grade B, after irradiation in the Low-Intensity Test Reactor at 260, 400, 450, and 550°F. Post-irradiation examination by impact testing showed no appreciable effect of irradiation for these materials irradiated at temperatures of less than 450°F. An increase of 100°F in the ductile-to-brittle transition temperature was observed for both steels. The increase was shown to be linear with the logarithm of the neutron-flux dosage for irradiation temperatures up to 450°F. The data from materials irradiated at 550°F showed a similar linearity, but displaced toward lower transition-temperature shifts.

Irradiation studies at Hanford[48,80] include a study on the effect of irradiation of iron- and nickel-base alloys at 650°C and the annealing kinetics for unalloyed iron. The iron- and nickel-base alloys were irradiated to 2.53×10^{20} nvt (thermal) in a graphite-helium environment. Control specimens were annealed in a similar environment at 650°C. The results are shown in Table IV-5. Recovery studies of irradiated iron by elevated-temperature annealing have shown property changes that have been related to mechanisms of irradiation. Recovery was shown to occur in iron exposed to 4×10^{18} neutrons/cm^2 in three stages associated with various temperatures that were dependent upon the irradiation level. These recovery ranges and stages were associated with various activation energies and mechanisms of the irradiation process.

Investigators at Hanford[48] examined, by burst testing at 337°C, eight Zircaloy-2 tubes after exposure to 1×10^{19} neutrons/cm^2. Initial hoop

Table IV-5 TENSILE PROPERTIES OF IRRADIATED AND UNIRRADIATED IRON- AND NICKEL-BASE ALLOYS[80]

Alloys	Unirradiated			Irradiated, 2.53×10^{20} nvt (thermal)		
	Yield strength, 1000 psi	Ultimate strength, 1000 psi	Elongation, %	Yield strength, 1000 psi	Ultimate strength, 1000 psi	Elongation, %
Ferral (modified)	73.6	97.5	15.5	76.0	76.0	3.0
AISI type 406 S.S.	67.0	88.6	23.0	70.0	91.0	25.0
Hastelloy X	51.7	116.0	30.0	37.0	108.0	34.0
Hastelloy R-235	91.0	157.5	16.5	97.0	158.0	19.0
Inconel	35.6	94.0	42.0	35.5	95.0	42.5
Inconel 702	97.0	155.0	27.0	97.0	154.0	31.0
AISI type 316 S.S.	29.5	81.0	62.0	27.0	78.0	56.0
AISI type 347 S.S.	52.8	100.0	43.5	52.0	95.0	39.0

Table IV-6 TENSILE PROPERTIES OF IRRADIATED M-388 AND M-257[9]

Alloy	Irradiation exposure, nvt (thermal)	Yield strength (0.2% offset), 1000 psi	Ultimate tensile strength, 1000 psi	Young's modulus, 10^6 psi	Total elongation, %
M-257	Unirradiated	28.3	36.2	10.0	8.0
M-257	7×10^{19}	28.3	35.3	11.7	10.0
M-257	3.19×10^{20}	34.7	38.6	11.4	6.0
M-257	6.25×10^{20}	35.5	40.2	11.3	6.0
M-388	Unirradiated	9.7	16.1	11.0	29.0
M-388	7×10^{19}	6.8	15.3		29.0
M-388	3.19×10^{20}	8.0	17.1	9.4	23.0
M-388	6.25×10^{20}	10.2	19.1	13.5	15.6

stresses were in the range 46,000 to 49,000 psi, which produced rupture times of 0.1 to 30 hr. Strength and ductilities were comparable to those of unirradiated Zircaloy-2.

Other materials that have been studied include beryllium, Inconel, niobium, and aluminum alloys. Investigation of tubular beryllium irradiated at 700°C to exposures of 1.8×10^{19} neutrons/cm^2 (>1 Mev) by Oak Ridge[78] shows a reduction in 100-hr rupture time by 23 per cent. The irradiation of two aluminum alloys (M-388, an aluminum-nickel alloy, and M-257, an SAP product) was carried out at Hanford.[48] Exposures were 7×10^{19}, 3.19×10^{20}, and 6.25×10^{20} neutrons/cm^2 (thermal). Tensile properties are compared in Table IV-6.

A good review of the effect of irradiation on structural properties was prepared by Hanford[81] personnel for materials associated with reactor construction. (F. R. Shober)

Selected Mechanical Properties of Cladding and Structural Materials

At Hanford[48] the activation energies for creep of Zircaloy-2 were investigated in the 50 to 275°C temperature range. Values are between 15,000 and 30,000 cal/mole in the 50 to 190°C range and 75,000 cal/mole at 277°C. The activation energies at the lower temperatures appear to be both stress- and strain-dependent, whereas the activation energy at the higher temperature appears to be related to strain aging in Zircaloy-2.

The creep and fatigue properties of Hastelloy X at elevated temperatures have been reported by Aerojet-General.[15] The rupture time for 1000-psi stress at 1750°F was found to be 6619 hr, and the specimen showed about 47 per cent elongation in 2 in. The 10-hr rupture strengths for coarse-grained Hastelloy-X tubing at 2000, 1800, 1600, and 1400°F were found to be 1600, 3000, 5100, and 24,000 psi, respectively. S-N curves for Hastelloy-X fuel-pin tubing indicate that failure will occur at 10^6 cycles under the following conditions:

Stress, psi	Temp., °F
35,000–38,000	1400
18,500	1600
8,700	1725
5,300	1800
3,200	2000

A review of recent developments of niobium and tantalum alloys has been prepared by the Defense Metals Information Center at Battelle Memorial Institute.[82] The properties of several promising alloys for high-temperature application are tabulated. One of particular interest was a niobium–14 wt.% tungsten alloy which has tensile strengths of 25,000 and 50,000 psi at 2400 and 3500°F, respectively. Good fabrication properties are reported for this alloy. (F. R. Shober)

Selected Metallurgical Aspects of Cladding and Structural Materials

Refractory Metals

Phase Studies of Tungsten-Molybdenum-Rhenium. Russian investigators[83] have plotted the constitution diagram of tungsten and molybdenum solid solutions with up to 50 wt.% rhenium. The alloys with cross sections parallel to tungsten-molybdenum, with contents of 10, 20, 30, 40, and 50 wt.% rhenium, were analyzed, and three isothermal cross sections of cast alloys, annealed at 1750°C for 3 hr and at 1000°C for 450 hr, were plotted. The solubility of the solid solution at 1000°C extends from the binary tungsten alloy with 32 wt.% rhenium to 46 wt.% rhenium. The system forms the σ phase; the binary $\alpha + \sigma$ phase is found between the σ phase and the ternary solid solution. The alloy with 40 wt.% tungsten–20 wt.% molybdenum is a single-phase ternary solid solution at the threshold of solubility, which transforms to binary two-phase $\alpha + \sigma$ at lowered temperatures.

Phase Studies of Chromium-Niobium-Molybdenum. Recent Russian[84] work has been concerned with investigation of the ternary alloy, chromium-niobium-molybdenum. Microstructural examination showed that the ternary α solid solution of chromium, niobium, and molybdenum was found in the chromium and niobium corner. This region expands with the increase in molybdenum. A large two-phase region of Cr_2Nb and ternary α solid solution is adjacent to the chromium-niobium side. The boundary was found for the Cr_2Nb two-phase region and α solid solution for 1500 to 1000°C. X-ray studies uncovered the ternary solid solution of chromium, niobium, molybdenum, and Cr_2Nb compound. The microhardness of the alloys

indicates two phase differences in microhardness, the Cr_2Nb compound with 1200 to 1850 kg/mm^2 and ternary α solid solution with 250 to 700 kg/mm^2.

Thermal Properties of Molybdenum, Tantalum, and ZrC. The heat capacities of molybdenum and tantalum are reported by Atomics International[85] to show a gradual rise above their Dulong and Petit values of 0.06253 and 0.03316 cal/(g)(°C), respectively, at elevated temperatures. At 2800°K, C_p (molybdenum) = 0.1350 cal/(g)(°C) and at 3200°K, C_p(tantalum) = 0.0667 cal/(g)(°C). These anomalies were noted in other transition metals. The per cent elongation, relative to room temperature of ZrC, was measured between 1000 and 2000°C and was found to vary linearly from 0.6 per cent at 1000°C to 1.6 per cent at 2300°C, with a permanent set occurring above 2300°C.

Epsilon Phases in Refractory Alloys. Argonne workers found[19] that the addition of 10 at.% iridium to a $NbNi_3$ alloy transformed the structure from the distorted hexagonal (actually orthorhombic) $TiCu_3$ type to a true hexagonal structure having no apparent ordering. Further investigation revealed similar phases in other systems, as shown in Table IV-7. Because of the resemblance to the epsilon phase reported by Raub* in the molybdenum-platinum system, these ternary phases are denoted epsilon phases.

Table IV-7 OCCURRENCE OF ϵ PHASES[19]

Composition, at.%	C_0, A	A_0, A	C/A
Nb–67.5 Ni–10 Ru	4.256	2.617	1.626
Nb–67.5 Ni–10 Os	4.263	2.622	1.626
Nb–67.5 Ni–10 Ir	4.285	2.620	1.636
Nb–50 Ni–17.5 Co–10 Ir	4.258	2.628	1.620
Nb–67.5 Pd–10 Ir	4.56	2.768	1.628
Ta–67.5 Ni–10 Os	4.26	2.61	1.63
Ta–67.5 Ni–10 Ir	4.26	2.60	1.64
Mo–67.5 Ni–10 Os	4.226	2.604	1.623
Mo–60 Ni–20 Ir	4.268	2.63	1.62

From the data in Table IV-7, it is noted that:

1. All nine ϵ phases lie adjacent to an AB_3 compound of either the $TiCu_3$ type or the $TiAl_3$ type.

2. All have c/a ratios fairly close to the ideal value of 1.633.

Alloying Behavior of Niobium. An investigation was made at Argonne[19] of the intermetallic compounds that exist in binary systems of niobium with the transition elements. A compound ($NbAu_2$) was discovered, having the AlB_2 type structure, c = 2.73 A, a = 4.63 A, and c/a = 0.59. In two binary systems (niobium-rhenium and niobium-osmium), a chi phase (α-manganese structure) pre-empts the Laves phase at the $NbRe_2$ and $NbOs_2$ compositions. The two chi phases were studied in some detail, and lattice parameters are given in Fig. IV-1, with recent data on niobium-rhenium by Knapton for comparison.

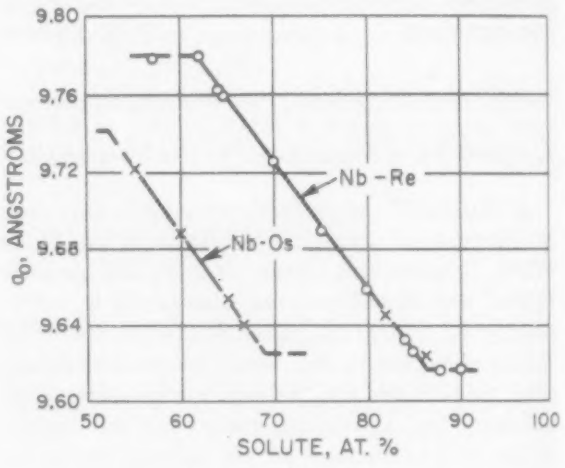

Fig. IV-1 Lattice parameters of chi phases in niobium-osmium and niobium-rhenium systems.[19] ×, ANL data. ○, Knapton data [*J. Less-Common Metals*, 1(6): 480 (1959)].

It was found that, in binary diagrams where niobium was placed on the left, the phases occur from left to right in the following order: bcc → Cr_3O → σ → Laves → chi (α-Mn) → cp hex variant → fc cube variant. No one system thus far known contains all these phases, but the order of occurrence is always followed.

Refractory-Metal References. The Office of Technical Services has published two extensive bibliographies. One contains about 380 references[86] on molybdenum and tungsten metals, alloys, carbides, and other compounds. The second contains about 240 references[87] covering

* E. Raub, Die Legierungen der Platin metalle mit Molybdän, *Z. Metallk.*, 45: 23 (1954).

the same type of information for niobium and tantalum.

A compilation of both binary and ternary phase diagrams of niobium, molybdenum, tantalum, and tungsten has been prepared by the Defense Metals Information Center[88] at Battelle. (J. A. DeMastry)

Fuel-Cladding Reactions

Studies of high-temperature reactions between various cladding materials and UO_2 and UC have been reported by Hanford.[48] The fuel weight changes during 10 min with various metals at 1000 and 1500°C are shown in Table IV-8. These data have only qualitative significance since they include no exact measurement

Table IV-8 FUEL WEIGHT CHANGES AFTER 10-MIN CONTACT WITH VARIOUS CLADDING MATERIALS[48]

	Weight change, %			
	1000°C		1500°C	
Cladding	UO_2	UC	UO_2	UC
Tungsten	−0.093	0.015	0.096	−0.037
Tantalum	0.005	0.110	0.011	0.388
Molybdenum	−0.054	0.070	−0.065	0.060
Zircaloy-2	−0.063	0.205	−0.100	0.215
Type 304L S.S.	−0.131	5.44	−0.121	
Inconel	−0.012	0.050		
Hastelloy F	0.110	0.97		
Fansteel-80	0.995	0.019	2.55	0.293
Fansteel-82	0.110	0.002	0.112	0.068

of the contact area between the specimen and the metal. Metallographic examination of each cladding material (after heating) in contact with UC revealed mixed carbides and fused base metal in all the higher temperature tests. Stainless steel was the only material to react appreciably at 1000°C. A polished cross section showed a hemispherical reaction zone extending 0.013 in. into the 0.015-in.-thick stainless steel. (J. A. DeMastry)

Scandium-Titanium System

The following details of the scandium-titanium phase diagram as determined by Ames[89] are reported:

1. A minimum in the solidus-liquidus curves at 1295°C and 49 wt.% scandium.

2. There is a solubility of about 5 wt.% of each of the metals in the alpha form of the other at about 850°C.

3. There appears to be complete solid solubility in the upper portion of the beta phases of these metals.

4. A monotectoid exists at approximately 55 wt.% scandium and 1050°C, with the immiscibility loop extending from 18 to 55 wt.% scandium with a temperature range of 1050 to 1110°C at its maximum. (J. A. DeMastry)

Hardness of Zirconium Alloys

In the light of the interest in conversion of Vickers and Knoop hardness measurements, Knolls[90] has published hardness-conversion curves in the 100 to 600 diamond pyramid hardness (DPH) range for zirconium-base alloys. Large standard deviations in the Knoop hardness scale are reported in the range of 500 to 600 Knoop hardness number (KHN) with an applied load of 10 g. (J. A. DeMastry)

Diffusion Studies

The extent of interdiffusion between 23 barrier and base metals annealed at 1700°C has been measured by metallographic examination, microhardness tests, and electron-probe microanalysis.[91] No diffusion coefficients were determined, but it was concluded, on the basis of minimum diffusion, that hafnium and iridium are the most promising barriers for tungsten at 1700°C, with vanadium as a third choice. Iridium appears to be the best choice for tantalum and molybdenum, with tantalum-zirconium and molybdenum-hafnium deserving further evaluation. It is reported that, because of melting of most of these couples at 1700°C, no recommendations could be made for niobium-base metal.

The electron-probe microanalyzer[92] was used to determine the composition and extent of phases occurring in a number of bimetal diffusion couples at 1100°C. The Naval Research Laboratory investigated six binary systems: niobium-platinum, niobium-selenium, niobium-zinc, niobium-cobalt, nickel-tantalum, and iron-molybdenum. It is reported that the niobium-selenium and niobium-zinc systems are somewhat alike in their phase formations in that niobium-selenium exhibits NbSe, Nb_2Se_3, and $NbSe_2$, whereas niobium-zinc produces NbZn, Nb_2Zn_3, $NbZn_2$, and $NbZn_3$. Diffusion between niobium and platinum formed Nb_3Pt, NbPt, $NbPt_2$, and $NbPt_3$ and would seem to preclude prolonged use of platinum thermocouples in

contact with niobium at 1100°C. The only phases produced in the niobium-cobalt system are previously unreported in the literature and are Nb_3Co_2 and $NbCo_4$. This system also exhibited an extended region containing about 5 wt.% niobium in cobalt, in agreement with the solubility limit shown in existing phase diagrams. Nickel-tantalum diffusion produced zones that showed strong cracking and grain formation. The phases $TaNi_3$, $TaNi_2$, TaNi, and Ta_3Ni_2 comprised the zones, with pure tantalum precipitating in the $TaNi_2$ phase on cooling from 1100°C. Iron-molybdenum produced only one phase, Mo_2Fe_3.

Diffusion in the uranium-niobium system is being investigated at Massachusetts Institute of Technology,[44] using incremental couples at 10 per cent intervals across the uranium-niobium binary system and temperatures from 800°C at the uranium-rich end to 1700°C at the niobium end of the binary system. The couples are being analyzed with an electron (microbeam) probe, but no results have yet been reported. Apparently, diffusion coefficients will be calculated later in this study. In the field of intermetallic diffusion, it should also be noted that a bibliography concerned with metal-metal diffusion has been issued by the French.[93] It covers the period from 1950 to 1960 and includes 241 references.

The self-diffusion of beta zirconium has been studied with the use of the Zr^{95} isotope by the French.[94] The self-diffusion coefficients determined in the temperature range 900 to 1240°C are represented by the equation

$$D\,(\mathrm{cm^2/sec}) = 4.2 \times 10^{-5} \exp\,(-24{,}000/RT)$$

This is in fair agreement with a value referenced in a previous issue of *Reactor Core Materials*, which was also determined using the radioactive-tracer technique. The study of self-diffusion and bonding (sintering) of Zircaloy-2, which was reviewed previously under the topics of Diffusion Studies and Diffusion Bonding, has been continued at Bettis.[18] The effect of hydrogen on the diffusivity is discussed in the Diffusion Bonding section of this issue.

Diffusion in metal-to-nonmetal systems is receiving increasing attention, and a number of reports have been issued describing research in this area. The diffusion coefficient of uranium in graphite at 1950°C has been determined[95] to be approximately 2×10^{-9} cm^2/sec. Experiments at General Atomic indicate that the phenomenon is complicated by the evaporation of small amounts of carbon from the surface of the specimens. Thermal diffusion in ThO_2-UO_2-graphite compacts has also been studied and is discussed qualitatively by General Atomic workers in terms of the intended application. The diffusion coefficient for beryllium in BeO has been measured for a group of identical polycrystalline BeO samples, as well as in other types of BeO samples.[96] It was determined at Atomics International that the temperature dependence follows two straight lines on a log D versus $1/T$ graph, the lines intersecting at 1725°C. The lines correspond to the equations

$$D = 1.37 \exp\,(-91{,}900/RT) \quad 1550 \text{ to } 1725°C$$

$$D = 1.10 \times 10^{-6} \exp\,(-36{,}150/RT) \quad 1725 \text{ to } 2000°C$$

where D is in the usual units of cm^2/sec. However, the diffusion coefficient at 1800°C for this particular set of samples is about 40 times less than that reported previously for a different type of BeO. This variation in D is not understood and does not correlate with any single material parameter; therefore the study is being continued.

In a Russian paper,[97] a study of the diffusion of silicon into niobium at 1100 to 1300°C is described. The diffusion zone produced at these temperatures is reported to be brittle and to consist of three layers, $NbSi_2$, Nb_5Si_3, and Nb_4Si. Diffusion constants calculated for the $NbSi_2$ phase, which had the most distinct boundaries, are given in Table IV-9.

Table IV-9 DIFFUSION CONSTANTS FOR THE NIOBIUM-SILICON SYSTEM

Temp., °C	D_t, cm^2/sec	D_0, cm^2/sec	Q, cal/mole
1100	0.51×10^{-8}		
1150	1.57×10^{-8}		
1200	4.50×10^{-8}	6×10^{-4}	29,300
1250	5.86×10^{-8}		
1300	9.52×10^{-8}		

The mechanism of helium diffusion in irradiated copper was studied at Harwell.[98] It was found that helium diffuses from the narrow layer in which it is originally deposited and precipitates asymmetrically into the material that has been damaged by the passage of the

incident alpha particles. The investigators suggest that the results can be best explained if the helium diffuses interstitially but is captured at the numerous bubble nuclei that exist in the irradiated material. Once out of solution, the helium is effectively trapped until very high temperatures are reached. A still further widening of the layer occurs at about 900°C, presumably because the helium escapes from the bubbles. (D. C. Carmichael)

References

1. B. Cox, The Oxidation and Corrosion of Zirconium and Its Alloys, XII. Hydrogen Absorption by Zircaloy-2 and Some Other Alloys During Corrosion in Steam, British Report AERE-R-3556, January 1961.
2. F. W. Albaugh, Reactor Fuels Research and Development Operation Monthly Report, January 1961, USAEC Report HW-68350-A, Hanford Atomic Products Operation, Feb. 15, 1961. (Classified)
3. Argonne National Laboratory, Reactor Development Program Progress Report, January 1961, USAEC Report ANL-6307, Feb. 15, 1961.
4. Hanford Atomic Products Operation, (Unpublished)
5. N. J. M. Wilkins et al., The Corrosion of Aluminum Alloy in High Temperature Flowing Water, British Report AERE-R-3649, February 1961.
6. J. E. Draley et al., Corrosion of Aluminum and Its Alloys in Superheated Steam, USAEC Report ANL-6207, Argonne National Laboratory, April 1961.
7. N. D. Stolica and G. S. Adams, Corrosion in Neutralized Radioactive Waste, USAEC Report IDO-14531, Phillips Petroleum Co., Oct. 4, 1960.
8. J. M. Atwood and W. A. Snyder (Eds.), Plutonium Recycle Program, Annual Report, Fiscal Year 1960, USAEC Report HW-67000, Hanford Atomic Products Operation, Aug. 15, 1960.
9. Oak Ridge National Laboratory, Aircraft Nuclear Propulsion Project Semiannual Progress Report for Period Ending April 30, 1961, USAEC Report ORNL-3144, July 17, 1961. (Classified)
10. Oak Ridge National Laboratory, Proceedings of the US/UK Meeting on the Compatibility Problems of Gas-Cooled Reactors Held at Oak Ridge National Laboratory February 24–26, 1960, USAEC Report TID-7597, Book 2, Mar. 3, 1961.
11. W. D. Klopp, Review of Recent Developments on Oxidation-Resistant Coatings for Refractory Metals, Report DMIC-Memo-120, Battelle Memorial Institute, Defense Metals Information Center, July 31, 1961.
12. J. C. Withers, Protective Coatings for Refractory Metals, Paper Presented at Fifth Meeting of Refractory Composites Working Group, Dallas, Texas, Aug. 8–10, 1961.
13. Aerojet-General Nucleonics, Army Gas-Cooled Reactor Systems Program Monthly Progress Report for March 1961, USAEC Report IDO-28570, Apr. 27, 1961.
14. Aerojet-General Nucleonics, The Army Gas Cooled Reactor Systems Program. A Preliminary Study of a 1000 Kw(e) Mobile Nuclear Power System, USAEC Report AGN-TM-390, December 1960.
15. Aerojet-General Nucleonics, Army Gas-Cooled Reactor Systems Program Monthly Progress Report for February 1961, USAEC Report IDO-28569, Mar. 27, 1961.
16. Aerojet-General Nucleonics, Army Gas-Cooled Reactor Systems Program Monthly Progress Report for November 1960, USAEC Report IDO-28566, Dec. 30, 1960.
17. Coriou et al., Stress Corrosion Cracking of Inconel in High Temperature Water, French Report CEA-1521, 1960.
18. Westinghouse Electric Corp., Bettis Atomic Power Laboratory, Materials. Technical Progress Report for the Period March 26, 1961 to June 25, 1961, USAEC Report WAPD-MRK-10. (Classified)
19. Argonne National Laboratory, Annual Report for 1960, Metallurgy Division, USAEC Report ANL-6330.
20. R. Caillat et al., Corrosion Inhibition of Magnesium Heated in Wet Air by Surface Fluorination, French Report CEA-1520, 1960.
21. North American Aviation, Inc., Compatibility of Materials with High Temperature Potassium, Third Quarterly Progress Report for November 1, 1960 Through January 31, 1961, Report NP-10147, Mar. 3, 1961.
22. J. J. Gill, Sodium-Graphite Interaction and Graphite Protective Coatings, USAEC Report NAA-SR-6094, Atomics International, May 1, 1961.
23. J. J. Gill and J. C. Bokros, Nitriding of Type 304 Stainless Steel in a Sodium-Nitrogen System, USAEC Report NAA-SR-6162, Atomics International, May 30, 1961.
24. R. C. Schulze et al., INOR-8–Graphite–Fused Salt Compatibility Test, USAEC Report ORNL-3124, Oak Ridge National Laboratory, June 15, 1961.
25. Oak Ridge National Laboratory, Molten-Salt Reactor Program Progress Report for Period from August 1, 1960, to February 28, 1961, USAEC Report ORNL-3122, June 27, 1961.
26. W. N. Crofford et al., Isothermal Study of Concentration and Transport of Radioactive Stainless Steel Components in Liquid Lithium, Report NRL-5572, Naval Research Laboratory, Oct. 6, 1960.
27. T. A. Kovacina and R. R. Miller, The Solubility of Nickel in Sodium by a Tracer Technique, *Nuclear Sci. and Eng.*, 10: 163–166 (June 1961).

28. L. F. Epstein, Correlation and Prediction of Explosive Metal-Water Reaction Temperatures, *Nuclear Sci. and Eng.*, 10: 247–253 (July 1961).
29. M. T. Barringer, Metal-Water Reactions: A Selective Literature Search of USAEC Reports, USAEC Report KAPL-M-MTB-1, Knolls Atomic Power Laboratory, Jan. 9, 1961.
30. E. Ruedi et al., Evidence for Focusing Collisions in Irradiated Platinum, *Phys. Rev. Letters*, 6(10): 530–532 (May 15, 1961).
31. G. S. Anderson and G. K. Wehner, Atom Ejection Patterns in Single-crystal Sputtering, *J. Appl. Phys.*, 31(12): 2305–2313 (December 1960).
32. G. K. Wehner et al., Surface Bombardment Studies. Report No. 2163, Annual Report for Period February 15, 1960 to February 14, 1961, USAEC Report TID-12431, General Mills, Inc., Mar. 1, 1961.
33. N. Laegreid and G. K. Wehner, Sputtering Yields of Metals for Ar^+ and Ne^+ Ions with Energies from 50 to 600 ev, *J. Appl. Phys.*, 32(3): 365–369 (March 1961).
34. G. D. Magnuson et al., Etch Effects From Oblique-Incidence Ion Bombardment, *J. Appl. Phys.*, 32(3): 369–374 (March 1961).
35. J. B. Ward and J. W. Kauffman, Low-temperature Recovery of Resistivity in Electron-irradiated Gold, *Phys. Rev.*, 123(1): 90–96 (July 1, 1961).
36. V. A. Pervakov and V. I. Khotkevich, Calorimetric Determination of the Formation Energy of Vacancies in Gold, *Doklady Akad. Nauk S. S. S. R.*, 134(6): 1328–1330 (Oct. 21, 1960). Translated in *Soviet Phys.-Doklady (USA)*, 5(5): 1051–1053 (March-April 1961).
37. S. N. Buckley, Irradiation Growth, British Report AERE-R-3674, March 1961.
38. A. Seeger et al., Observation of Interstitial Atoms in F.C.C. Metals, *Phil. Mag.*, (8)5: 853–857 (1960).
39. H. Kronmuller et al., Ferromagnetic Hysteresis by Interstitial Atoms in Neutron-irradiated Nickel, *Z. Naturforsch.*, 15a: 740–741 (August 1960).
40. K. D. Chaudhuri et al., The Effect of Radiation Damage on the Thermal Conductivity of Superconductors, *Cryogenics*, 1: 47–48 (September 1960).
41. L. M. Clarebrough et al., The Influence of Impurities on the Annealing of Nickel After Cold Work, *Acta Met.*, 8: 797–803 (November 1960).
42. G. R. Piercy and R. H. Tuxworth, The Effect of Fast-Neutron Irradiation on the Density, X-Ray Lattice Parameter, and Line Breadth of Metals, Canadian Report CRRM-1010 (AECL-1251), March 1961.
43. D. L. Gray and W. V. Cummings, Jr., An X-Ray Diffraction Study of Irradiated Molybdenum, *Acta Met.*, 8: 446 (1960).
44. R. E. Ogilvie and J. T. Norton, Physical Metallurgy of Uncommon Metals, USAEC Report TID-12600, Massachusetts Institute of Technology, Apr. 25, 1961.
45. M. J. Makin et al., Dislocation Loops and Hardening in Neutron Irradiated Copper, *Phil. Mag.*, 6(63): 464–468 (March 1961).
46. I. G. Greenfield and H. G. F. Wilsdorf, Effect of Neutron Irradiation on the Plastic Deformation of Copper Single Crystals, *J. Appl. Phys.*, 32(5): 827–839 (May 1961).
47. S. Yoshida and J. S. Koehler, Influence of Plastic Deformation on the Annealing of Quenched Gold, *Acta Met.*, 8: 878–881 (December 1960).
48. F. W. Albaugh, Reactor and Fuels Research and Development Operation Monthly Report, April 1961, USAEC Report HW-69408A, Hanford Atomic Products Operation, May 15, 1961. (Classified)
49. W. G. Nilson, The Effect of Quenching and Neutron Irradiation on Internal Friction of Aluminum–5 Magnesium Alloy, *Can. J. Phys.*, 39: 119–132 (January 1961).
50. D. Hull and I. L. Mogford, Precipitation and Irradiation Hardening in Iron, *Phil. Mag.*, 6(64): 535–546 (April 1961).
51. G. T. Murray, Precipitation of Helium Along Dislocations in Aluminum, *J. Appl. Phys.*, 32(6): 1045–1051 (June 1961).
52. I. V. Batenin et al., The Influence of Neutron Irradiation on Crystal Fine Structure and the Properties of Metals and Alloys, *Doklady Akad. Nauk S. S. S. R.*, 134(4): 802–805 (Oct. 1, 1960).
53. I. V. Batenin et al., The Problem of the Influence of Neutron Irradiation on the Fine Crystal Structure of Metals and Alloys (in Russian), *Fiz. Metal. i Metalloved. Akad. Nauk S. S. S. R., Ural.' Filial*, 7: 243–246 (1959).
54. P. J. Bray, Radiation Damage Studies in Solids; Nuclear Resonance Absorption Technique; Progress Report for November 1, 1959 Through November 1, 1960, USAEC Report TID-11057, Brown University, Nov. 1, 1960.
55. F. E. Pretzel and R. L. Petty, Interstitial Defects in LiH and NaCl Irradiated at Low Temperatures, *Phys. Rev.*, 123(2): 464–465 (July 15, 1961).
56. Kazuhiko Izui and F. Eiichi Fujita, Observation of Lattice Defects in Fission Fragment-Irradiated Graphite, *J. Physiol. Soc. Japan*, 16(5): 1032–1033 (1961); *J. Physiol. Soc. Japan*, 14(12): 1829–1830 (1959).
57. W. Bollmann, Electron Microscope Study of Radiation Damage in Graphite, *J. Appl. Phys.*, 32(5): 869–876 (May 1961).
58. L. C. F. Blackman, Properties of Graphite. Part III. Crystal Compounds and Irradiated Graphite, *Research (London)*, 13: 492–502 (December 1960).
59. W. N. Reynolds et al., Aggregation and Disposal of Radiation Damage in Graphite, *Nature*, 189: 824–826 (Mar. 11, 1961).
60. D. L. Hetrick, On the Release of Stored Energy in Irradiated Graphite, USAEC Report NAA-SR-

131(Del.), North American Aviation, Inc., June 27, 1951.

61. S. E. Wisnewski et al., An Investigation of the Anisotropic Lattice Defects in Natural and Synthetic Quartz by Fast Neutron Irradiation, USAEC Report NYO-9622, Rutgers University, Jan. 15, 1961.
62. W. Primak et al., Frequency Factors for Annealing Fast-Neutron Induced Density Changes in Vitreous Silica, *J. Appl. Phys.*, 32(4): 660–668 (April 1961).
63. G. Mayer and M. Lecomte, Effect of Fast Neutrons on Crystalline Quartz and Vitreous Silica, *J. Phys. Radium*, 21: 846–852 (December 1960).
64. P. B. Price, Direct Observations of Ion Damage in Cadmium, *Phys. Rev. Letters*, 6(11): 615–617 (June 1, 1961).
65. C. Lehmann and G. Leibfried, Fokussierende 110-Strossfolgen in Flächenzentrierten Kristallen bei Kleinen Winkeln, *Z. Physik*, 162: 203–214 (1961); also in Report NP-9814.
66. J. B. Gibson et al., Dynamics of Radiation Damage, *Phys. Rev.*, 120: 1229 (1960).
67. N. A. Protopopov et al., A Method of Studying Slowing-Down Processes for Fission Fragments in Metals, *Atomnaya Energ.*, 10: 166–168 (February 1961).
68. A. Sosin, Point-Defect Migration and Binding in Metals, *Phys. Rev.*, 122: 1112–1116 (May 15, 1961).
69. Reference cancelled.
70. G. H. Vineyard, Some Recent Developments in the Theory of Radiation Damage, *Energia nucleare (Milan)*, 8(1): 9–15 (1961).
71. S. T. Kishkin, The Effect of Irradiation on the Structure and Properties of Structural Metals, Russian Translation NP-tr-574 (from a publication of the State Publishing House of the Defense Industry, Moscow), 1958.
72. W. Uhlmann, Radiation Effects on Aluminum, Magnesium, Zirconium, and Their Alloys: A Literature Survey, Swedish Report VDIT-22, February 1961.
73. A. L. Houwink and B. J. Spit (Eds.), The Proceedings of the European Regional Conference on Electron Microscopy, Delft, 1960, Vol. 1 (De Nederlandse Vereniging Electronenmicroscopie, Delft).
74. R. J. Ailio (Ed.), Summaries of the AEC Basic Research Programs in Metallurgy, Solid State Physics and Ceramics, USAEC Report TID-4005 (Pt. 1, 6th ed.), June 1961.
75. V. J. Linnenbom, The Effects of Radiation on Materials, Part 3, Radiation Damage Mechanisms. Insulating Materials, *Insulation*, 6(3): 11–15 (March 1960).
76. L. Weil, Cryogenics and Radiation Damage, *Cryogenics*, 1(3): 129–134 (March 1961).
77. E. N. Aqua and R. J. Allio, Radiation Effects upon and the Recovery of the Mechanical Properties of Metals, USAEC Report KAPL-2103, Knolls Atomic Power Laboratory, Oct. 25, 1960.
78. Oak Ridge National Laboratory, May 4, 1961. (Unpublished)
79. L. E. Steele and J. R. Hawthorne, Effect of Irradiation Temperature on Neutron-induced Changes in Notch Ductility of Pressure-Vessel Steels, Report NRL-5629, Naval Research Laboratory, Apr. 13, 1961.
80. F. W. Albaugh, Reactor and Fuels Research and Development Operation Monthly Report for March 1961, USAEC Report HW-69062A, Hanford Atomic Products Operation, Apr. 15, 1961. (Classified)
81. S. H. Bush, Irradiation Effects in Core Structural Materials, USAEC Report HW-68747, Hanford Atomic Products Operation, Mar. 6, 1961.
82. E. S. Bartlett and F. F. Schmidt, Review of Recent Developments in the Technology of Columbium and Tantalum, Report DMIC-Memo-115, Battelle Memorial Institute, Defense Metals Information Center, July 7, 1961.
83. M. A. Tylkina et al., Phase Studies of Tungsten-Molybdenum-Rhenium Alloys, *Zhur. Neorg. Khim*, 5: 2458–2461 (1960) (in Russian).
84. N. N. Kurnakov and M. Ya Troneva, Studies of Ternary Cr-Nb-Mo Alloy at Chromium and Niobium Angle, *Zhur. Neorg. Khim*, 5: 2403–2409 (November 1960) (in Russian).
85. G. W. Lehman, Thermal Properties of Refractory Materials, Report WADD-TR-60-581, Atomics International, July 1960.
86. Office of Technical Services, Molybdenum and Tungsten. OTS Selective Bibliography, Report SB-415, June 1960.
87. Office of Technical Services, Columbium and Tantalum. OTS Selective Bibliography, Report SB-414, June 1960.
88. J. J. English, Binary and Ternary Phase Diagrams of Columbium, Molybdenum, Tantalum, and Tungsten, Report DMIC-152, Battelle Memorial Institute, Defense Metals Information Center, Apr. 28, 1961.
89. Ames Laboratory, Annual Summary Research Report in Chemistry, July 1, 1959–June 30, 1960, USAEC Report IS-192, September 1960.
90. F. K. Blechinger and F. W. Kunz, Hardness Conversion for Zirconium-Base Alloys, USAEC Report KAPL-M-FKB-1, Knolls Atomic Power Laboratory, Feb. 16, 1961.
91. E. M. Passmore et al., Investigation of Diffusion Barriers for Refractory Metals, Report WADD-TR-60-343, Manufacturing Laboratories, Inc., August 1960.
92. R. E. Seebold and L. S. Birks, Elevated Temperature Diffusion in the Systems Nb-Pt, Nb-Se, Nb-Zn, Nb-Co, Ni-Ta, and Fe-Mo, Report NRL-5520, Naval Research Laboratory, Sept. 19, 1960.

93. C. Pinchon, Diffusion Metal-Metal, French Report CEA-Bib-13, November 1960 (in French).
94. D. Volokoff et al., Study of the Autodiffusion of Zirconium in the Body Centered Cubic Beta Phase, French Report CEA-1833, 1961.
95. General Atomic Div., General Dynamics Corp., 40-Mw(e) Prototype High-Temperature Gas-Cooled Reactor Research and Development Program, Quarterly Progress Report for the Period Ending September 30, 1960, USAEC Report GA-1774, April 1961.
96. S. B. Austerman, Diffusion of Beryllium in Beryllium Oxide. Part II, USAEC Report NAA-SR-5893, Atomics International, May 1, 1961.
97. P. M. Arzhanyi et al., The Structure and Phase Composition of Diffusion Coating of Niobium by Silicon, Russian Translation NP-tr-567, Nov. 7, 1960 from [*Izvest. Akad. Nauk S. S. S. R., Otdl. Tekh. Nauk Met. i Toplivo*, No. 6: 127–129 (1959)].
98. C. J. Beevers and R. S. Barnes, The Diffusion of Helium in Irradiated Copper, British Report AERE-R-3589, December 1960.

Section V

SPECIAL FABRICATION TECHNIQUES

Melting, Hot and Cold Working

In studies at National Lead Company of Ohio[1] to determine the effects of various types of vacuum-induction furnace charge materials on the yields and chemical purity of uranium feed stock, it was concluded that: (1) the hydrogen content was higher in ingot melted from charges containing more derby (as-reduced metal) material; (2) oxygen, nitrogen, and carbon contents were higher in the top than in the bottom of the ingot; (3) crude ingot yields were lowest when charges were made up of pigots, briquettes (compacted machine chips), and derbies high in slag and oxide; (4) pigots in the charge were deleterious to ingot purity; and (5) degreased "drip crop" (ingot tops) and dingot extrusion scrap were deleterious to fabricated-fuel-element yields.

Several review type articles concerned with factors of interest in the melting of high-temperature or refractory metals were published recently. For example, Moss and Richards[2] of the Armament Research and Development Establishment of England published a historical survey of various methods used for arc melting refractory metals. Included are discussions of arc-melting processes and techniques in general, and multiple melting and semicontinuous casting in particular. Alloy segregation, ingot defects, and methods of overcoming these occurrences are also discussed. The authors conclude that the most satisfactory method of producing homogeneous high-purity ingots is to combine multiple melting with continuous casting.

The electron-beam-melting techniques continue to be of interest. Pecher[3] discusses some of the purification effects of melting a variety of metals. Specifically he has presented data on the effects of electron-beam melting, as compared with arc melting, on the interstitial contents of cobalt and hafnium, and on the mechanical properties of beryllium, hafnium, vanadium, tungsten, and niobium alloys, tantalum-tungsten alloys, and cobalt.

In an article written in a similar vein, some of the metals and newer alloys used in less severe service between 1200 and 1800°F are discussed.[4] Included are some of the cobalt-, nickel-, and iron-base alloys in the technological transition area between development and production. Induction melting in vacuum and consumable-electrode arc melting in vacuum and under a flux are covered.

In a report on the preparation of niobium-base alloys, Du Pont[5] discusses the particular techniques that proved to be satisfactory in the preparation of 8-in.-diameter ingots. The objective of the development reported on is the preparation of aircraft-quality 10-ft-long T sections. Although the development is incomplete, 4-in. billets of D-31 (niobium–10 wt.% titanium–10 wt.% molybdenum alloy) suitable for reextrusion to T sections have been prepared by the following technique. In the first melt a $6\frac{1}{2}$-in.-diameter ingot is prepared by consumable-electrode vacuum arc melting. After a second melt by consumable-electrode vacuum arc melting, an 8-in.-diameter ingot is produced. This ingot is surface conditioned, canned in mild steel, and extruded at a reduction ratio of 4 to 1 with glass lubricant.

Notable for its current interest is a recent survey of literature on the fabrication of molybdenum and molybdenum-base alloys by Lockheed.[6] This annotated bibliography cites rolling, forming, welding and brazing, riveting, shearing, and spinning references published since 1958.

Zircaloy-2 continues to receive considerable attention in the areas of melting and fabrication. Knolls[7] reports the effect of melting

procedures on the weldability, corrosion resistance, and stringer content; the Advanced Technology Laboratories (ATL)[8] reports information regarding the cold extrusion of heavy-walled tubes. Data from the Knolls tests (comparisons of double vacuum-arc-melted, vacuum- and inert-atmosphere- (argon) arc-melted, and inert-atmosphere double-arc-melted materials) indicate that materials other than double vacuum-arc-melted Zircaloy-2 should not be considered for procurement. Zircaloy-2 has been successfully extruded at ATL at temperatures from room temperature to 400°C with reductions of 50, 65, and 80 per cent. Although fabricators conclude that the cold extrusion of heavy-walled tubes is economical (if production volume is sufficient) and that the production of thin-walled fuel containing tubes with integral end caps appears promising, complete evaluation of cold extrusion must await more testing. Corrosion and orientation tests indicated that the product was similar to hot-extruded material, but control of concentricity and surface finish of the tubes was only fair. (E. L. Foster, Jr.)

Cladding

Cladding by Rolling and Swaging

Major interest this quarter was centered on swage cladding. One of the most significant advances was made in swage cladding with high-strength and refractory metals. Another interesting concept reported, although not a cladding process, is the forming of spiral and ribbon-candy fuel assemblies from as-rolled composite sheets.

Millhollen[9] has made a series of out-of-reactor proof and acceptance tests developed for inspection of the Plutonium Recycle Test Reactor (PRTR) fuel assemblies. The fuel elements were 19-rod clusters of Zircaloy-clad swaged UO_2. The tests were designed to inspect both the individual fuel rods and the final fuel-rod clusters.

To determine whether hot swaging had any effect on hydrogen pickup in Zircaloy-4, several fuel rods were swaged both in air and under an argon blanket at Hanford.[10–12] These rods were then corrosion tested and examined for hydride precipitation. It was concluded that there was no noticeable effect of swaging on hydrogen pickup.

The swage cladding of UO_2 with high-temperature materials[11,12] is being investigated. The cladding materials of interest are Inconel X, Hastelloy F, and two niobium alloys (Fansteel-80 and -82). Samples containing −60-mesh fused UO_2 in Inconel X and Hastelloy F tubes have been hot swaged in the temperature range of 850 to 1200°C with no cladding ruptures. Initial attempts to swage Fansteel-80 were unsuccessful because of induction coil temperature limitations. Modifications are being made to permit operation in the 1400 to 1600°C range.

A U. S. patent on swaging wire fuel elements has been granted.[13] These fuel elements, measuring as small as 0.035 in. in diameter, were formed by encasing uranium rod in a Zircaloy sheath. This assembly was then coated with MgO, BeO, or ZrO_2 and encased in a steel tube. The entire assembly was then reduced to the desired diameter by swaging at 800 to 900°C. Finally, the steel and oxide were removed.

Forming procedures for producing spiral and ribbon-candy fuel elements from rolled composite sheets are being investigated by Nuclear Metals.[14–16] The spirals were formed by wrapping the sheet around a circular mandrel. Spacing was maintained by a series of dimples pressed into the fuel plate. Since there is a possibility that hot spots may develop in these dimples, a current investigation deals with a procedure whereby plates consisting of unfueled areas for dimpling are rolled.

A ribbon-candy fuel element was also being investigated as a potential fuel-element subassembly. The composite fuel plates were first bent to a 30° included angle. The plates were brought parallel by pinching the bends in a pinch die. Spacing was maintained by dimpling the plates. (H. D. Hanes)

Pressure Bonding

The term pressure bonding, or isostatic bonding, refers to a process that involves the use of gas pressure at an elevated temperature. Materials to be bonded or compacted are sealed in an evacuated container. The sealed assembly is subjected to an external gas pressure at an elevated temperature. The process is essentially an ideal hot-pressing operation and has been effectively utilized for the bonding and joining of reactor components and for the

densification of ceramic, cermet, and dispersion fuels.

The simultaneous densification and cladding of UO_2 is being investigated at Battelle and Sylvania.[17–20] Sylvania has completed work on its low-cost fuel-element program and is preparing a topical report. A similar program at Battelle is being continued to fabricate stainless-steel-clad specimens for irradiation testing in the Vallecitos Boiling-Water Reactor (VBWR). Evaluation of GE and superactive type ceramic oxides is continuing. The best ceramic oxide will be mixed in various proportions with fused oxides to produce, after pressure bonding, a density of 98 per cent of the theoretical density.

Other studies at Battelle have demonstrated[19] that beryllium can be successfully joined by gas-pressure bonding at 1500 to 1650°F and 10,000 psi for 4 hr. Also being investigated is the basic mechanism of pressure bonding. The prior history, crystal structure, surface roughness, and efficiency of vacancy sinks are being evaluated.[20] (E. S. Hodge)

Canning

A Belgian patent[21] describes the canning of a 5 to 15 wt.% UC or PuC fuel using a mixture of SiC and silicon pressed onto the fuel rod as a protective barrier layer. Several layers can be used to form a metallic bond with the fuel. Another Belgian patent[22] describes a fuel-element-canning operation in which a can is extrusion clad by passing it through a die that forces the can into contact with the fuel. The canning material is first heated, and the entire operation requires an inert atmosphere. Bonding between the can and element is achieved by the use of a liquid or solid phase introduced during the extrusion operation. Fuel elements produced in this manner show no change in size or shape from the original fuel and cladding dimensions.

Investigators at Worcester Polytechnic Institute have been concerned with studies to determine the feasibility of cladding uranium with zirconium by direct casting.[23] The process would have molten zirconium in contact with molten uranium throughout a thin interface. Solidification should then result in a metallurgical bond, thereby permitting fabrication by simply casting the zirconium and uranium into appropriate shapes. Such a process would represent a considerable cost savings by the elimination of expensive machining and fabrication operations.

Preliminary exploratory studies were devoted to aluminum-copper and copper-steel components. No bonding could be achieved between the aluminum and copper. The formation of a brittle intermetallic phase at the interface was believed to have impeded bonding. Copper and steel composites were then investigated because their melting-temperature range approximates that of uranium and zirconium. Also, no intermetallic phases were expected with this binary system. Bonding was achieved with these materials, and it was found necessary to melt only one of the components. The use of a flux was helpful in preventing oxidation at the molten interface; clean surfaces were necessary for the mating surfaces to bond. The interface remains straight if one of the metals is held solid or maintained in the solid state. When both metals are molten at the interface, the steel erupts into the copper.

Future bimetallic casting studies using uranium and zirconium are planned on the basis of the favorable results of the preliminary work. The metals will be melted in vacuum under better-controlled conditions than have previously been used.

Fuel-development studies for EBR-II core 2 have continued at Argonne.[24] Previous investigations have resulted in the uranium–20 wt.% plutonium–10 wt.% fissium alloy being chosen as the reference fuel. Materials being considered for cladding the fuel are vanadium, steel, niobium, niobium–1 wt.% zirconium, Inconel X, and type 304 stainless steel. A 0.0005-in.-thick vanadium barrier layer is being used with the Inconel X and type 304 stainless-steel specimens. Development work is now under way on the fabrication of tubing from the above-mentioned cladding materials.

Twenty-one 2-in.-long pin specimens have been jacketed and sodium bonded into niobium, niobium–1 wt.% zirconium alloy, vanadium, Inconel X, and type 304L stainless-steel jackets for irradiation testing. To prevent alpha contamination of the jackets, a disposable polyethylene loading funnel was inserted into the jacket tubes, and the plutonium-containing pins were dropped through this funnel onto the solid sodium at the bottom of the tubes. The sodium was melted, and end plugs were fusion welded to the jacket materials.

Only one specimen required decontamination. Leak detection was accomplished by the mass-

spectrometer method. X-ray and eddy-current inspection revealed an improper sodium level in two specimens, a displacement of the vanadium barrier foil in one specimen, and a bond void in another specimen.

Studies in France[25] have been concerned with the use of sintered aluminum powder (SAP) as a canning material. There are three essential problems associated with this application for SAP material: (1) diffusion of fission products into SAP; (2) the appearance of postules and cracks from prolonged heating, giving rise to leakage paths; and (3) the implications for using SAP to supply all the mechanical support in a fuel element.

The behavior of fuel elements in unsupported cans at a given temperature, when submitted to a uniform external pressure, is a criterion for selection. Only creep stresses are of concern in an unsupported fuel can because there would be no bond between fuel and cladding to produce thermal stresses. Creep data for SAP material between 400 and 500°C indicate that its creep strength is comparable to that of beryllium. (E. G. Smith)

Nonelectrolytic Chemical-Plating Techniques

A British patent describes[26] the formation of protective metallic coatings for chromium-plated uranium by immersion in molten aluminum, aluminum–12 wt.% silicon, zinc–1 wt.% aluminum, or zinc–5 wt.% aluminum, with or without flux. The formation of WSi_2 coatings on tungsten by immersion in molten copper-silicon alloy, by pack siliconizing, and by hydrogen reduction of $SiCl_4$ was investigated.[27,28] Similar immersion coatings also can be produced on molybdenum.[29] Effort is being made to improve a current commercial pack process for forming proprietary protective coatings on molybdenum.[30]

Epitaxial films of silicon of controlled thickness and electronic behavior can be grown on single-crystal silicon substrates at 1270°C by hydrogen reduction of $SiCl_4$ to which appropriate amounts of PCl_3 or BBr_3 have been added.[31]

A general treatment of an iodide chemical-vapor-deposition process for metal refining was presented in which the complex relations among the various parameters involved in the process were demonstrated.[32] This development permits correlation of metal yield, duration of run, deposition rate, and power losses in closed-cycle Van Arkel–de Boer systems for which the change in dimensions of the deposition surface, as a result of metal deposition, significantly affects the diffusion path between deposit and feed and the heat loss from the deposition surface.

Methods used to purify $MoCl_5$ for subsequent use in chemical-vapor deposition of molybdenum were described.[33] Work was continued on the formation of vapor-deposited tungsten coatings on refractory nonmetallic substrates (e.g., BeO).[34]

The deposition of pyrolytic graphite at 2400°C from an atmosphere containing 5 per cent methane was recently investigated.[35] Experimental evidence was presented by Diefendorf[36a] indicating the relative importance of the gas phase and surface reactions as well as the influence of the substrate on the deposition of pyrolytic graphite. Modification of the properties of pyrolytic graphite by the addition of metal alloying elements can be accomplished by vapor-deposition techniques.[36b] Hirt and Palmer[36c] have reported that very pure C_3O_2, at low concentration in pure helium carrier gas, decomposes at a useful rate at temperatures between 600 and 800°C to produce a tenacious and hard polycrystalline carbon film on a glazed porcelain surface. Other research presented recently deals with the deposition of pyrolytic carbon on heated graphite rods and in the pores of bonded and unbonded carbon powders.[36d,36e]

Conditions for the deposition of stoichiometric TaC, NbC, and HfC coatings from halide-methane atmospheres were established by High Temperature Materials.[37,38] The Knoop hardness of stoichiometric NbC is 2600 to 2800, whereas that of HfC is 2700 to 2900.

A U. S. Patent[39] was issued describing conditions for the formation of carbide coatings on graphite by chemical-vapor deposition.

(E. M. Sherwood)

Electroplating

In a study of diffusion-bonding processes for fabricating PWR plate type fuel elements, chemical displacement (immersion) coatings for Zircaloy were investigated at Bettis.[40] The continuity of adherent displacement coatings of copper was greatly improved by high agitation rates, which also accelerated plating rates. Surface smoothness had less influence on the continuity of the coating when specimens were

rapidly agitated or when the solution was pumped at high speed over the specimen surfaces. Uniform deposits of 0.15 and 0.2 mil were produced in 8 and 10 min, respectively, in copper nitrate–hydrofluoric acid solutions. Although displacement coatings of iron were improved in continuity, adherence, and uniformity by introducing rapid agitation and by adding sodium acetate to the ferric chloride–hydrochloric acid solutions, adherence and continuity were not so good as they were for the copper coatings. Composites of copper and iron were judged satisfactory, but copper-tin composites were poorly adherent.

During research at Battelle,[19] electroplating facilitated joining operations for thorium and uranium. Thorium was successfully joined to thorium and uranium by soldering after electroplating with nickel, copper, and tin. Uranium was joined to uranium by silver brazing after plating with nickel and copper, but brazing temperatures (<1100°F) caused bond failures between nickel and thorium when electroplated thorium was joined by silver brazing. Neither soldered nor brazed joints imposed galvanic couples that affected corrosion resistance adversely.[20]

Electrodeposits of thorium and neptunium on aluminum were reported by Russian researchers.[41] In a solution of thorium nitrate, water, and ethyl alcohol, layers of Th^{230} and Np^{237} with a thickness of 1 mg/cm^2 (30 μin. for thorium) or more were obtained by "repeated electrolytic deposition." The deposition rate was favored by high current densities and high concentrations of thorium nitrate. No X-ray or other data were offered to show that the deposits were metallic, although metal oxide deposits are a possibility.

An account[42] of the improvement in accuracy and life that is obtained by chromium plating high-velocity gun barrels summarizes the results of an engineering study that produced information useful in the conduct of any investigation of electroplating for improving the surface properties of engineering materials. Unlike many investigations, the Bureau of Standards researchers utilized previously known data on the properties of chromium plate to demonstrate optimum plating conditions for maximum performance. Desirable and undesirable properties of different kinds of chromium plate and their effect on gun-tube performance were taken into account at an early stage in the investigation. This rudimentary, but important, procedure is too often bypassed in the conduct of other research investigations.

Two new bibliographies on electroplating references have been compiled. One bibliography[43] on chromium and nickel electroplating contains 461 references for the period from 1955 to 1959. The other includes 400 references during the period of 1950 to 1960 on metal coatings.[44] (W. H. Safranek)

Ceramic Coatings

In a program to develop plate type UO_2 fuel elements using plasma-jet spraying techniques, ATL[45] has applied coatings of calcium-stabilized zirconia and UO_2. Coatings of the latter, having 87 per cent of the theoretical density and oxygen-to-uranium ratios of nearly 2.00, have been deposited regularly with efficiencies of about 40 per cent. To date, the best results have been obtained with –200 +325-mesh fused UO_2. A major problem is the preparation of the substrate. Various techniques are being tried. (B. W. King)

Welding and Brazing

The current status of mechanical joining and welding was appraised by a Materials Advisory Board subpanel assigned the subject of joining refractory sheet metals.[46] Specific comments related to various joining processes and to the joining of specific types of materials are discussed. The materials covered are molybdenum and its alloys, tungsten, niobium alloys, and tantalum and its alloys. Four specific recommendations are presented in the report: (1) to support a program to define laboratory mechanical tests suitable for simulating various severities of service that refractory-metal joints must sustain; (2) to include in future alloy-development programs a minimum-weldability test at a much earlier stage in the alloy-development program (the minimum-weldability test suggested is a longitudinal-weld tensile specimen); (3) a study of brazing or braze-welding techniques in which high-remelt-temperature development would be emphasized; (4) a basic study to evaluate joining processes that involve the composite use of pressure, time, temperature, and relative movement.

An Air Force-supported program to investigate the physical metallurgy of joining tungsten

and niobium at General Electric is continuing.[47] Recent work has included studies of fusion welding of tungsten, the physical metallurgy of welds in tungsten and tungsten-base alloys, and the brazing of niobium and tungsten. Further studies have been made of the welding characteristics of powder-metallurgy and electron-beam-melted tungsten sheet. Welds have been made by the inert-gas-shielded tungsten-arc process and by the electron-beam process. These studies have confirmed that the removal of weld surfaces increases the ductility of tungsten weld joints. Electron-beam welds made on powder-metallurgy tungsten sheet have shown considerable gas evolution. This gas evolution leads to porosity in the weld metal. Effort in the physical-metallurgy field has been concentrated on studies of the deformation properties of electron-beam-melted and powder-metallurgy sheet, fracture mechanisms in arc weldments, and the recrystallization and grain-growth characteristics of several dilute tungsten alloys. The brittle-ductile bend transition temperature of both types of sheet in the recrystallized condition occurs in the range of 200 to 225°C. Weldments made in powder-metallurgy sheet have a bend transition temperature about 25 to 50°C higher than that of the recrystallized material. Of the various alloy additions that have been evaluated, an addition of 0.03 per cent boron has proved to be effective in retarding grain growth.

The brazing studies to date have been concerned primarily with a screening evaluation of various potential alloys. Alloys with melting ranges of 2100 to 2500°F for use on niobium or niobium alloys have been identified. Other alloys with melting ranges between 3000 and 3500°F have been identified for brazing niobium alloys such as F-48. Definite selection of the best brazing alloys to be used in more extensive studies has not been made as yet.

A "cold-wall" vacuum furnace utilizing tantalum heating elements is being used to develop brazing materials and procedures for refractory metals.[48] The furnace has a work space equal to a 1-ft cube and is capable of attaining temperatures as high as 4500°F. No ceramics or nonmetallic materials that get hot are used in the chamber. Consequently the low pressure necessary (1×10^{-6} mm Hg) for the 4500°F operating temperature can be maintained. Temperature measurement is by tungsten-rhenium thermocouple insulated with beryllium oxide and sheathed with tantalum. Several niobium alloys have been studied in conjunction with several brazing alloys. Most of the work was on the niobium–33 wt.% tantalum–0.7 wt.% zirconium alloy. The following five brazing materials were studied:

Material	Brazing temp., °F
Palladium	2900
Platinum	3300
Titanium	3300
90 wt.% platinum–10 wt.% iridium	3300
90 wt.% platinum–10 wt.% rhodium	3450

All these materials work well, with the exception of the 90 wt.% platinum–10 wt.% rhodium alloy, which erodes seriously and produces brittle joints. Pure titanium gave the best results as a brazing filler metal for use with the niobium–33 wt.% tantalum–0.7 wt.% zirconium alloy. It produced a strong ductile joint, but some base-metal solid-solution alloying between the titanium and the niobium-base parent metal did occur. Shear strengths of lap joints having an area of 0.08 sq in. brazed with titanium at 3300°F ranged downward from about 7000 psi at room temperature to 1000 psi at 2600°F and 300 psi at 3000°F.

Two bibliographies covering ultrasonic welding literature were recently published.[49,50] The bibliography prepared by Lockheed[6] is annotated and covers 58 references from the unclassified literature for the period from 1958 to 1960.

(R. E. Monroe)

Explosive Forming

A paper describing a technique developed for compacting metal powders by the use of detonating explosives has been prepared by Montgomery and Thomas.[51] Several metal powders, including W-titanium (a granular titanium obtained by the sodium reduction process), aluminum, copper, iron, and steel, have been compacted during their experimentation. These metal powders were compacted by placing the powder in a waterproofed thin-walled aluminum tube, wrapping a continuous spiral of Cordtex detonating fuse around the aluminum container, immersing the container and charge in a suitable water bath, and detonating the charge. In this manner the powders were successfully com-

pacted into cylindrical type shapes as large as 4½ in. in diameter and up to 20 in. long. Hexagonal and fluted cross-section cylinders were also successfully compacted. A study is also being conducted to include the explosive compaction of nonmetals such as graphite and to modify the technique to permit the compaction of tubular shapes.

Table V-1 gives some of the results obtained during this investigation. Note that the explosively compacted densities were near theoretical in most cases. During this testing, it was also found that effective compaction was related to the initial particle size of the metal powders.

Table V-1 COMPACTING OF METAL POWDERS BY DETONATING EXPLOSIVES[51]

(Container for Metal Powder: 17.5 × 5.5 Cm in Diameter; 100 Per Cent of Metal Powders Passed 69 SB Sieve)

Weight of explosive, g	Metal powder	Bulk density of metal powder, g/cm³	Weight of metal powder, g	Weight of metal powders: weight of explosive	Av. dia. of compacted mass, cm	Density of solid metal, g/cm³	Av. density of compacted mass	
							G/cm³	Per cent of theoretical density
60.3	W-titanium	1.53	675	11.2	3.5	4.5	4.0	88.9
59.9	Aluminum	1.29	575	9.6	3.8	2.7	2.7	100
130.5	Copper	5.25	2154	16.5	4.2	8.9	8.45	95
130.1	Iron	2.5	1080	8.3	3.2	7.9	7.65	96.8

The basic principles for the explosive compaction of metal powders have been established during this investigation; however, additional development will be required before the maximum potential of the process can be applied to any specific use in powder metallurgy. It is unlikely that explosive compaction will ever replace mechanical methods of powder compaction in areas in which satisfactory results are presently being obtained; however, in cases where mechanical methods are not adequate, explosives may prove to be a very useful tool. The principal advantage of explosive compaction is that much greater pressures are made available for compaction than are obtainable by conventional mechanical methods. The process may thus find considerable application in the compaction of rare metals and their alloys.

A report describing the explosive-forming process has been prepared by Polhemus.[52] The deformation process that takes place during explosive forming is described in terms of slip. The types of explosives and the forms in which they are available, as well as the uses of explosive metalworking, are discussed in this report.

A general review of explosive forming has also been prepared by Tardif.[53] The main variables involved in explosive forming, the materials and shapes formed, and the metallurgical and dimensional aspects of the process are discussed. The theories describing the mechanism of explosive forming and other explosive metalworking operations, such as hardening, welding, and powder compaction, are also reported.

Research is being conducted at Hanford[11] on the compaction of UO_2 powder by high-energy impact with a Dynapak machine. Experiments have been conducted for the purpose of simultaneously defining the roles of temperature, pressure, and oxygen-to-uranium ratio on the high-energy impaction of UO_2. Densities and oxygen-to-uranium ratios of these specimens have been determined. Preliminary indications are as follows:

1. In the 1000 to 1200°C temperature range at 500,000 psi, temperature has very little effect; however, as pressures are decreased and oxygen-to-uranium ratios are increased, higher temperatures tend to result in higher densities.

2. Greater initial oxygen-to-uranium ratios (in the oxygen-to-uranium ratio range of 2.01 to 2.26) result in greater UO_2 density.

3. The pressure requirement for compacting uranium dioxide to ≥ 99 per cent of the theoretical density may be as low as 400,000 psi. This may be accomplished under controlled conditions of temperature and oxygen-to-uranium ratio in a conventional impact die using a carbide punch instead of the more complicated, modified Bridgman anvil apparatus.

Electrodeposited UO_2 crystals of approximately −28 +48 mesh have been compacted by high-energy impact at 1100°C and 500,000 psi to 10.88 g/cm^3 (99.2 per cent of the theoretical density). Photomicrographs and electron micrographs of the compacted UO_2 revealed that extensive plastic deformation of the crystals had occurred.

Micronized UO_2 − 0.5 wt.% TiO_2 and micronized UO_2 − 0.1 wt.% TiO_2 have been high-energy impacted at 1100°C and 500,000 psi to densities of 97.3 and 97.8 per cent of the theoretical density, respectively. Photomicrographs of the compacted UO_2 revealed that no reaction, such as the formation of a liquid eutectic phase that lowers the sintering temperature of these mixtures, had occurred between the TiO_2 and UO_2.

Thoria, alumina, and a 50 wt.% $ThO_2-Al_2O_3$ mixture were compacted by high-energy impact at 1200°C and 500,000 psi to densities of 9.59 g/cm^3 (95.9 per cent of the theoretical density), 3.37 g/cm^3 (84.9 per cent of the theoretical density), and 6.33 g/cm^3 (90.0 per cent of the theoretical density), respectively.

Uranium monocarbide, fused and crushed to −6 mesh, has also been compacted by high-energy impact at 1200°C and 500,000 psi to a machinable solid possessing a density of 13.28 g/cm^3 (97.4 per cent of the theoretical density).

The design, operation, capabilities, and limitations of the pneumatically actuated Dynapak machine are described in a report prepared by Reimann.[54] The report contains a detailed description of the operational features of the Dynapak, with particular emphasis on the functional relation of components during the firing cycle. A general comparison is made between standard high-energy equipment and the high-energy-rate Dynapak. The application of basic extrusion theory to high-energy-rate extrusion also is described. Particular emphasis is placed on the energy requirements necessary to extrude a given volume of material at various reduction ratios and on the conditions that produce inertial separation. (C. C. Simons)

Nondestructive Testing

Ultrasonic Techniques

Many factors complicate the establishment of acceptance standards for ultrasonic nondestructive testing (NDT). The work of Sinclair and Nanda at the Electric Boat Company[55] to develop tentative acceptance standards for butt weldments in ship plate which would be approximately equivalent to the standards established by radiographic inspection demonstrated this fact. An ultrasonic standard sensitive enough to reject cracks of the size rejected by radiography was not sensitive enough to reject equally objectionable inclusions and porosity. Sinclair and Nanda used a $\frac{3}{8}$-in.-diameter, 2.25-Mc, 45° angle-beam search unit. The instrument-sensitivity and flaw-acceptance levels were established with reference to a $\frac{1}{16}$-in.-diameter by $\frac{1}{2}$-in.-deep hole in a 1-in.-thick HY-80 (80,000-psi yield strength) steel plate. They could not establish separate standards for each type of defect because it was impossible to determine with confidence the type of flaw from the pattern of the ultrasonic signal.

Oak Ridge[56] is using a through-transmission method of inspecting for nonbond areas in duplex tubing, consisting of an inner niobium tube and an outer stainless-steel tube bonded together with copper. Two probes have been constructed to evaluate two sizes of tubing: 0.250 and 0.315 in. in inside diameter. The probes consist of an ID transmitting crystal and an outside collimated receiving crystal in fixed reference to each other. A "B"-scan presentation of the circumference of the tube is used to simplify interpretation. The tube is rotated as the probes are moved longitudinally. Through transmission is not a new method of detecting nonbonded areas, but successfully applying the method to such small tubing as 0.250 in. in inside diameter in the manner described is an achievement.

Also, Oak Ridge[56] has successfully used the "ringing" technique to evaluate "can"-to-copper braze of a four-disk test section in which the can thickness seemed to be uniform. Very good correlation existed between indications of nonbond by ringing and destructive-test data. This technique is expected to be used in a full-scale boiler prototype.

Surface waves may be useful for detecting bond defects in ceramic coatings if the elastic properties of the coatings are not too different from the substrate, according to Armour Research.[57] However, poor results were obtained using this method with zirconium oxide coatings.

Armour's[57] intermodulation method of detecting bond defects appears to be promising. In this method a low-frequency continuous wave (approximately 14 kc) and a high-frequency

continuous wave (5 to 10 Mc) are transmitted in a direction normal to the bond area. If the ceramic-metal bond is defective in the region intersected by the high-frequency beam, the electrical output voltage is modulated at the frequency of the bond stress. The percentage of modulation, rather than the amplitude of the received signal, is used as indication of defective bonding. Thus variations in coupling normally encountered in scanning large areas will not mask variations due to defects.

The measurement of acoustic properties of solid-suspensoid systems is of interest in the field of nondestructive testing. Slurry- and gaseous-suspensoid core blanket and heat-transfer media present problems of settling, particle fracture, and agglomeration leading to operating problems involving fouling of heat-transfer surfaces, erosion of pump and valving equipment at elevated flow, and uncertainty concerning the concentration and form of the fuel in the core region. Aeroprojects[58] has been using a standing-wave-ratio method, which indicates changes in acoustic impedance, to determine concentrations of nickel-powder–water slurries. Although, supposedly, the method should be sensitive to concentrations of 3-μ nickel particles as low as 300 g/liter, Aeroprojects has been able to detect concentrations to only 1000 g/liter because of noise believed to be due to excess gas in the slurry and to interaction between their 20-kc source and the walls of the container.

Because an increase both in particle size and in concentration leads to increases in impedance ratios, poor discrimination has been obtained between the two. Methods of improving discrimination under study are (1) lowering the frequency to obtain measurements sensitive only to concentration and (2) seeking a relation between the velocity of sound and the concentration. In a measurement of the resonance frequency of the acoustic system between 800 and 1000 g/liter, the frequency changed about 200 cycles per 100 g/liter. Temperature effects were not reported. (D. Ensminger)

Magnetic, Eddy-Current, and Other NDT Techniques

A sensitive magnetic test[59] has been developed for the detection of iron particles in fuel powder. After the particles are magnetized in a strong magnetic field, which aligns their magnetic axes, they are detected with a sensitive magnetic field meter. No description was given of the type of meter used or the level of field strength involved. However, the laboratory setup has detected less than 200 ppm of residual particles in samples of production powder.

A unique method[59] for detecting discontinuities in chromium plate on boron stainless steel is described. An attempt is made to electroplate the part or specimen with copper. By using low voltage in a copper sulfate–sulfuric acid bath, the copper will selectively plate on the bare stainless steel. The results of the test are red (copper) colored indication on a white background. The test is extremely sensitive and will define the hairline cracks that are common in chrome plate. After inspection, the copper is removed by a brief rinse in mild nitric acid.

Some investigators of chromium plating[59] indicate that eddy-current tests are best for the measurement of plate thickness. They say that it can be measured to the nearest 0.0001 in. with a precision of ± 0.00002 in. The questions that always arise, of course, in such a sweeping statement relate to whether this holds true for all chromium plating or whether the base material contributes to the success of this particular application. No clarifying data were given.

A fiber optic camera[59] has been successfully applied to the inspection of channels in core assemblies. The pictures taken by the camera have shown that interpretable results can be expected from all channels in the core. Although some highlighting from the rib pattern of the blanket plates is still evident, it is sufficiently different in character from the appearance of corrosion products that it is readily interpreted.

The old problem of attempting to fabricate defects that will provide meaningful data for evaluating and calibrating nondestructive-testing equipment is being discussed and considered by many people. One group[60] has made arrangements with a vendor to fabricate artificial defects in Inconel tubing. These defects are being made in redraw stock by inflicting drilled holes, deep scratches, gouges, and etched notches prior to the final drawing operation. These samples will be used to evaluate electromagnetic and ultrasonic methods. This is certainly a step in the right direction. It will be necessary, of course, to provide some correlation between these fabricated defects and those occurring naturally in the Inconel tubing.

Electromagnetic testing of Inconel tubing has indicated a considerable electromagnetic "noise" that apparently clouds critical evaluation of this technique to detect defects. Tests with the Radac and new Magnetic Analysis Single Frequency Tester have shown that, although the instruments are less sensitive to the electromagnetic "noise" than Probolog, abrupt but minor tube-wall-thickness variations continue to produce large indications. These investigators doubt that signals from such variables as localized tube-wall repairs can ever be filtered out. (C. L. Seale)

References

1. R. Burgett (Ed.), Summary Technical Report for the Period January 1, 1961, to March 31, 1961, USAEC Report NLCO-826, National Lead Co. of Ohio, May 5, 1961.
2. A. R. Moss and D. T. Richards, The Arc Melting of Nb, Ta, Mo, and W, *J. Less-Common Metals*, 2(11): 405–425 (December 1960).
3. D. Pecher, Electron Beam Melting: What It Does for Metals, *Materials in Design Eng.*, 53(3): 101–106 (March 1961).
4. H. J. Henning and F. W. Boulger, Superalloy Forgings, Report DMIC-Memo-86 (PB-161236), Battelle Memorial Institute, Defense Metals Information Center, Feb. 10, 1961.
5. A. W. Dana, Jr., Cb and Cb Alloy Extrusion Program. Phase II: Billet Process Development, Interim Report II, Report AMC-TR-7-775 (II), E. I. du Pont de Nemours & Co., Inc., Feb. 6, 1961.
6. M. A. Pearcy (Comp.), The Fabrication of Mo—An Annotated Bibliography, Report SB-60-41, Lockheed Aircraft Corp., December 1960.
7. Knolls Atomic Power Laboratory, Nuclear Core Operation Manufacturing Engineering Quarterly Report for February 1–May 1, 1961, USAEC Report KAPL-2500-1, May 1961. (Classified)
8. Advanced Technology Laboratories, Div. of American-Standard, Investigations of the Technical Feasibility of Cold Extrusion for Zircaloy-2 Tubing Production, Quarterly Technical Progress Report for January–March 1961, USAEC Report ATL-A-119.
9. M. K. Millhollen, Out-of-Reactor Evaluation of Components and Assemblies—Mark I Swaged UO_2 PRTR Fuel Element, USAEC Report HW-66910, Hanford Atomic Products Operation, Sept. 1, 1960.
10. F. W. Albaugh, Reactor and Fuels Research and Development Operation Monthly Report for March 1961, USAEC Report HW-69062-A, Hanford Atomic Products Operation, Apr. 15, 1961. (Classified)
11. F. W. Albaugh, Reactor and Fuels Research and Development Operation Monthly Report for April 1961, USAEC Report HW-69408-A, Hanford Atomic Products Operation, May 15, 1961. (Classified)
12. F. W. Albaugh, Reactor and Fuels Research and Development Operation Monthly Report for May 1961, USAEC Report HW-69822-A, Hanford Atomic Products Operation, June 15, 1961. (Classified)
13. J. L. Zambrow, Method of Making Wire Fuel Elements, U. S. Patent 2,947,676.
14. Nuclear Metals, Inc., Fundamental and Applied Research and Development in Metallurgy, Progress Report for October 1960, USAEC Report NMI-2090, Nov. 21, 1961.
15. Nuclear Metals, Inc., Fundamental and Applied Research and Development in Metallurgy, Progress Report for December 1960, USAEC Report NMI-2092, Feb. 7, 1961.
16. Nuclear Metals, Inc., Fundamental and Applied Research and Development in Metallurgy, Progress Report for January 1961, USAEC Report NMI-2093, Mar. 20, 1961.
17. J. L. Zambrow, Quarterly Technical Progress Report for Period Ending June 30, 1960, USAEC Report SCNC-313, Sylvania-Corning Nuclear Corp., September 1960.
18. Sylvania-Corning Nuclear Corp., Informal Letter Progress Report for October 1960, USAEC Report TID-11065.
19. R. W. Dayton and C. R. Tipton, Jr., Progress Relating to Civilian Applications During April 1961, USAEC Report BMI-1514, Battelle Memorial Institute, May 1, 1961. (Classified)
20. R. W. Dayton and C. R. Tipton, Jr., Progress Relating to Civilian Applications During May 1961, USAEC Report BMI-1518, Battelle Memorial Institute, June 1, 1961. (Classified)
21. Fuel Elements for Nuclear Reactors, Belgian Patent 571,786 (to DEGUSSA), Oct. 16, 1957.
22. M. Gauthron and G. Beernaert (to Commissariat à l'Énergie Atomique), New Canning Process and Equipment, Belgian Patent 573,642, Dec. 19, 1957.
23. Worcester Polytechnic Institute, June 1961. (Unpublished)
24. Argonne National Laboratory, Reactor Development Program Progress Report, USAEC Report ANL-6343, March 1961.
25. C. Bridoux et al., Sintered Aluminum Powder as a Canning Material, *Nuclear Eng.*, 6(60): 189–192 (May 1961).
26. United Kingdom Atomic Energy Authority, Application of Metallic Coatings to Chromium-Plated Uranium Surfaces (to UKAEA), British Patent 858,301, Jan. 11, 1961.
27. C. G. Goetzel and P. Landler, Refractory Coatings for Tungsten, Report WADD-TR-60-825, New York University, Nov. 1, 1960.

28. C. G. Goetzel and P. Landler, Refractory Coatings for Tungsten, *Planseeber. Pulvermet.*, 9: 36–38 (April 1961).

29. K. Sedlatschek and H. J. Stadler, Refractory Coatings for Molybdenum, *Planseeber. Pulvermet.*, 9: 39–43 (April 1961).

30. H. Blumenthal and N. Rothmann, Development of a Powder and/or Gas Cementation Process for Coating Molybdenum Alloys for High-Temperature Protection, Second Quarterly Progress Report for WADD (October 1–December 31, 1960), Chromalloy Corp., Dec. 31, 1960.

31. H. Theuerer, Epitaxial Silicon Films by Hydrogen Reduction of $SiCl_4$, *J. Electrochem. Soc.*, 108(7): 649–653 (July 1961).

32. J. H. Oxley and J. M. Blocher, Jr., Mass and Heat Transfer During the Chemical Vapor Deposition of Metals, *J. Electrochem. Soc.*, 108(5): 460–464 (May 1961).

33. Alloyd Research Corporation, Research on Production of Ultrapure Molybdenum, Progress Report No. 3 for March 2–May 2, 1961, May 2, 1961.

34. F. W. Hoertel, Vapor Deposition of Tungsten on Graphite Rocket Nozzle Inserts, Monthly Progress Report No. 12, Bureau of Mines, April 1961.

35. J. D. Batchelor, Improvement of the Usefulness of Pyrolytic Graphite in Rocket Motors, Monthly Progress Report for March 20–April 20, 1961, Atlantic Research Corp., Apr. 26, 1961.

36. Fifth Biennial Conference on Carbon, Pennsylvania State University, University Park, Pennsylvania, June 19–23, 1961.
   a. R. J. Diefendorf, The Deposition of Pure Pyrolytic Graphite: II, Paper No. 12.
   b. B. Bovarnick, On the Establishment of Pyrolytic Graphite Alloys, Paper No. 18.
   c. T. J. Hirt and H. B. Palmer, Carbon Films from Carbon Suboxide Deposition, Paper No. 5.
   d. K. W. Corley-Macauly and M. Mackenzie, Studies on the Deposition of Pyrolytic Carbons, Paper No. 14.
   e. R. L. Bickerdike et al., The Deposition of Pyrolytic Carbon in the Pores of Bonded and Unbonded Carbon Powders, Paper No. 15.

37. High Temperature Materials, Inc., Pyrolytic Carbide Development Program, Monthly Progress Report for April 1961, Apr. 30, 1961.

38. High Temperature Materials, Inc., Pyrolytic Carbide Development Program, Monthly Progress Report for May 1961, Report NP-10374, May 31, 1961.

39. I. E. Campbell (to USAEC), Method of Obtaining Uniform Coatings on Graphite, U. S. Patent 2,978,358, Apr. 4, 1961.

40. C. R. Woods and T. R. Padden, Chemical Replacement Plating of Zircaloy, USAEC Report WAPD-238, Westinghouse Electric Corp., Bettis Atomic Power Laboratory, May 1961.

41. G. I. Khlebnikov and Y. P. Dergunov, Preparation of Thick Layers of Thorium, Uranium, Neptunium, Plutonium, and Americium, *At. Energ.*, 9(5): 406–408 (1960).

42. V. A. Lamb and J. P. Young, Plating Gun Bores, *Ordnance*, 725–727 (March–April 1961).

43. B. H. Nagel, Annotated Bibliography on Plating with Nickel and Chromium, Report AD-242211, Autonetics Div., North American Aviation, Inc., Feb. 10, 1960.

44. Office of Technical Services, Metal Coatings (1950–1960), OTS Selective Bibliography, Report SB-409.

45. Advanced Technology Laboratories, Div. of American-Standard, Development of Clad Ceramic Fuel Plates by Spray-Coating Techniques, Quarterly Technical Progress Report for January–March 1961, USAEC Report ATL-A-117.

46. National Research Council Materials Advisory Board, Joining of Refractory Sheet Metals, Report MAB-171-M, Mar. 20, 1961.

47. W. H. Kearns et al., Investigation of the Physical Metallurgy of Joining Tungsten and Columbium, preliminary information under Air Force Contract No. 33(616)-7484, General Electric Co.

48. M. M. Schwartz, Brazing of Sandwich Structures of Columbium Alloys, *Welding J.*, 40(4): 377–382 (April 1961).

49. G. I. Chandler, Literature Search on Ultrasonics in Welding and Other Ultrasonic Joining Processes, Report AD-242215, Autonetics Div., North American Aviation, Inc., Apr. 15, 1960.

50. M. A. Pearcy (Comp.), Ultrasonic Welding—An Annotated Bibliography, Report SB-61-2, Lockheed Aircraft Corp., February 1961.

51. W. T. Montgomery and H. Thomas, The Compacting of Metal Powders by Explosives, *Powder Met.*, No. 6: 125–128 (1960).

52. F. C. Polhemus, Explosive Forming of Metals, USAEC Report TID-12501, Union Carbide Nuclear Co., Y-12 Plant, Mar. 24, 1961.

53. H. P. Tardif, High-Energy-Rate Forming of Metals, Canadian Report CARDE-TM-290/59, Aug. 3, 1959.

54. G. A. Reimann, High-Energy-Rate Extrusion, Interim Technical Progress Report No. 1 for the Period September 23, 1960 to January 23, 1961, Report ASC-TR-7-882 (I), Westinghouse Electric Corp., Materials Manufacturing Dept., February 1961.

55. N. A. Sinclair and M. M. Nanda, Ultrasonic Inspection of Submarine Steel Weldments, *Nondestructive Testing*, 19(1): 58–64 (January–February 1961).

56. R. W. McClung, Oak Ridge National Laboratory, July 1961. (Unpublished)

57. W. E. Lawrie, Ultrasonic Methods for Nondestructive Evaluation of Ceramic Coatings, Report WADD-TR-61-91 (Pt.1), Illinois Institute of Tech-

nology, Armour Research Foundation, Feb. 23, 1961.
58. Aeroprojects, Inc., February 1961. (Unpublished)
59. Westinghouse Electric Corp., Bettis Atomic Power Laboratory, Pressurized-Water Reactor (PWR) Project, Technical Progress Report for the Period February 24 to April 23, 1961, USAEC Report WAPD-MRP-91.
60. Westinghouse Electric Corp., Bettis Atomic Power Laboratory, Materials — Technical Progress Report for the Period March 26 to June 25, 1961, USAEC Report WAPD-MRK-10. (Classified)

Index | *VOLUME 4*

Included in this issue is the index for Volume 4 of *Reactor Core Materials*. Future indexes for this quarterly will be prepared annually and will appear in the final (Number 4) issue. Here the bold numbers denote issues, and the other numbers denote pages.

A

Adhesive bonds, ultrasonic testing, **2**: 60
Alfenol, corrosion, **1**: 41
Alkali halides (irradiated), fission-fragment tracks, **3**: 33
  Frenkel defects, **2**: 37
Alkali metals
  See Metals (alkali)
Alloys
  See also specific alloys
  casting, **2**: 51; **3**: 52
  degassing, **2**: 51
  diffusion bonding, **1**: 65–6
  electron-beam applications, **2**: 51
  explosive forming and working, **3**: 60–3
  melting, **2**: 51; **3**: 52
  nondestructive testing, **3**: 64
  welding, **3**: 60; **4**: 56
Alloys (302, 406, 406(Mod.), 410, 430), corrosion, **1**: 41
Alloys (brazing), corrosion, **1**: 41–2, 45
  flow properties, **1**: 24–5
Alloys (irradiated), damage, **3**: 35; **4**: 40
  fission-product slowing, **4**: 41
  phase transformations, **3**: 35
  surface effects, **3**: 32
Alloys (ordered) (irradiated), damage and recovery, **3**: 34
Alloys (powder metallurgical), corrosion and tensile strength, **1**: 49
Alloys (structural) (irradiated), effects, **1**: 58
Aluminum, bonding, **4**: 53
  cladding corrosion, **3**: 4
  coating corrosion, **3**: 3
  corrosion, **1**: 42; **4**: 33–4
  diffusion in U, **3**: 2
  diffusion in UAl_4, **1**: 52
  manual, **1**: 49
  mechanical properties, **1**: 49
  Ni diffusion, **1**: 53
  nondestructive metallography, **3**: 22
  nuclear applications, **1**: 49
  phase studies, **1**: 49
  physical properties, **1**: 49
  plating of U, **2**: 60; **3**: 58
  self-diffusion, **3**: 44
  ultrasonic roll bonding, **3**: 53
  U diffusion, **1**: 53
  Xe diffusion, **2**: 45–6
Aluminum (irradiated), C-ion energy loss and ranges, **3**: 32
  damage annealing, **3**: 31
  damage recovery, **2**: 35
  density, **4**: 38
  effects, **1**: 53–5; **2**: 36; **4**: 41
  fission-fragment stopping, **4**: 41
  fission-fragment tracks, **2**: 13
  He release, **1**: 52
  O-ion energy loss and ranges, **3**: 32
  X-ray lattice parameter and line breadth, **4**: 38
Aluminum (molten), reactions with water, **1**: 17; **3**: 30; **4**: 36
Aluminum (Np-coated), preparation, **4**: 55
Aluminum (Th-coated), preparation, **4**: 55
Aluminum (Ti-coated), chemical plating, **3**: 57
Aluminum alloy (1S) cladding, extrusion, **2**: 56
Aluminum alloy dispersions, corrosion and tensile strength, **3**: 38
Aluminum alloys, corrosion, **1**: 41; **4**: 33–4
  extrusion, **3**: 38–9
  nondestructive metallography, **3**: 22
  strength, **1**: 49
  tensile strength, **1**: 41
  ultrasonic roll bonding, **3**: 53
Aluminum alloys (irradiated), effects, **4**: 41

Aluminum alloys (356) (irradiated), tensile properties, **3**: 36
Aluminum alloys (1000 A) (irradiated), damage, **4**: 39
Aluminum alloys (1100), corrosion, **1**: 44–5
tensile strength, **2**: 10
Aluminum alloys (2024), **3**: 38–9
Aluminum alloys (2024) (irradiated), tensile properties, **3**: 36
Aluminum alloys (3003), **3**: 38–9
Aluminum alloys (5083), **3**: 38–9
Aluminum alloys (6061) (irradiated), tensile properties, **3**: 36
Aluminum alloys (7075), **3**: 38–9
Aluminum alloys (A-288), corrosion, **4**: 33
Aluminum alloys (M-257 and M-388) (irradiated), tensile properties, **4**: 43
Aluminum alloys (X-8001), corrosion, **2**: 32; **4**: 33
Aluminum alloys (X-8001)–dysprosium oxide dispersions, development, **2**: 30
Aluminum-beryllium-germanium-silver alloys, density, **3**: 20
ductility, **2**: 18
elasticity, **3**: 20
plastic deformation, **3**: 20
strength, **3**: 20
Aluminum-boride dispersions, compatibility, **3**: 26
Aluminum–boron carbide dispersions, corrosion, **2**: 30
Aluminum-boron-gadolinium-oxygen-uranium system (irradiated), effects, **1**: 6–7
Aluminum-boron-uranium alloys (irradiated), effects, **1**: 6–7
Aluminum-boron–uranium oxide dispersion fuels, development, **1**: 11
Aluminum-carbon-uranium system, phase studies, **2**: 8
Aluminum-chromium-iron alloys, corrosion, **1**: 41
Aluminum-chromium-iron-molybdenum-nickel-titanium-tungsten alloys, (D-979), creep properties, **1**: 48
Aluminum-chromium-tantalum-titanium alloys, oxidation, **1**: 43
Aluminum-copper alloys (irradiated), atomic mobility, **3**: 33
Aluminum-copper-magnesium-zirconium alloys, extrusion, **3**: 38–9
recrystallization, **3**: 38–9
Aluminum-Fiberglas dispersion fuels, fabrication, **1**: 10
tensile strength, **1**: 10; **2**: 10
Aluminum-Fiberglas-uranium dispersion fuels, fabrication, **2**: 10
Aluminum-Fiberglas–uranium oxide dispersion fuels, development, fabrication, and tensile strength, **3**: 6–7
Aluminum foils (irradiated), lattice constants, **4**: 39
Aluminum-gadolinium-oxygen-uranium system (irradiated), effects, **1**: 6–7
Aluminum-iron alloys, ductility, **2**: 43
Aluminum-iron alloys (irradiated), annealing and magnetic properties, **3**: 33
Aluminum-iron dispersions, corrosion, **2**: 32–3
Aluminum-iron-nickel alloys, corrosion, **2**: 32; **4**: 34
Aluminum-iron-nickel dispersions, corrosion, **2**: 32–3
Aluminum-iron-titanium alloys, corrosion and mechanical properties, **2**: 33
Aluminum-iron-zirconium alloys, corrosion and mechanical properties, **2**: 33
Aluminum-lithium alloys (irradiated), He precipitation, **4**: 39–40
Aluminum-magnesium alloys (irradiated), internal friction, **4**: 39
Aluminum-magnesium couples, ignition, **3**: 29
Aluminum-magnesium-manganese-zinc alloys (AZ31), corrosion, **1**: 44
Aluminum-molybdenum-nickel alloys, phase studies, **1**: 50
Aluminum-molybdenum-tin-zirconium alloys, fabricability and tensile properties, **1**: 47
Aluminum-molybdenum-uranium alloy fuels (Al-clad), pressure bonding, **2**: 54
Aluminum-molybdenum-uranium alloys, **1**: 3–4
Aluminum-molybdenum-zirconium alloys, creep and impact properties, **2**: 46
Aluminum-nickel alloys, corrosion, **1**: 41
diffusion bonding, **1**: 65
Aluminum-nickel alloys (M-388) (irradiated), corrosion, **1**: 41
Aluminum-nickel cladding, Xe diffusion, **2**: 45–6
Aluminum-nickel compounds, solubility in Mo-Ni-Si alloys, **1**: 50
Aluminum-nickel diffusion couple, analysis, **3**: 44
Aluminum-nickel dispersions, corrosion, **2**: 32–3
Aluminum-nickel-plutonium alloys, corrosion, **1**: 8; **3**: 5–6
Aluminum-nickel-plutonium-silicon system, corrosion, **1**: 8; **3**: 5–6
Aluminum-nickel-plutonium-titanium alloys, corrosion, **3**: 5–6
Aluminum-nickel-silicon system, corrosion, **2**: 32
Aluminum-niobium alloys, phase studies, **1**: 50
tensile properties, **1**: 48
Aluminum-niobium-titanium alloys, oxidation, **3**: 28
Aluminum-niobium-vanadium alloys, corrosion, **1**: 43
Aluminum oxide, Cr and Fe diffusion, **2**: 45
reaction with PuO_2, **1**: 15
Aluminum oxide (irradiated), effects, **1**: 55–6
surface heterogeneity, **2**: 37
Aluminum oxide coatings on UO_2, **1**: 67–8; **2**: 59; **3**: 57–8
Aluminum oxide powder, explosive compaction, **4**: 58
Aluminum oxide powder (Ni-coated), preparation, **2**: 58
Aluminum oxide–thorium dioxide powder, explosive compaction, **4**: 58

Aluminum oxide–uranium dioxide dispersions, phase studies and UO_2 migration, **2**: 7
Aluminum oxide–uranium dioxide system, phase studies, **1**: 14
Aluminum-oxygen-uranium system, phase studies, **3**: 11; **4**: 3
Aluminum-plutonium alloy fuels [Al alloy (X-8001)-clad], coextrusion, **3**: 55–6
Aluminum-plutonium alloys, corrosion, **1**: 8; **3**: 5–6
density, **2**: 4
extrusion, **3**: 53
hardness, **2**: 4
heat-treatment effects, **4**: 3
injection casting, **3**: 52
linear coefficient of expansion, **2**: 4; **3**: 5
load capacity, **4**: 3
reaction with Zircaloy-2, **3**: 5
Aluminum-plutonium alloys (irradiated), effects, **1**: 8; **4**: 3
Aluminum-plutonium-oxygen compounds, crystallography, **3**: 13
melting point, **1**: 15
Aluminum-plutonium-silicon system, corrosion, **1**: 8; **3**: 5–6
Aluminum-plutonium-uranium alloys, corrosion, **1**: 8
Aluminum-plutonium-zirconium alloys, corrosion, **1**: 8; **3**: 5–6
Aluminum powder, explosive compaction, **4**: 56–7
Aluminum powder (sintered), canning applications, **4**: 54
Aluminum-silicon system cladding, extrusion, **2**: 56
Aluminum-silicon-tantalum-titanium system, oxidation, **1**: 43
Aluminum-tantalum-titanium alloys, oxidation, **1**: 43
Aluminum-thorium alloys, diffusion bonding, **1**: 66
Aluminum-thorium compounds, corrosion, **2**: 5; **3**: 13
density, **2**: 5
hardness, **4**: 5
Aluminum-thorium-uranium alloys, hot hardness, **1**: 10
Aluminum-thorium-uranium compounds, corrosion and density, **2**: 5
hardness, **4**: 5
Aluminum-tin-uranium alloys, **1**: 7
Aluminum-tin-zirconium alloys, fabricability, **1**: 47
Aluminum tubing, nondestructive testing, **1**: 73
Aluminum-uranium alloys, diffusion, **2**: 45; **4**: 3
diffusion bonding, **1**: 65
fabrication, **1**: 11
properties, **4**: 3
Aluminum-uranium alloys (Al-clad), rolling, **1**: 65
Aluminum-uranium alloys (irradiated), effects, **1**: 6–7
Aluminum-uranium alloys (molten), reaction with water, **3**: 30
Aluminum–uranium carbide dispersion fuels, development, **2**: 10
Aluminum-uranium compounds, Al diffusion, **1**: 52
Aluminum–uranium dicarbide dispersion fuels, corrosion, **1**: 11
Aluminum–uranium oxide dispersion fuels, development, **1**: 11
reactions, **1**: 11
ultrasonic roll bonding to Al, **3**: 53
Aluminum–uranium oxide dispersion fuels (Al-clad), development, **2**: 9–10
rolling, **1**: 65
Aluminum–uranium oxide dispersion fuels (irradiated), effects, **1**: 11
Aluminum–uranium sulfide dispersion fuels, development, **2**: 10
Aluminum-uranium-zirconium alloys, **1**: 7
Argon, diffusion in graphite, **2**: 46

B

Barium (irradiated), vacancy relaxation, **1**: 56
Barium oxide, diffusion in graphite, **2**: 46
Barium oxide–uranium dioxide system, phase studies, **4**: 12
Barium plutonium oxide, crystallography, **3**: 13
Barium sulfate (irradiated), lattice strains, **3**: 33
Beryllium, aging, **3**: 22; **4**: 25
alloying, **1**: 22
analysis, **1**: 22–3, 30
annealing, **4**: 24–5
applications, **1**: 22
beta-phase stabilization, **1**: 26
bibliographies, **1**: 30; **4**: 27
brazing, **1**: 24–5, 30; **3**: 60; **4**: 23
brittleness, **1**: 27–8
C diffusion, **4**: 24
carburization, **2**: 23
casting, **1**: 22–3, 30, 63; **4**: 22
chemical properties, **1**: 29–30; **3**: 20
cladding, **1**: 28–30
coating, **2**: 21; **3**: 60
compatibility with stainless steel, **1**: 30
compatibility with UO_2, **4**: 23–4, 26
composite structures, **2**: 19
compression properties, **3**: 23
constitution, **2**: 22
corrosion, **1**: 22, 29; **2**: 23–4; **3**: 24; **4**: 26
crack propagation, **2**: 22, 24; **3**: 23
creep properties, **3**: 23, 48
cross sections, **1**: 22
crystal deformation, **1**: 27
design data, **3**: 22
diffusion in BeO, **4**: 26
diffusion bonding, **1**: 24–5
dimensional stability, **2**: 22
drilling, **4**: 23
ductility, **1**: 27; **2**: 21–3; **3**: 22–3; **4**: 24–5
dynamic modulus, **3**: 22
economics, **3**: 20

Beryllium (Continued)
elastic limit, **2**: 22
electrical conductivity, **1**: 28
electrical resistivity, **1**: 22, 28; **2**: 22; **3**: 23–4
electronic structure, **1**: 28; **2**: 22
etching, **3**: 22
explosive welding, **1**: 70
extrusion, **1**: 24, 30; **3**: 21; **4**: 22
fabrication, **1**: 22–5, 30; **2**: 18–20; **3**: 22; **4**: 22–3
fastener properties, **3**: 22
fatigue properties, **3**: 22–3
flight structures, **1**: 22
forging, **2**: 24
forming, **2**: 18; **3**: 21; **4**: 23
fracture, **2**: 22; **3**: 22; **4**: 25–6
fusion welding, **2**: 19–20; **3**: 60
hardness, **1**: 26–7; **3**: 21; **4**: 25
health hazards, **1**: 22
heat-treatment effects, **2**: 20–1; **4**: 25
high-temperature properties, **3**: 23
hot hardness, **4**: 25
impact properties, **3**: 22
impact testing, **3**: 23
impurity precipitation, **1**: 27–8
joining, **1**: 22, 24–5; **2**: 18–20; **3**: 21–2; **4**: 23–4
lattice parameters, **2**: 22
lattice reorientation, **1**: 26–7
literature survey, **2**: 24
machining, **2**: 18–19
magnetic properties, **2**: 24
mechanical properties, **1**: 22, 28–9; **2**: 22–3; **3**: 20, 22; **4**: 24
melting, **1**: 22
metallography, **2**: 24; **3**: 22
metallurgy, **1**: 22, 25–8; **2**: 20–1; **3**: 20; **4**: 24–5
microscopy, **4**: 24
multiple yielding, **4**: 25
notch sensitivity, **3**: 22–3; **4**: 25
nuclear properties, **1**: 22
occurrence, **3**: 20
oxidation, **1**: 29; **2**: 23; **3**: 22; **4**: 24–7
O determination, **1**: 22, 30
physical properties, **1**: 22, 28–9; **2**: 22; **3**: 20, 22
plastic anisotropy, **3**: 22
plastic deformation, **2**: 21
plating, **4**: 27
polishing, **1**: 30; **2**: 24
preferred orientation, **1**: 26–7
preparation, **2**: 24; **4**: 22
pressure bonding, **2**: 54; **4**: 23, 53
prestraining effects, **2**: 22
production, **1**: 22; **3**: 20
purification, **1**: 23; **3**: 20–1
radiation-activation analysis, **1**: 22
reaction with air, **1**: 29
reaction with CO_2, **1**: 29; **3**: 55; **4**: 26–7
reaction with CO, **1**: 29
reaction with water vapor, **4**: 27
reaming, **4**: 23
reduction, **1**: 22
research and development, **1**: 22; **2**: 18
resources, **1**: 22
rolling, **2**: 19; **4**: 24
self-bonding, **3**: 55
shear properties, **3**: 23
shrink fitting, **3**: 21
soldering, **1**: 24–5
strain-rate effects, **4**: 25
strength, **2**: 18, 21; **3**: 23; **4**: 24–5
stress corrosion, **1**: 29
stress-rupture properties, **3**: 23
structure, **1**: 25–7; **2**: 20–1
superconductivity, **4**: 25
surface effects, **2**: 22; **3**: 23
temperature effects, **4**: 24–5
tensile properties, **1**: 28; **3**: 22–3; **4**: 25
testing, **1**: 28–9
thermal properties, **1**: 28–30; **3**: 23–4
twinning, **2**: 21
welding, **1**: 24–5, 30; **2**: 19–20, 60–1; **3**: 21, 60; **4**: 23
yield strength, **2**: 22
X-ray microscopy, **3**: 22
Beryllium (Be-coated), preparation, **4**: 23
Beryllium (forged), tensile properties, **2**: 19
Beryllium (high-porosity), production, **4**: 23
Beryllium (irradiated), anisotropic growth, **4**: 38
annealing, **2**: 24; **4**: 26
ductility, **4**: 26
effects, **1**: 22, 30, 56
embrittlement, **3**: 38
hardness, **2**: 23
mechanical properties, **4**: 26
porosity, **3**: 38
stress rupture, **4**: 26
swelling, **2**: 23–4
Beryllium alloys, mechanical properties and melting, **4**: 51
Beryllium-cadmium alloys, mechanical properties, **2**: 20
microstructure, **1**: 27
phase studies, **2**: 20
tensile properties, **1**: 27
Beryllium carbide, formation, **1**: 29
Beryllium-cerium alloys, transformation, **2**: 20
Beryllium-chromium alloys, beta-phase stability, **3**: 22
mechanical properties, **2**: 20
microstructure, **1**: 27
phase studies, **2**: 20
tensile properties, **1**: 27
transformation, **2**: 20
Beryllium-cobalt alloys, phase studies, solidus line, and transformation, **2**: 20
Beryllium-cobalt-iron-nickel alloys, beta-phase stability, **3**: 22
Beryllium compounds, **1**: 22; **2**: 24
Beryllium-copper alloys, **1**: 27; **2**: 20; **4**: 24

Beryllium crystals, ductility, 3: 20
mechanical properties, 2: 22–3
microhardness, 3: 21
tensile testing, 4: 22
Beryllium diboride crystals, preparation, 4: 24
Beryllium difluoride–lithium fluoride–uranium tetrafluoride (molten), compatibility with graphite and INOR-8, 4: 35–6
Beryllium dust, collection, 2: 24
Beryllium extrusions, textures, 2: 21
Beryllium foil, plasticity and production, 2: 20
Beryllium-germanium alloys, 1: 27; 2: 20
Beryllium-hafnium alloys, phase studies, 2: 20
Beryllium hexaboride crystals, preparation, 4: 24
Beryllium honeycomb, compression tests, 3: 23
development, 2: 19
tensile strength, 2: 19
Beryllium iodide, preparation, 3: 21
Beryllium-iron alloys, beta-phase stability, 3: 22
mechanical properties, 2: 22
solidus line, 2: 20
transformation, 2: 20
Beryllium-iron-nickel alloys, beta-phase stability, 3: 22
Beryllium-lanthanum alloys, casting, 2: 18
grain refinement, 2: 18
transformation, 2: 20
Beryllium-lithium alloys, 1: 27; 2: 20
Beryllium-magnesium alloys, 4: 22
Beryllium-manganese alloys, 1: 27; 2: 20
Beryllium-nickel alloys, 2: 20; 3: 22; 4: 24
Beryllium-nickel-palladium alloys, transformation, 2: 20
Beryllium-niobium alloys, intermetallics, 4: 24
transformation, 2: 20
Beryllium oxide, 1:22
Be diffusion in, 4: 46
reactions with N and water, 3: 19
thermal properties, 1: 30
Beryllium oxide (W-coated), development, 4: 54
Beryllium oxide–gadolinium oxide system, phase studies, 2: 31; 3: 27
Beryllium oxide powder, explosive compaction, 3: 62
Beryllium oxide–samarium oxide system, phase studies, 2: 31; 3: 27
Beryllium oxide–uranium dioxide ceramics (irradiated), dimensional changes, 2: 24
Beryllium oxide–uranium dioxide dispersions (irradiated), stability, 4: 27
Beryllium-palladium alloys, transformation, 2: 20
Beryllium-platinum alloys, transformation, 2: 20
Beryllium powder, explosive compaction, 3: 62
Beryllium-rhenium alloys, hardness and phase studies, 4: 24
Beryllium sheet, 4: 23–6
Beryllium-silicon system, beta-phase stability, 3: 22
transformation, 2: 20
Beryllium-silver alloys, beta-phase stability, 3: 22
transformation, 2: 20
Beryllium strip, fabrication and tensile properties, 2: 19
Beryllium-thorium compounds, corrosion, 2: 5; 3: 13; 4: 5
density, 2: 5
hardness, 4: 5
Beryllium-thorium-uranium alloys, corrosion, 2: 5
creep strength, 1: 10
density, 2: 5
Beryllium-thorium-uranium compounds, hardness, 4: 5
Beryllium-titanium alloys, phase studies, 2: 20
Beryllium tubing, corrosion, 2: 19
ductility, 3: 23
extrusion, 2: 19
fabrication, 2: 19
nondestructive testing, 2: 19
preferred orientation, 2: 19
stress-rupture properties, 3: 23, 48
ultrasonic welding, 2: 19
Beryllium tubing (finned), development, 4: 23
Beryllium tubing (irradiated), rupture, 4: 43
Beryllium-uranium alloys (irradiated), swelling, 1: 3–4
Beryllium-uranium-Zircaloy-2 alloys, phase studies and structure, 3: 40
Beryllium-vanadium alloys, transformation, 2: 20
Beryllium wire, drawing, 1: 24
Beryllium-yttrium alloys, mechanical properties, 2: 20
microstructure, 1: 27
oxidation, 3: 29
phase studies, 2: 20; 3: 42
tensile properties, 1: 27
Beryllium-zinc alloys, 1: 27; 2: 20
Beryllium-Zircaloy-2 alloys, phase studies and structure, 3: 40
Beryllium-zirconium alloys, casting, 2: 18
grain refinement, 2: 18
phase studies, 1: 25–6; 2: 20
transformation, 2: 20
Bismuth-magnesium-uranium-zirconium alloys (molten), corrosive effects, 2: 34
Bismuth-magnesium-uranium-zirconium alloys (molten) (irradiated), effects, 2: 34–5
Bismuth-thorium compounds ($ThBi_2$), formation, 1: 15
Bismuth-uranium alloys (molten), corrosive effects, 1: 46; 2: 34
Blanket wafers, radiographic testing, 1: 73
Bonds, ultrasonic testing, 2: 60
Boron, corrosion, 2: 30
Boride-metal dispersions, compatibility, 3: 26
Boron, coating on steel, 2: 57
fabrication of fuels containing, 1: 36–7
Boron carbide, applications, 4: 31
compatibility, 4: 31
He diffusion, 3: 26

Boron carbide (Continued)
production of spherical particles, **2**: 30
properties, **4**: 31
Boron carbide (irradiated), effects, **2**: 30–1; **4**: 31
He diffusion, **1**: 36
H release, **4**: 31
Boron carbide burnable-poison plates (irradiated), effects, **1**: 36
Boron carbide ceramic (irradiated), effects, **2**: 40
Boron carbide–copper cermet (S.S.-clad) (irradiated), effects, **2**: 40
Boron carbide–graphite dispersions, control applications, **4**: 31
Boron carbide–graphite dispersions (irradiated), dimensional changes, **4**: 31
Boron carbide–metal dispersions, compatibility, **3**: 26
Boron carbide–silicon carbide burnable-poison plates (irradiated), effects, **1**: 36
Boron carbide–silicon carbide dispersions (irradiated), effects, **2**: 30–1
Boron carbide–stainless steel–uranium dioxide dispersion fuels (S.S.-clad), production, **2**: 53
Boron-carbon system, phase studies, **3**: 26; **4**: 31
Boron-chromium-nickel alloys, corrosion, **1**: 41–2
Boron-iron absorber sections (clad) (irradiated), burnup, **1**: 36
Boron-iron alloys, poison applications, **1**: 37, 39
Boron-nickel cermets, production, **3**: 26
Boron-niobium alloys, poison applications, **1**: 37, 39
Boron nitride ceramics and cermets (irradiated), effects, **2**: 40
Boron–stainless steel alloys, corrosion, **2**: 30
poison applications, **1**: 37, 39
properties, **1**: 39
Boron–stainless steel–uranium dioxide dispersion fuels, fabrication, **1**: 12
Boron-thorium compounds (ThB_4), corrosion, **3**: 13
hardness, **4**: 5
Boron-thorium-tungsten alloys, X-ray diffraction, **2**: 5
Boron-thorium-uranium compounds, hardness, **4**: 5
Brass (irradiated), effects, **1**: 55
sputtering, **4**: 38
Brass (Si), corrosion, **1**: 42
Brass-magnesium couples, ignition, **3**: 29
Bronze, corrosion, **1**: 42

C

Cadmium (irradiated), anisotropic growth, **4**: 38
dislocation loops, **4**: 41
Cadmium-indium-silver alloys, corrosion, **2**: 30
Cadmium-indium-silver-tin alloys, corrosion, **2**: 30
Calcium (irradiated), vacancy relaxation, **1**: 56
Calcium-erbium alloys, phase studies, **3**: 41
Calcium hexaboride–iron cermet (S.S.-clad) (irradiated), effects, **2**: 40
Calcium oxide–lanthanum oxide–uranium dioxide solid solutions, stability, **2**: 6
Calcium oxide–uranium dioxide–yttrium oxide solid solutions, stability, **2**: 6
Calcium oxide–uranium dioxide–zirconium dioxide ceramics, fabrication, **4**: 12
Calcium oxide–uranium dioxide–zirconium dioxide system, phase studies, **2**: 7
Calcium oxide–uranium dioxide–zirconium dioxide system (irradiated), corrosion and effects, **2**: 7
Calcium-yttrium alloys, phase studies, **3**: 41
Carbon
See also Graphite
coatings, **1**: 67–8; **2**: 59; **3**: 57–8; **4**: 9
diffusion in Be, **4**: 24
Carbon (irradiated), C- and O-ion energy loss and ranges, **3**: 32
Carbon-iron-silicon system, diffusion, **3**: 44
Carbon-oxygen-uranium system, lattice parameters and phase studies, **3**: 13
Carbon-thorium-titanium system, corrosion, **2**: 5
Carbon-uranium system, cladding applications, **4**: 3
Carbon-uranium system (irradiated), swelling, **3**: 3
Ceramic oxide fuels, pressure bonding, **4**: 53
Ceramics, coatings, **3**: 57; **4**: 58–9
compatibility with PuO_2, **3**: 13
Cerium-cobalt-plutonium alloys, corrosive effects, **1**: 44
Cerium-cobalt-plutonium alloys (molten), fuel applications, **4**: 4
Cerium dioxide–uranium dioxide solid solutions, phase studies, **4**: 12
Cerium-uranium alloys (irradiated), swelling, **1**: 3–4
Chromium, activation energy, **1**: 43
C solubility, **1**: 52
coating, **1**: 67; **2**: 58–9; **4**: 35
diffusion, **1**: 52; **2**: 45
high-temperature applications and properties, **1**: 51–2
H solubility, **1**: 52
N solubility, **1**: 52
oxidation, **1**: 43
O solubility, **1**: 52
plating, **1**: 67–8; **2**: 60; **3**: 58; **4**: 55, 59
self-diffusion, **3**: 44
Chromium alloys, ductility, hardness, and twinning, **2**: 42
Chromium-iron alloys, Fe diffusion, **2**: 45
oxidation, **2**: 34
Chromium-iron-manganese-molybdenum-nickel-titanium alloys (W-545), creep properties, **1**: 48
Chromium-iron-molybdenum-niobium-titanium alloys, **1**: 47
Chromium-iron-titanium alloys, hardness and phase studies, **1**: 50
Chromium-molybdenum-niobium alloys, phase studies, **4**: 43–4

Chromium-molybdenum-uranium alloys (irradiated), effects, 1: 2; 3: 3
Chromium-nickel alloys, transformation, 3: 39
Chromium-nickel-niobium alloys, phase studies, 3: 39
Chromium-nickel-tungsten alloys, electrical resistance and hardness, 2: 44–5
Chromium-niobium alloys, creep properties, 2: 47
oxidation, 1: 43
tensile properties, 1: 48; 2: 47
Chromium-niobium-uranium alloys (irradiated), effects, 1: 2
Chromium-niobium-zirconium alloys, properties, 2: 47
Chromium oxide, Cr and Fe diffusion, 2: 45
Chromium-oxygen-plutonium compounds, crystallography, 3: 13
Chromium-rhenium alloys, 2: 42
Chromium-tantalum-titanium alloys, oxidation, 1: 43
Chromium-uranium alloys (irradiated), effects, 1: 2
Chromium–uranium dioxide cermets, modulus of rupture, 1: 12
preparation, 3: 7
thermal conductivity, 3: 8
Chromium–uranium dioxide cermets (clad), pressure bonding, 2: 54
Chromium–uranium dioxide dispersion fuels (clad), fabrication, 2: 10
Chromium–uranium dioxide dispersion fuels (clad) (irradiated), effects, 2: 10
Chromium–uranium dioxide–Zircaloy-2 dispersion fuels (Zircaloy-2-clad), development, 1: 11–21
Chromium–uranium nitride cermet fuels (clad), pressure bonding, 2: 54
Chromium-vanadium alloys (irradiated), effects, 1: 3–4
Chromium-yttrium alloys, ductility and oxidation, 3: 29
Chromium-zirconium compounds, hydriding, 4: 28
Cladding materials (irradiated), damage and mechanical properties, 3: 34
Cobalt, 3: 44; 4: 51
Cobalt (irradiated), effects, 1: 56
Cobalt-60, diffusion in Mo-Ni alloys, 2: 45
Cobalt alloys, diffusion, 2: 45
melting, 4: 51
Cobalt–europium oxide–gadolinium-samarium dispersions, development, 2: 30
Cobalt-iridium-nickel-niobium alloys, phase studies, 4: 44
Cobalt-iron alloys (irradiated), magnetic properties, 3: 33
Cobalt-molybdenum alloys, extrusion and mechanical properties, 2: 51
Cobalt-niobium alloys, diffusion, 4: 45–6
recrystallization, 1: 50
Cobalt–samarium oxide dispersions, development, 2: 30
Colmonoy 5 and 6, corrosion, 1: 42
Copper, bonding to Al and steel, 4: 53
diffusion in Zircaloy, 1: 53
lattice deformations, 2: 38
plating, 1: 68; 2: 60; 3: 58
pressure bonding, 2: 54–5
U diffusion, 1: 52–3
vacancy-vacancy interaction, 2: 37
Copper (irradiated), annealing, 3: 31, 34; 4: 38
damage recovery, 2: 35, 37
density, 4: 38
diffusion, 3: 31
dislocation loops, 4: 39
effects, 1: 53–4, 56; 2: 35–6, 38
energy release, 3: 31
hardness, 3: 31; 4: 39
He diffusion, 4: 46–7
He precipitation, 3: 31
H_2 diffusion, 1: 54
interstitials, 3: 34
plastic deformation, 4: 39
recoil-atom ranges, 3: 32
resistivity, 3: 32
sputtering, 4: 38
vacancy relaxation, 1: 56
X-ray lattice parameter and line breadth, 4: 38–40
Copper [S.S.(304)-clad], ultrasonic testing, 3: 64
Copper (W-coated), preparation, 2: 58
Copper alloys (molten), fuel applications, 4: 4
Copper bonding film, X-ray fluorescent testing, 1: 73
Copper brazing, testing by "ringing," 4: 58
Copper crystals (irradiated), atomic collisions, 3: 30–1
Copper-erbium alloys, phase studies, 3: 41
Copper-gold compounds (CuAu) (irradiated), surface effects, 3: 32–3
Copper hexaboride–metal dispersions, compatibility, 3: 26
Copper-molybdenum-zirconium alloys, corrosion and strength, 1: 46–7
Copper-nickel alloys, graphitization, 2: 43; 4: 21–2
Copper-niobium-zirconium alloys, 3: 46
Copper powder, explosive compaction, 4: 56–7
Copper-uranium alloys, diffusion, 2: 45
Copper-yttrium alloys, phase studies, 3: 41
Copper-zinc alloys, diffusion bonding, 1: 66
Copper-zirconium alloys, hardening and transformation, 2: 41
Croloys, corrosion, 1: 41–2
Crystals, elastic constants, 1: 72
Crystals (irradiated), atomic collisions, 3: 34
defect cascades, 3: 34
diffusion coefficients, 1: 57
effects, 1: 56–7; 2: 38; 3: 35

D

Deuterium-zirconium compounds, thermal properties, **4**: 27–8
Dynapak machine, **4**: 58
Dysprosium, fabrication, **4**: 31
Dysprosium-zirconium alloys, phase studies, **3**: 40

E

Electromagnetic testing, evaluation, **4**: 59
Engineering materials (irradiated), effects, **1**: 57
Erbium, fabrication, **4**: 31
Erbium alloys, phase studies, **3**: 41
Europium, fabrication, **4**: 31
Europium hexaboride–metal dispersions, compatibility, **3**: 26
Europium oxide, reaction with Si in steels, **1**: 36
Explosives, characteristics, **3**: 62

F

Fansteel-80 and -82, reactions with UC, **4**: 45
reactions with UO_2, **4**: 11, 45
Fecral, oxidation, **1**: 43
Ferral, corrosion, **1**: 41
Ferral (modified) (irradiated), tensile properties, **4**: 42
Fiberglas dispersion fuels (clad), fabrication and tensile strength, **1**: 10
Fiberglas-uranium fuels (Al alloy-clad), rolling, **1**: 65
Fissium-plutonium-uranium alloys, **2**: 5; **3**: 5; **4**: 3–4, 53–4
Fissium-uranium alloy fuels [S.S.(304)-clad] (irradiated), effects, **2**: 1–2
Fissium–uranium dioxide system, oxidation, **2**: 11–12; **3**: 9
Fluoride coatings, **3**: 60
Fluoride salts (molten), chemistry, **4**: 36
compatibility with graphite and INOR-8, **4**: 35–6
corrosive effects, **1**: 45; **3**: 29
permeation of graphite, **1**: 45–6
FS 26, corrosion, **1**: 42

G

Gadolinium, fabrication, **4**: 31
hardness, **1**: 39
Gadolinium-iron alloys, phase studies, **2**: 28
Gadolinium-nickel alloys, phase studies, **2**: 28
Gadolinium oxide–samarium oxide, compatibility with alloys, **3**: 26–7
Gadolinium-titanium alloys, hardness and phase studies, **1**: 39
Gadolinium-zirconium alloys, hardness, **1**: 39
phase studies, **1**: 39; **3**: 41–2
Germanium (irradiated), effects, **1**: 55
sputtering, **4**: 38
vacancy-interstitial pairs, **3**: 33–4
Germanium films (irradiated), damage, **4**: 39
Glass, coatings on graphite, **2**: 60
Glass (borated), stability in stainless steel, **1**: 36
Glass and zircon, coatings on W, **2**: 60
Gold, diffusion in U, **3**: 2
Gold (irradiated), annealing, **4**: 38–9
atomic collisions, **3**: 30–1
C-ion energy loss and ranges, **3**: 32
damage recovery, **2**: 35
density, **4**: 38
effects, **1**: 54, 56; **2**: 35–6
electrical resistivity recovery, **4**: 38
fission-fragment stopping, **4**: 41
O-ion energy loss and ranges, **3**: 32
recoil-atom ranges, **3**: 32
sputtering, **4**: 38
trivacancy structure energy, **3**: 34
X-ray lattice parameter and line breadth, **4**: 38–9
Gold-nickel alloys, corrosion, **1**: 41–2
Gold-niobium alloys, intermetallics, **4**: 44
Graphite
See also Carbon
Ar diffusion, **2**: 46
BaO diffusion, **2**: 46
cladding, **1**: 47
coatings, **3**: 59; **4**: 35
compatibility with INOR-8 and molten fluoride salts, **4**: 35–6
elastic modulus, **2**: 17
electrical resistivity, **2**: 17
fission-product diffusion, **2**: 46
flexural strength, **2**: 17
furfural alcohol impregnation, **2**: 17
He diffusion, **2**: 46
molten-fluoride-salt permeation, **1**: 45–6
oxidation, **2**: 17; **3**: 19
permeability reduction, **4**: 21
production of impermeable, **2**: 17
reaction with metals and alloys, **4**: 21–2, 35
reaction with UO_2, **2**: 17–18
SrO diffusion, **2**: 46
thermal expansion, **2**: 17
ultimate tensile strength, **2**: 17
U diffusion in, **4**: 46
vapor deposition of TiN coating, **3**: 57
Xe-135 diffusion, **2**: 46
Y_2O_3 diffusion, **2**: 46
ZrO_2 diffusion, **2**: 46
Graphite (carbide-coated), preparation, **4**: 54
Graphite (Cu-Ni alloy-clad), graphitization, **2**: 43
Graphite (glass-coated), preparation, **2**: 60
Graphite (irradiated), annealing, **4**: 40
effects, **1**: 22, 55–7; **2**: 18; **3**: 19, 33–5
lattice defects, **4**: 40
stored-energy release, **4**: 40

Graphite (irradiated) (Continued)
structure, **4**: 40
Graphite (Ni-coated), preparation, **2**: 60
Graphite (pyrolytic), deposition, **4**: 54
development, **1**: 67
Graphite (pyrolytic C-coated), impermeability and preparation, **2**: 57
Graphite (Si-SiC coated), oxidation, **3**: 59
reactions, **2**: 43
Graphite (W-coated), development, **1**: 67
preparation, **2**: 58
Graphite-matrix fuels, thermal conductivity, **4**: 7
Graphite molds, **1**: 63
Graphite powder, explosive compaction, **3**: 62; **4**: 57
Graphite–thorium dicarbide–uranium dicarbide fuels (irradiated), effects, **4**: 12–13
Graphite–thorium dioxide–uranium dioxide compacts, thermal diffusion, **4**: 46
Graphite–uranium dicarbide dispersions (irradiated), dimensional changes, **1**: 15
Graphite–uranium dicarbide fuel pellets (irradiated), dimensional changes, **4**: 21
Graphite–uranium dioxide, casting and melting, **3**: 14
Graphite–uranium dioxide (Al_2O_3-coated) fuels, fabrication, **4**: 6–7
Graphite–uranium dioxide (Al_2O_3-coated) fuels (irradiated), evaluation, **4**: 9

H

Hafnium, casting, **1**: 63
corrosion, **2**: 30
density, **2**: 30
diffusion barrier for Mo and W, **4**: 45
electrolytic recovery, **3**: 59
electron-beam welding, **4**: 51
forging, **2**: 30
interstitial contents, **4**: 51
rolling, **2**: 30
separation from Zr, **3**: 59
tensile properties, **2**: 30
weldability, **2**: 30
Hafnium alloys, mechanical properties and melting, **4**: 51
Hafnium carbide, coatings, **2**: 57–8; **3**: 57; **4**: 54
hardness, **4**: 54
Hafnium diboride (irradiated), structure, **4**: 31
Hafnium diboride–metal dispersions, compatibility, **3**: 26
Hafnium-molybdenum alloys, phase studies, **1**: 51; **2**: 43
Hafnium-molybdenum-niobium alloys, tensile properties, **1**: 48
Hafnium-niobium alloys, phase studies and recrystallization, **1**: 50
Hafnium-rhenium alloys, phase studies, **1**: 51; **2**: 43
Hafnium-tungsten alloys, phase studies, **2**: 43
Hafnium-vanadium alloys, hydriding, **4**: 28
Halides
See Alkali halides (irradiated)
Hastelloy B, H diffusion, **1**: 52
Hastelloy F, reactions with UC and UO_2, **4**: 45
Hastelloy R-235 (irradiated), tensile properties, **4**: 42
Hastelloy X, compatibility with Gd_2O_3-Sm_2O_3, **3**: 26–7
corrosion, **1**: 42; **3**: 28–9; **4**: 34–5
creep properties, **1**: 48; **4**: 43
ductility, **1**: 48; **3**: 29; **4**: 34–5
fatigue properties, **4**: 43
nitriding effects, **3**: 29
rupture, **4**: 43
tensile properties, **3**: 47; **4**: 42
Hastelloy X tubing, fatigue properties, **2**: 47
Hastelloys, corrosion, **1**: 41
Haynes 25, compatibility with Gd_2O_3-Sm_2O_3, **3**: 26–7
corrosion, **1**: 42; **3**: 29
oxidation effects on creep strength, **3**: 29
Haynes 25 (coated), corrosion, **3**: 29
Haynes 40, 41, 90, and 8589, corrosion, **1**: 42
Haynes Stellite alloy 25 powder, explosive compaction, **3**: 62
Helium, diffusion in B_4C, **1**: 36; **3**: 26
diffusion in graphite, **2**: 46
Hydrides, internuclear distances, **3**: 24
Hydrogen-magnesium system, decomposition pressures and thermodynamic properties, **4**: 28
Hydrogen-oxygen-zirconium system, phase studies, **2**: 24–5
Hydrogen-uranium-zirconium system, **3**: 4; **4**: 28

I

Inconel, corrosion, **1**: 41–2, 45; **3**: 28–9
creep properties, **3**: 47
ductility, **3**: 47
fatigue properties, **1**: 48
nondestructive testing, **4**: 59–60
reaction with Si-SiC, **2**: 43
reaction with UC, **4**: 45
reaction with UO_2, **4**: 45
rupture properties, **3**: 47
stress corrosion, **1**: 41; **4**: 35
Inconel (Cr-plated), corrosion, **1**: 41
Inconel (irradiated), effects, **4**: 43
rupture life, **2**: 40
tensile properties, **4**: 42
Inconel 702, corrosion, **4**: 34–5
creep properties, **1**: 48; **3**: 47
ductility, **4**: 34–5
oxidation effects on creep strength, **3**: 29
rupture strength, **3**: 47
Inconel 702 (coated), corrosion, **3**: 29

Inconel 702 (irradiated), tensile properties, **3**: 36; **4**: 42
Inconel 713C, creep properties, **1**: 48
creep-rupture properties, **2**: 47
ductility, **2**: 47
fatigue properties, **3**: 47
Inconel X, cladding applications, **4**: 53
creep-rupture properties, **1**: 48
heat-treatment effects, **3**: 47
oxidation effects, **3**: 29
properties, **3**: 47
Inconel X (coated), corrosion, **3**: 29
Inconel X DA and X SA (irradiated), tensile properties, **3**: 36
Indium, applications in neutron radiography, **1**: 73
Indium-thorium alloys, hardness and recrystallization, **4**: 5
INOR-8, compatibility with graphite and molten fluoride salts, **4**: 35–6
corrosion, **1**: 45; **3**: 29
Insulators (irradiated), damage, **4**: 41
Intermetallic compounds, hydriding, **4**: 28
Iridium, diffusion barrier for Mo, Ta, and W, **4**: 45
Iridium-molybdenum-nickel alloys, phase studies, **4**: 44
Iridium-nickel-niobium alloys, phase studies, **4**: 44
Iridium-nickel-tantalum alloys, phase studies, **4**: 44
Iridium-niobium-palladium alloys, phase studies, **4**: 44
Iridium-platinum alloys, brazing with, **4**: 56
Iridium-thorium alloys, intermetallics, **4**: 44
Iridium-titanium alloys, phase studies, **2**: 28, 30
Iron, compatibility with UN, **2**: 10
corrosion, **2**: 34
detection in fuel powders, **4**: 59
diffusion, **1**: 52; **2**: 45; **3**: 44
plating on U, **1**: 68
Iron (irradiated), annealing, **3**: 32; **4**: 42
C precipitation, **4**: 39
damage recovery, **2**: 36–8
density, **4**: 38
effects, **1**: 54–6; **2**: 36, 38
hardening, **4**: 39
mechanical properties, **2**: 39
resistivity, **3**: 32
sputtering, **4**: 38
vacancy relaxation, **1**: 56
X-ray lattice parameter and line breadth, **4**: 38, 40
Iron (W-coated), preparation, **2**: 58
Iron alloys, carburization, **1**: 42
melting, **4**: 51
Iron alloys (irradiated), tensile properties, **4**: 42
X-ray line half-width, **4**: 40
Iron-molybdenum alloys, diffusion, **4**: 45–6
Iron-molybdenum-titanium alloys, beta-phase stability, **2**: 44
Iron-nickel alloys (irradiated), effects, **1**: 55
magnetic properties, **3**: 33
Iron-niobium alloys, recrystallization, **1**: 50
Iron-niobium-titanium-tungsten alloys, oxidation, **1**: 43
Iron-plutonium alloy fuels, corrosive effects, **1**: 44
Iron-plutonium-silicon system (molten), corrosive effects, **4**: 4
Iron powder, explosive compaction, **4**: 56–7
Iron-silicon system (irradiated), magnetic properties, **3**: 33
Iron-yttrium alloys, phase studies, **3**: 41

K

Kennametal 3047 and K163B1, corrosion, **1**: 42
Krypton-85*m*, diffusion, **4**: 10–11
Krypton-88, diffusion, **3**: 10; **4**: 10–11

L

Lanthanum, diffusion in U, **2**: 45
Lanthanum oxide–uranium dioxide solid solutions, stability, **2**: 6
Lanthanum-thorium alloys, solubility, **1**: 9
Lead (irradiated), vacancy relaxation, **1**: 56
Lead oxide–silicon dioxide–uranium dioxide glass fuels, development, **2**: 7
Liquids, gamma-ray spectroscopic testing, **1**: 73
Lithium (molten), corrosive effects, **2**: 34; **4**: 36
Lithium deuteride, literature survey, **2**: 25
Lithium fluoride (irradiated), damage, **4**: 40
Li precipitation, **3**: 33
Lithium hydride, **1**: 33; **2**: 25
Lithium hydride (irradiated), interstitial defects, **4**: 40
Lithium hydride (molten), corrosive effects, **4**: 28
Ti hydride and Zr hydride solubility, **1**: 33
Lithium hydride vapor, literature survey, **2**: 25

M

M252, oxidation effects on creep strength, **3**: 29
M252 (coated), corrosion, **3**: 29
Magnesium, corrosion, **1**: 44–5; **3**: 29
ignition, **3**: 29
mechanical properties, **3**: 48
nondestructive metallography, **3**: 22
oxidation, **4**: 35
physical properties, **3**: 48
plating on, **4**: 27
Magnesium (irradiated), effects, **4**: 38, 41
Magnesium alloys, canning applications, **1**: 49
corrosion, **3**: 29
ignition, **3**: 29
mechanical properties, **3**: 48
nondestructive metallography, **3**: 22
physical properties, **3**: 48

Magnesium alloys (irradiated), effects, **4**: 41
properties, **3**: 48
Magnesium hydride, thermodynamic properties, **4**: 28
Magnesium-manganese alloys, creep properties, **1**: 49
Magnesium-manganese-zirconium alloys, creep properties, **1**: 49
Magnesium-nickel couples, ignition, **3**: 29
Magnetic compounds (irradiated), effects, **1**: 58
Magnox A.12, ductility and fatigue, **1**: 49
Manganese (irradiated), effects, **1**: 56
Manganese alloys (molten), fuel applications, **4**: 4
Manganese-molybdenum-titanium alloys, beta-phase stability, **2**: 44
Manganese-nickel alloys, corrosion, **1**: 41–2
Materials (irradiated)
See also Engineering materials (irradiated) and Reactor materials
effects, **1**: 57; **3**: 34
Materials (structural) (irradiated), properties, **4**: 41–3
Mercury, containment by clad steel, **2**: 34
Metal borides, metallography, **4**: 31
Metal carbide–uranium carbide systems, evaluation, **3**: 13
Metal coatings, bibliography, **4**: 55
corrosion, **1**: 68
Metal films (irradiated), damage, **4**: 17
Metal hydrides, **1**: 30
Metal–metal boride dispersions, compatibility, **3**: 26
Metal plates, ultrasonic thickness testing, **2**: 60–1
Metal powders, compatibility with PuO_2, **3**: 13
explosive compaction, **3**: 61–2
pressure bonding for cladding, **2**: 54
Metal powders (Ni- and Ta-coated), preparation, **2**: 58
Metals, casting, **1**: 63; **2**: 51; **3**: 52
degassing, **2**: 51
diffusion, **2**: 45; **4**: 46
diffusion bonding, **1**: 65–6
drawing, **3**: 53
electron-beam applications, **2**: 51; **3**: 52
explosive working, **1**: 71; **3**: 60–3; **4**: 57
extrusion, **3**: 53
gas diffusion, **1**: 52
melting, **2**: 51; **3**: 52
nondestructive testing, **3**: 64
reactions with water, **1**: 17
ultrasonic testing, **1**: 73
vapor deposition, **4**: 54
welding, **3**: 60; **4**: 56
Metals (alkali) (irradiated), effects, **1**: 56
Metals (body-centered) (irradiated), damage, **3**: 34
Metals (cubic) (irradiated), anisotropic growth, **4**: 38
Metals (fissionable) (irradiated), swelling, **4**: 17
Metals (irradiated), atomic displacements, **1**: 57
bubble formation, **3**: 35
damage, **3**: 35; **4**: 40
displaced atoms, **1**: 56
effects, **1**: 56–7; **2**: 35; **3**: 32, 34
fission-product slowing, **4**: 41
imperfections, **2**: 38
impurity resistance, **2**: 38
lattice effects, **1**: 57; **4**: 41
mechanical-property recovery, **4**: 41
phase transformations, **3**: 35
point-defect annealing, **4**: 41
rare-gas location and motion, **3**: 32
stresses, **1**: 57
vacancy annealing, **1**: 56
Metals (molten), embrittlement, **3**: 30
reactions with water, **4**: 36–7
Metals (Mo-coated), development, **1**: 67
Metals (noble) (irradiated), damage recovery, **3**: 34
effects, **1**: 58; **2**: 37; **3**: 34
Metals (reactive), consumable-electrode melting and purification, **2**: 51
Metals (refractory), carbide–uranium carbide systems, **3**: 13
casting, **4**: 51
coatings, **3**: 57
diffusion barriers, **4**: 45
explosive forming, **3**: 63
high-temperature applications and properties, **1**: 51–2
melting, **1**: 63; **4**: 51
Metals (structural) (irradiated), effects, **4**: 41
Metals (transition), hydrides, **1**: 30
vacancy annealing, **3**: 31–2
Metals (transition) (irradiated), vacancy annealing, **3**: 31–2
Mica (irradiated), fission-fragment tracks, **3**: 33
Minerals (irradiated), damage, **3**: 35
Molybdenum, bibliography, **4**: 44
C solubility, **1**: 52
casting, **2**: 51; **4**: 51
cladding, **2**: 54
coating, **1**: 67; **2**: 58–9; **4**: 34, 54
compatibility with UO_2, **2**: 6; **4**: 11
compatibility with UN, **2**: 10
deformation twinning, **2**: 42
diffusion barriers for, **4**: 45
diffusion fissium-Pu-U alloys, **2**: 5; **4**: 4
explosive forming, **1**: 68–70; **3**: 63
explosive welding, **1**: 70
fabrication, **2**: 42; **4**: 51
fracture, **2**: 42
graphitization, **4**: 21–2
heat capacity, **4**: 44
H solubility, **1**: 52
joining, **4**: 55
mechanical properties, **3**: 48
melting, **2**: 51; **4**: 51
N solubility, **1**: 52
oxidation, **1**: 42–3
O solubility, **1**: 52
plating, **1**: 68
purification, **4**: 54

Molybdenum (Continued)
reactions with UC and UO_2, **4**: 45
self-diffusion, **2**: 45; **3**: 44
W diffusion, **2**: 45
U diffusion, **1**: 52
vacancy annealing, **3**: 31–2
Molybdenum (Al-Cr-Si alloy-coated), properties, **3**: 59
Molybdenum (Al_2O_3-glass-coated), oxidation, **3**: 59
Molybdenum (Chromalloy W-2-coated), properties, **3**: 59
Molybdenum (diffusion-coated), preparation, **2**: 58
Molybdenum (irradiated), damage recovery, **3**: 34
density, **4**: 38
divacancy migration, **3**: 32
effects, **1**: 54–5; **2**: 36
embrittlement, **2**: 39–40
lattice interactions, **3**: 32
mechanical properties, **2**: 39
sputtering, **4**: 38
vacancy annealing, **3**: 31–2
X-ray lattice parameter and line breadth, **4**: 38–9
Molybdenum (Linde LM-5-coated), properties, **3**: 59
Molybdenum (silicide-coated), oxidation, **2**: 33
Molybdenum (W-coated), preparation, **2**: 58
Molybdenum alloys, arc casting, **2**: 52
bibliography, **4**: 44
ductility, **2**: 42
extrusion, **2**: 52
fabrication, **4**: 51
hardness, **2**: 42
joining, **4**: 55
phase studies, **4**: 45
powder metallurgy, **2**: 52
production, **2**: 52
properties, **2**: 52
strength, **1**: 48–9
strength-weight ratios, **1**: 48–9
twinning, **2**: 42
Molybdenum carbides, bibliography, **4**: 44
oxidation, **3**: 6
Molybdenum compounds, bibliography, **4**: 44
Molybdenum-nickel alloys, Co^{60} diffusion, **2**: 45
Molybdenum-nickel alloys (INOR-8), weldment cracking, **3**: 60
Molybdenum-nickel-niobium alloys, weldment cracking, **3**: 60
Molybdenum-nickel-osmium alloys, phase studies, **4**: 44
Molybdenum-nickel-silicon system, phase studies and solubility of Al-Ni compounds in, **1**: 50
Molybdenum-niobium alloys, oxidation, **1**: 43
tensile properties, **1**: 48
Molybdenum-niobium-titanium alloys, canning, **4**: 51
oxidation, **1**: 43
Molybdenum-niobium-tungsten-zirconium alloys, electron-beam melting, **3**: 52
Molybdenum-niobium-uranium alloys, cladding applications, **4**: 3
hardness, **3**: 2
lattice parameters, **3**: 2
phase studies, **3**: 2; **4**: 2
Molybdenum-niobium-vanadium alloys, **3**: 39
Molybdenum-niobium-vanadium-zirconium alloys, tensile properties, **1**: 48
Molybdenum-niobium-zirconium alloys, physical properties, **1**: 51
Molybdenum-rhenium alloys, ductility, fabricability, and twinning, **2**: 42
Molybdenum-rhenium-tungsten alloys, phase studies, **4**: 43
Molybdenum-rhodium alloys, phase studies, **2**: 41–2
Molybdenum-ruthenium-uranium alloys, gamma-phase decomposition, **2**: 4
Molybdenum sheet, development, **1**: 63
Molybdenum silicide coatings, **2**: 58; **4**: 35
Molybdenum silicide powder, explosive compaction, **3**: 62
Molybdenum silicide–zirconium diboride powder, explosive compaction, **3**: 62
Molybdenum-silicon-uranium system, **1**: 3–4
Molybdenum-tantalum-uranium alloys, mechanical properties, **2**: 4
Molybdenum-thorium-uranium alloys, creep strength, **1**: 9–10
hot hardness, **1**: 10
Molybdenum-titanium alloys, explosive forming, **1**: 68–70; **3**: 63
explosive welding, **1**: 70
extrusion, **2**: 51
mechanical properties, **2**: 51
Molybdenum–titanium nitride dispersions, stability, **3**: 40
Molybdenum-titanium-vanadium alloys, beta-phase stability, **2**: 43–4
Molybdenum-titanium-zirconium alloys, mechanical properties and strength, **3**: 48
Molybdenum-uranium alloys, annealing, **4**: 2
bond structure, **3**: 3
casting, **4**: 2
cladding applications, **4**: 3
corrosion, **1**: 6; **3**: 2–3
creep properties, **1**: 3–4
electrical resistivity, **3**: 3
fracture, **4**: 2
gamma-phase decomposition, **2**: 4
Hall effect, **3**: 3
magnetic susceptibility, **3**: 3
mechanical properties, **2**: 4
oxidation, **1**: 5; **2**: 2; **4**: 16
phase studies, **1**: 1
phase transformation, **1**: 3
production, **1**: 6
soft X-ray band, **3**: 3
specific heat, **3**: 3
strength, **2**: 4
stress-rupture properties, **1**: 2–3
tensile properties, **1**: 2–3
thermal cycling, **1**: 2–3; **2**: 2

Molybdenum-uranium alloys (Continued)
thermoelectric power, **3**: 3
Molybdenum-uranium alloys (clad), canning, **2**: 57
coextrusion, **1**: 66; **2**: 56
fabrication, **1**: 23
forging, **1**: 65
rolling, **1**: 65; **3**: 53
Na bonding, **1**: 66–7; **2**: 57
Molybdenum-uranium alloys (clad) (irradiated), effects, **2**: 2
Molybdenum-uranium alloys (irradiated), effects, **1**: 3, 5; **3**: 3–4
Molybdenum–uranium carbide dispersion fuels, development, **2**: 10
Molybdenum–uranium dioxide cermet fuels, modulus of rupture, **1**: 12
preparation, **3**: 7
thermal conductivity, **3**: 8
Molybdenum–uranium dioxide cermet fuels (clad), pressure bonding, **2**: 54
Molybdenum–uranium dioxide dispersion fuels (clad), fabrication, **2**: 10
Molybdenum–uranium dioxide dispersion fuels (clad) (irradiated), effects, **2**: 10
Molybdenum–uranium nitride cermet fuels (clad), pressure bonding, **2**: 54
Molybdenum–uranium sulfide dispersion fuels, development, **2**: 10
Molybdenum-zirconium alloys, hardening and transformation, **2**: 41
Monel, corrosion, **1**: 42
graphitization, **4**: 21–2
reaction with Si-SiC, **2**: 43
Multimet, compatibility with Gd_2O_3-Sm_2O_3, **3**: 26–7

N

NaK, corrosion of Nb-Zr alloys, **2**: 34
Neptunium (irradiated), effects, **4**: 16–17
Neptunium-uranium alloys, phase studies, **1**: 1
Nickel, Al diffusion, **1**: 53
coatings, **2**: 58, 60; **4**: 35
corrosion, **1**: 42
diffusion in U, **1**: 52
graphitization, **4**: 21–2
high-temperature applications and properties, **1**: 51–2
plating, **1**: 67–8; **2**: 59–60; **3**: 5, 58–9; **4**: 55
reaction with Si-SiC, **2**: 43
self-diffusion, **3**: 44
solubility in molten Na, **4**: 36
U diffusion, **1**: 53
Nickel (irradiated), annealing, **4**: 38–9
C-ion energy loss and ranges, **3**: 32
damage recovery, **2**: 35
effects, **1**: 55–7
ferromagnetic hysteresis, **3**: 32
hardness, **3**: 31
mechanical properties, **2**: 39
O-ion energy loss and ranges, **3**: 32
sputtering, **4**: 38
vacancy relaxation, **1**: 56
X-ray lattice parameter and line breadth, **4**: 39
Nickel (W-coated), preparation, **2**: 58
Nickel alloys, carburization, **1**: 42; **4**: 21–2
melting, **4**: 51
properties, **3**: 47
Nickel alloys (diffusion-coated), preparation, **2**: 58
Nickel alloys (irradiated), tensile properties, **4**: 42
Nickel alloys (molten), fuel applications, **4**: 4
Nickel aluminum oxide, Cr and Fe diffusion, **2**: 45
Nickel chromium oxide, Cr and Fe diffusion, **2**: 45
Nickel foils (irradiated), fission-product vapor transport, **4**: 17
Nickel-niobium alloys, Ir-addition effects, **4**: 44
Nickel-niobium-osmium alloys, phase studies, **4**: 44
Nickel-niobium-ruthenium alloys, phase studies, **4**: 44
Nickel-niobium-titanium-tungsten alloys, oxidation, **1**: 43
Nickel-osmium-tantalum alloys, phase studies, **4**: 44
Nickel powder–water slurries, nondestructive testing, **4**: 59
Nickel-tantalum alloys, diffusion, **4**: 45–6
Nickel-uranium alloys, diffusion, **2**: 45
Nickel–uranium dioxide powder, explosive compaction, **3**: 62
Nickel-yttrium alloys, phase studies, **3**: 41
Nickel-zirconium alloy plate, **3**: 59
Niobium, bibliography, **4**: 44–5
brazing, **4**: 56
C diffusion and solubility, **1**: 52
CO_2 and CO embrittlement, **3**: 28
carburization, **1**: 50–1
casting, **2**: 51; **4**: 51
chemistry, **1**: 51
cladding, **2**: 54; **4**: 53
coating, **1**: 42–3, 67; **4**: 34
compatibility with UO_2, **2**: 6
corrosion, **1**: 43; **4**: 35
development, **3**: 48
diffusion-barrier studies, **4**: 45
diffusion with fissium-Pu-U alloys, **2**: 5; **4**: 4
ductility, **1**: 48
explosive forming, **1**: 68; **3**: 63
explosive welding, **1**: 70
fabricability, **3**: 48
gas effects, **1**: 51
hardness, **3**: 48
H diffusion and solubility, **1**: 52
joining, **4**: 55–6
melting, **2**: 51; **4**: 51
metallurgy, **1**: 51
N diffusion and solubility, **1**: 52
oxidation, **1**: 42–3; **2**: 33; **3**: 28; **4**: 34
O diffusion and solubility, **1**: 52

Niobium (Continued)
plating, 1: 68
reactions with CO_2 and CO, 1: 43
self-diffusion, 1: 52
Si diffusion in, 4: 46
stacking faults, 3: 39
tensile yield strength, 3: 48
thermal conductivity, 1: 8
U diffusion, 1: 53
vacancy annealing, 3: 31–2
welding, 2: 60
Niobium (Cr-Si-Ti-coated), oxidation, 1: 43
Niobium (Cr-Ti alloy–Si-coated), preparation and properties, 2: 33
Niobium (irradiated), effects, 2: 36; 4: 43
oxidation, 3: 28
rupture life, 2: 40
thermal conductivity, 4: 38
vacancy annealing, 3: 31–2
Niobium (MoS_2-coated), preparation and properties, 2: 33
Niobium (Zn-coated), oxidation, 2: 42
vapor deposition, 3: 57
Niobium alloys, bibliography, 4: 44–5
brazing, 4: 56
development, 3: 48; 4: 43
high-temperature applications and properties, 1: 51–2
joining, 4: 55
mechanical properties, 4: 51
melting, 4: 51
oxidation, 4: 34
phase studies, 4: 45
strength, 1: 48–9
strength-weight ratios, 1: 48–9
welding, 2: 60
Niobium alloys (F-48 and F-50), corrosion, 1: 43
Niobium alloys ($MoSi_2$-coated), preparation, 2: 58
Niobium alloys (silicide-coated), preparation, 2: 58
Niobium carbide, bibliography, 4: 44–5
coatings, 3: 57; 4: 54
hardness, 4: 54
Niobium carbide system, oxidation, 3: 6
Niobium compounds, bibliography, 4: 44–5
Niobium crystals, elastic constants, 3: 39
Niobium hydride, phase studies, 2: 25
Niobium–niobium carbide system, lattice parameters and phase studies, 3: 39
Niobium-osmium alloys, intermetallics, 4: 44
Niobium oxide, phase studies, 2: 33
production, 3: 28
Niobium oxide–titanium dioxide–uranium dioxide solid solutions, stability, 2: 6
Niobium-palladium alloys, oxidation, 3: 28
Niobium-platinum alloys, diffusion, 4: 45–6
Niobium-plutonium-zirconium alloys, hardness and phase studies, 3: 6
Niobium-rhenium alloys, intermetallics, 4: 44
phase studies, 1: 50–1; 2: 43
recrystallization, 1: 50
Niobium-selenium system, diffusion, 4: 45
Niobium sheet, development, 1: 63
Niobium-silicon system, diffusion, 4: 46
Niobium–stainless steel tubing, through-transmission testing, 4: 58
Niobium-tantalum alloys, 1: 50
Niobium-tantalum-tungsten-zirconium alloys (silicide-coated), properties, 2: 58
Niobium-tantalum-zirconium alloys, brazing, 4: 56
Niobium-tantalum-zirconium alloys (silicide-coated), properties, 2: 58
Niobium-thorium-uranium alloys, creep strength, 1: 9–10
hot hardness, 1: 10
Niobium-tin alloys, hardness, 2: 42
oxidation, 2: 42; 3: 28
phase studies, 2: 42
Niobium-tin-zirconium alloys, hardness and heat treatability, 1: 51
Niobium-titanium alloy–uranium carbide dispersion fuels, development, 2: 10
Niobium-titanium alloy–uranium sulfide dispersion fuels, development, 2: 10
Niobium-titanium alloys, carburization, 1: 43
ductility, 1: 43
oxidation, 1: 43
reactions with CO_2 and CO, 1: 43
reactions with Si-SiC, 2: 43
recrystallization, 1: 50
Niobium-titanium-tungsten alloys, oxidation, 1: 43
Niobium-titanium-tungsten-vanadium alloys, oxidation, 1: 43
Niobium-titanium-vanadium alloys, oxidation, 1: 43
Niobium-tungsten alloys, fabrication, 4: 43
oxidation, 1: 43
recrystallization, 1: 50
tensile properties, 1: 48; 4: 43
Niobium-tungsten-vanadium alloys, tensile properties, 1: 48
Niobium-tungsten-vanadium-zirconium alloys, tensile properties, 1: 48
Niobium-uranium alloys, cladding applications, 4: 3
corrosion, 1: 5, 7–8; 2: 33
creep resistance, 1: 8
diffusion, 4: 45
fabrication, 1: 8
oxidation, 2: 33
phase studies, 4: 2–3
recrystallization, 1: 8
stress-rupture properties, 1: 8
thermal conductivity, 1: 8
Niobium–uranium carbide dispersion fuels, development, 2: 10
Niobium–uranium dioxide cermet fuels, microstructure, 3: 8
pressure bonding, 3: 7–8
thermal conductivity, 1: 12; 3: 8

Niobium–uranium dioxide cermet fuels (clad), pressure bonding, **2**: 54
Niobium–uranium dioxide dispersion fuels, development, **1**: 12
Niobium–uranium dioxide dispersion fuels (clad), fabrication and radiation effects, **2**: 10
Niobium–uranium nitride cermet fuels (clad), pressure bonding, **2**: 54
Niobium–uranium sulfide dispersion fuels, development, **2**: 10
Niobium-uranium-zirconium alloys, cladding applications, **4**: 3
corrosion, **1**: 5
Niobium-uranium-zirconium alloys (irradiated), corrosion and dimensional stability, **3**: 3
Niobium-uranium-zirconium alloys (Zircaloy-2-clad) (irradiated), dimensional stability, **3**: 3
effects, **1**: 4–5
Niobium-vanadium alloy coatings, preparation on UO_2 spheres, **2**: 58
Niobium-vanadium alloys, compatibility with fissium-Pu-U alloys, **4**: 4
preparation, **1**: 67
properties, **2**: 47
Niobium-vanadium-zirconium alloys, tensile properties, **1**: 48
Niobium-zinc alloys, diffusion, **4**: 45
phase studies, **2**: 42–3
reaction with Si-SiC, **2**: 43
Niobium-zirconium alloys, aging, **3**: 39–40
CO_2 and CO embrittlement, **3**: 28
carburization, **1**: 43
cladding applications, **4**: 53
corrosion by molten metals, **2**: 34
corrosion by molten K, **4**: 35
corrosion by molten NaK, **2**: 34
creep properties, **2**: 47, **3**: 47
ductility, **1**: 43
hardening, **2**: 41
H heat of transport, **3**: 41
H solubility, **3**: 40–1
martensite tempering, **2**: 41
oxidation, **1**: 43
phase studies, **2**: 41; **3**: 40
reaction with CO, **1**: 43
recrystallization, **1**: 50
tensile properties, **1**: 48; **2**: 46–7
transformation, **2**: 41
welding, **1**: 71
Zr diffusion, **2**: 45

O

Osmium-tantalum alloys, phase studies, **1**: 51; **2**: 43
Osmium-thorium alloys, intermetallics, **4**: 4
Osmium-tungsten alloys, phase studies, **1**: 51; **2**: 43

P

Palladium, brazing, **4**: 56
Palladium (irradiated), damage, **4**: 39
damage recovery, **2**: 35
density, **4**: 38
effects, **2**: 36
X-ray lattice parameter and line breadth, **4**: 38
Palladium-thorium alloys, intermetallics, **4**: 4
Platinum, brazing with, **4**: 56
Platinum (irradiated), damage, **4**: 39
damage recovery, **2**: 35
density, **4**: 38
effects, **1**: 55; **2**: 36–7
focusing collisions, **4**: 36–8
X-ray lattice parameter and line breadth, **4**: 38–9
Platinum-rhodium alloys, brazing with, **4**: 56
Platinum-thorium alloys, intermetallics, **4**: 4
Platinum–uranium dioxide–platinum system, thermoelectric power, **4**: 9
Plutonium, casting, **3**: 52
colorimetric testing of fuels, **1**: 73
formability, **3**: 5
melting, **3**: 52
temperature effects on tensile properties, **3**: 5
viscosity, **4**: 3
Plutonium (irradiated), effects, **4**: 16–17
Plutonium (Zircaloy-clad), rolling, **3**: 53
Plutonium alloys, casting and melting, **3**: 52
Plutonium aluminate, crystallography, **3**: 13
melting point, **1**: 15
Plutonium carbide, density, **3**: 15
formation, **4**: 16
melting, **4**: 15–16
powder metallurgy, **3**: 15
preparation, **1**: 16; **2**: 9
properties, **1**: 14; **2**: 8
shattering, **4**: 16
thermal expansion, **2**: 8; **3**: 13
transformation, **2**: 8
vaporization, **2**: 8
Plutonium carbide (Si-SiC-canned), fabrication, **4**: 53
Plutonium carbide–uranium carbide system, density, **3**: 15
development, **2**: 9
evaluation, **2**: 8
melting, **3**: 13
preparation, **3**: 15
Plutonium chromate, crystallography, **3**: 13
Plutonium compounds, fabrication and preparation, **1**: 16
Plutonium dioxide, characteristic temperature, **1**: 15
compatibility with ceramics and metal powders, **3**: 13
decomposition, **3**: 13
dissolution from glass fibers, **4**: 15

Plutonium dioxide (Continued)
dry pressing, **4**: 15
melting, **2**: 7; **3**: 13
reaction with Al_2O_3, **1**: 15
reaction with C, **4**: 16
reaction with ZrO_2, **1**: 15
sintering, **4**: 15
temperature effects on O/Pu ratio, **2**: 8
thermal expansion, **3**: 12
vapor pressure, **3**: 13; **4**: 13
vaporization, **2**: 8
Plutonium dioxide–silicon dioxide–sodium dioxide glass fibers, fabrication, **4**: 15
Plutonium dioxide–thorium dioxide system, sintering, **2**: 8
solid-state reactions, **2**: 8
vapor pressure, **3**: 13
weight losses, **2**: 8
Plutonium dioxide–uranium dioxide system, phase studies, **2**: 7; **3**: 12
Plutonium dioxide–zirconium dioxide system, phase studies, **2**: 8; **3**: 13
Plutonium nitride, preparation, **1**: 16
Plutonium oxides, properties, **2**: 8
Plutonium powder, production, **1**: 8
Plutonium-thorium alloys, phase studies, **2**: 5
recrystallization, **3**: 6
strength, **2**: 5
Plutonium-thorium alloys (irradiated), stability, **4**: 5
Plutonium-thorium-zirconium alloys, phase studies and strength, **2**: 5
Plutonium-uranium alloys, phase studies, **1**: 9
Plutonium–vanadium oxide system, crystallography, **3**: 13
Potassium (molten)
See also NaK
corrosive effects, **2**: 34; **3**: 29; **4**: 35
Potassium oxide–silicon dioxide–sodium oxide–uranium dioxide glass fuels, development, **2**: 7

Q

Quartz (irradiated), effects, **4**: 40–1

R

Radiation effects, theory, **4**: 41
Reactor-core assemblies, channel inspection, **4**: 59
Reactor fuel cans, fabrication, **3**: 56
Reactor fuel-cladding fins, cold swaging, **1**: 65
Reactor fuel particles (pyrolytic C-coated), preparation, **2**: 59; **3**: 58
Reactor fuel plates, eddy-current coolant-channel width measurement, **2**: 62
Reactor fuel slugs (canned), heat-transfer testing, **3**: 56
Reactor fuel tubes, coextrusion, **2**: 55–6
ultrasonic testing, **2**: 60
Reactor fuels, canning, **2**: 56–7
cyclographic bond testing, **2**: 62
development, **3**: 13
diffusion bonding, **1**: 66
eddy-current plate-spacing measurement, **3**: 65
fiber-optic testing, **3**: 65
nondestructive testing, **1**: 73
pressure bonding, **4**: 52–3
swaging, **1**: 64–5
ultrasonic testing, **2**: 61; **3**: 64
welding, **1**: 71; **2**: 60
Reactor fuels (Al-clad), plating with Ni, **3**: 59
Reactor fuels (Al-Si alloy-clad), extrusion, **2**: 56
Reactor fuels (canned), extrusion, **4**: 53
Reactor fuels (clad), canning, **3**: 57
diffusion-bond strength, **2**: 55
eddy-current testing, **3**: 64
fabrication, **1**: 64
pressure bonding, **2**: 54–5
ultrasonic testing, **3**: 64
Reactor fuels (irradiated), bubble formation, **3**: 15
nondestructive testing, **1**: 73
Reactor fuels (1S Al alloy-clad), extrusion, **2**: 56
Reactor fuels (Nb-plated, Al-clad), bonding, **3**: 55
fabrication, **3**: 56
Reactor fuels (ribbon-candy), fabrication, **4**: 52
Reactor fuels (spiral), fabrication, **4**: 52
Reactor fuels (S.S.-clad), pressure bonding, **4**: 53
Reactor fuels (steel-plated Zr-clad), canning, **2**: 57
Reactor fuels (thermoelectric), development, **2**: 9
swaging, **1**: 65
Reactor fuels (wire), swaging, **4**: 52
Reactor materials, development, **3**: 13
Reactor materials (irradiated), effects, **1**: 58
Reactor poisons, **1**: 36–9; **2**: 55
Refractory metals
See Metals (refractory)
René 41, creep properties, **3**: 47
oxidation effects on creep strength, **3**: 29
rupture strength, **3**: 47
René 41 (coated), corrosion, **3**: 29
Rhenium, compatibility with UO_2, **2**: 6
Rhenium-tantalum alloys, phase studies, **1**: 51; **2**: 43
Rhenium-tantalum-tungsten alloys, phase studies, **2**: 43
Rhenium-tungsten alloys, **2**: 42
Rhodium, applications in neutron radiography, **1**: 73
Rhodium-thorium alloys, intermetallics, **4**: 4
Rubidium (molten), corrosion of Nb-Zr alloys, **2**: 34
Ruthenium-tantalum alloys, phase studies, **1**: 51; **2**: 43
Ruthenium-tantalum-tungsten alloys, phase studies, **1**: 51
Ruthenium-tungsten alloys, phase studies, **1**: 51; **2**: 43

S

S Monel
See also Monel
corrosion, **1**: 42
Samarium, fabrication, **4**: 31
Scandium hydride, preparation and properties, **4**: 28
Scandium-titanium alloys, phase studies, **4**: 45
Selenium-thorium compounds, crystal structure, **1**: 9
Selenium-uranium compounds, corrosion, **3**: 13
density, **3**: 13
development, **2**: 9
fuel applications, **2**: 9
Semiconductors (irradiated), damage, **3**: 35
Silica (irradiated), effects, **4**: 40–1
light scattering, **3**: 33
Silicide coatings, **2**: 58; **4**: 34
Silicon, coating, **1**: 67
diffusion in Nb, **4**: 46
diffusion in U, **1**: 52
reaction with Eu_2O_3 in steels, **1**: 36
Silicon (irradiated), effects, **1**: 55
sputtering, **4**: 38
Silicon carbide, coatings, **4**: 35
oxidation, **3**: 6
Silicon carbide–uranium carbide dispersions, preparation, **3**: 14
Silicon dioxide (irradiated), damage recovery, **2**: 37
effects, **1**: 55–6; **2**: 37; **4**: 40–1
Silicon dioxide–uranium dioxide glasses, devitrification, **2**: 7
Silicon films, preparation, **4**: 54
Silicon nitride coatings, **4**: 35
Silicon–silicon carbide coatings, electropotential testing, **3**: 65
on graphite, **3**: 59
oxidation, **3**: 59
reactions with metals and alloys, **2**: 43
Silicon-thorium compounds, corrosion and density, **2**: 5
Silicon-thorium-uranium compounds, corrosion and density, **2**: 5
hardness, **4**: 5
Silicon-uranium compounds
See Uranium silicides
Silicon-uranium system, behavior and properties, **2**: 2
Silicon-uranium system (irradiated), effects, **1**: 6; **3**: 3
Silicon-uranium system fuels (Be-clad), coextrusion, **1**: 23; **2**: 56
Silver (irradiated), C-ion energy loss and ranges, **3**: 32
damage recovery, **2**: 35
effects, **1**: 54, 56
O-ion energy loss and ranges, **3**: 32
recoil-atom ranges, **3**: 32
Silver crystals (irradiated), atomic collisions, **3**: 30–1
disoriented crystallites, **3**: 32
Sodium, corrosive effects, **1**: 44, 56
thermodynamic properties, **3**: 30
Sodium (irradiated), vacancy relaxation, **1**: 56
Sodium (molten)
See also NaK
corrosion of Nb-Zr alloys, **2**: 34
Ni solubility in, **4**: 36
reaction with graphite, **4**: 35
Sodium chloride (irradiated), interstitial defects, **4**: 40
Solid-suspensoid systems, nondestructive testing, **4**: 59
Solids, ultrasonic testing, **3**: 64
Solids (inorganic)(irradiated), effects, **4**: 41
Solids (irradiated), collision focusing, **3**: 34
spectrum effects on damage, **3**: 34
surface heterogeneity, **2**: 37
Stainless steel, borated glass stability in, **1**: 36
compatibility with Be, **1**: 30
compatibility with Th-U alloys, **1**: 10
decontamination, **1**: 42
graphitization, **4**: 21–2
high-temperature applications and properties, **1**: 51–2
rare-gas diffusion, **1**: 52
welding, **2**: 60
Xe diffusion, **2**: 45–6
Stainless steel (17-4 PH)(irradiated), tensile properties, **3**: 36
Stainless steel (17-7 PH), creep properties and rupture strength, **3**: 47
Stainless steel (302), creep properties and rupture strength, **3**: 47
Stainless steel (304), carburization, **1**: 44; **2**: 33
cladding applications, **4**: 53
corrosion, **1**: 44–5; **4**: 34
creep properties, **1**: 47; **3**: 47
impact properties, **1**: 47
nitriding, **4**: 35
oxidation, **1**: 41; **2**: 33
reaction with Si-SiC, **2**: 43
rupture properties, **1**: 47
stress-rupture properties, **1**: 47
tensile properties, **1**: 47
ultrasonic roll bonding, **3**: 53
Stainless steel (304)(irradiated), annealing effects, **3**: 38
rupture life, **2**: 40
stress rupture, **4**: 42
tensile properties, **3**: 36, 38
Stainless steel (304B), reactions with SrB_6 and YB_6, **1**: 36
Stainless steel (304 ELC)(irradiated), rupture life, **2**: 40
Stainless steel (304L), corrosion, **4**: 34
reactions with UC and UO_2, **4**: 45
Stainless steel (310), explosive welding, **1**: 70

Stainless steel (316), corrosion, **3**: 29; **4**: 34
creep properties, **3**: 47
creep-rupture properties, **2**: 47
oxidation, **1**: 43
reaction with Si-SiC, **2**: 43
rupture strength, **3**: 47
Stainless steel (316)(irradiated), tensile properties, **3**: 36; **4**: 42
Stainless steel (316L), creep and creep-rupture properties, **3**: 47
Stainless steel (318), brazing to Be, **3**: 60
Stainless steel (347), compatibility with Gd_2O_3-Sm_2O_3, **3**: 26–7
corrosion, **4**: 34, 36
creep properties, **3**: 47
diffusion with fissium-Pu-U alloys, **2**: 5; **4**: 4
Stainless steel (347)(irradiated), annealing effects, **3**: 38
effects, **1**: 57
tensile properties, **3**: 36, 38; **4**: 42
Stainless steel (406)(irradiated), tensile properties, **4**: 42
Stainless steel (410), cold-roll joining to Zircaloy-2, **3**: 53–4
Stainless steel (410, 12 Cr), corrosion, **1**: 44–5
Stainless steel (430), diffusion with fissium-Pu-U alloys, **2**: 5; **4**: 4
reaction with Si-SiC, **2**: 43
Stainless steel (430T), **1**: 47
Stainless steel (430 Ti), reaction with Si-SiC, **2**: 43
Stainless steel (446), corrosion, **4**: 34
Stainless steel (A-286), creep properties and rupture strength, **3**: 47
Stainless steel (AM-350), tensile properties, **3**: 38
Stainless steel (AM-350)(irradiated), tensile properties, **3**: 37–8
Stainless steel (austenitic), **1**: 47; **4**: 28
Stainless steel (boron), corrosion, **2**: 30
Stainless steel (boron)(Cr-plated), nondestructive testing, **4**: 59
Stainless steel (irradiated), yield strength, **3**: 38
Stainless-steel (430T) cladding, **1**: 47
Stainless steel–titanium dioxide–uranium dioxide dispersion fuels (irradiated), fission-gas release, **3**: 12
Stainless-steel (304) tubing, collapse, **2**: 47
creep buckling, **2**: 47
rupture properties, **3**: 47
Stainless-steel (304) tubing (irradiated), burst properties, **3**: 35
Stainless-steel (410) tubing, explosive joining to Zr, **3**: 63
Stainless steel–uranium dioxide cermet fuels, radiation effects, **2**: 10
Stainless steel (302B)–uranium dioxide cermet fuels, modulus of rupture, **1**: 12
preparation, **3**: 7
thermal conductivity, **3**: 8
Stainless steel–uranium dioxide cermet fuels (clad), pressure bonding, **2**: 54
Stainless steel–uranium dioxide dispersion fuels, burnup, **1**: 11
development, **1**: 12
fabrication, **1**: 36–7; **2**: 10
Stainless steel–uranium dioxide dispersion fuels (irradiated), effects, **2**: 10
fission-gas release, **3**: 12
Stainless steel (347B)–uranium dioxide dispersion fuels [S.S.(347)-clad], **3**: 7; **4**: 5
Stainless steel (347)–uranium dioxide–zirconium diboride dispersion fuels, development, **4**: 5
Stainless steel (347)–uranium nitride cermet fuels (clad), pressure bonding, **2**: 54
Stainless-steel (304) welds (irradiated), mechanical properties, **3**: 35
Stainless steel (304)–zirconium dioxide dispersion control rod [S.S.(304)-clad], coextrusion, **2**: 55
Steel, bonding to Cu, **4**: 53
cladding applications, **4**: 53
corrosion, **1**: 46
ultrasonic testing, **3**: 65
Steel (13 Cr ferritic-martensitic)(irradiated), mechanical properties, **2**: 39
Steel (17 Cr ferritic)(irradiated), mechanical properties, **2**: 39
Steel (17-4 PH), stress-corrosion cracking, **4**: 35
Steel (502), heat-treatment effects on mechanical properties, **2**: 47
Steel (1018 carbon), corrosion, **1**: 44–5
Steel (4130 alloy), corrosion, **1**: 44–5
Steel (4340), explosive welding, **1**: 70–1
Steel (ASTM A-212)(irradiated), damage recovery, **2**: 38–9
Steel (ASTM A-212B), notch toughness, **2**: 47
Steel (ASTM A-212B)(irradiated), notch ductility, **4**: 42
Steel (ASTM A-302B)(irradiated), notch ductility, **4**: 42
Steel (austenitic)(irradiated), mechanical properties, **2**: 39
Steel (Be-coated), preparation, **4**: 23
Steel (B-coated), preparation, **2**: 57
Steel (carbon), corrosion, **1**: 42; **2**: 33–4
decontamination, **1**: 42
Steel (carbon)(clad), Hg containment, **2**: 34
Steel (Cr-Mo), creep properties, **3**: 47
creep-rupture properties, **2**: 47; **3**: 47
Steel (Cr-Mo)(irradiated), corrosion, **2**: 34–5
Steel (Cr-Mo ferritic), corrosion and mechanical strength, **1**: 44
Steel (Cr-Ni austenitic)(irradiated), mechanical properties, **2**: 39
Steel (Cr-plated), corrosion, **1**: 68
Steel (diffusion-coated), preparation, **2**: 58
Steel (EN2)(irradiated), embrittlement, **2**: 40
Steel (ferritic Cr-Mo), **1**: 47
Steel (irradiated), annealing effects on mechanical properties, **3**: 35, 37–8
damage recovery, **2**: 38
effects, **1**: 57; **2**: 38

Steel (irradiated) (Continued)
transition temperature, **2**: 38
Steel (low-alloy), corrosion, **2**: 33–4
oxidation, **4**: 35
Steel (low-alloy)(irradiated), effects, **1**: 57
Steel (Mn-Mo-V austenitic), age hardening, **2**: 43
Steel (Ni-plated), properties, **1**: 67
Steel (Si), Eu_2O_3 reaction with Si, **1**: 36
Steel (Swedish 21YY)(irradiated), damage recovery, **2**: 39
Steel (T-1), corrosion, **1**: 42
Steel (TiC-coated), preparation, **2**: 58
Steel powder, explosive compaction, **4**: 56–7
Steel weldments, ultrasonic testing, **4**: 58
Stellites, corrosion, **1**: 42
Strontium, diffusion in U, **2**: 45
Strontium boride, reaction with S.S.(304B), **1**: 36
Strontium oxide, diffusion in graphite, **2**: 46
Structural materials (irradiated), effects, **1**: 57; **2**: 38

T

Tantalum, bibliography, **4**: 44–5
C diffusion, **1**: 52
C solid solubility, **2**: 41
C solubility, **1**: 52
casting, **2**: 51; **4**: 51
chemistry, **1**: 51
coating, **1**: 43; **2**: 58
compatibility with UO_2, **2**: 6; **4**: 11
compatibility with UN, **2**: 10
corrosion, **1**: 44; **4**: 4
creep properties, **3**: 47
diffusion barriers for, **4**: 45
diffusion with fissium-Pu-U alloys, **2**: 5; **4**: 4
diffusion in Zr, **2**: 45
explosive forming, **1**: 68; **3**: 63
gas effects, **1**: 51
heat capacity, **4**: 44
high-temperature properties, **3**: 47
H diffusion and solubility, **1**: 52
joining, **4**: 55
mechanical properties, **2**: 40
melting, **2**: 51; **4**: 51
metallurgy, **1**: 51
N diffusion, **1**: 52
N solid solubility, **2**: 41
N solubility, **1**: 52
oxidation, **1**: 42–3; **2**: 33; **3**: 22, 28
O diffusion, **1**: 52
O solid solubility, **2**: 41
O solubility, **1**: 52
reactions with UC and UO_2, **4**: 45
self-diffusion, **3**: 44
tensile properties, **3**: 47
vacancy annealing, **3**: 31–2
welding, **1**: 71
Tantalum (Al-Ta alloy-coated), oxidation, **3**: 28
Tantalum (irradiated), compatibility with UC, **4**: 12
effects, **1**: 54
H diffusion, **1**: 54
Tantalum (silicide-coated), oxidation, **2**: 28
Tantalum alloys, bibliography, **4**: 44–5
development, **4**: 43
joining, **4**: 55
phase studies, **4**: 45
strength and strength-weight ratios, **1**: 48–9
Tantalum alloys (silicide-coated), preparation, **2**: 58
Tantalum capsules, fabrication, **1**: 64
Tantalum carbides, bibliography, **4**: 44–5
coatings, **2**: 57–8; **3**: 57; **4**: 54
Tantalum compounds, bibliography, **4**: 44–5
Tantalum crucibles, Pu and Pu alloy melting and casting, **3**: 52
Tantalum crystals, elastic constants, **3**: 39
Tantalum hydride, electrical properties, **1**: 33
Hall coefficient, **1**: 33
Tantalum (thoriated) powder, explosive compaction, **3**: 62
Tantalum sheet, development, **1**: 63
Tantalum-tungsten alloys, mechanical properties, **2**: 40; **4**: 51
melting, **4**: 51
Tantalum-tungsten alloys (irradiated), mechanical properties, **2**: 40
Tantalum-zirconium alloys, Zr diffusion, **2**: 45
Technetium, melting, **3**: 52–3
Technetium-thorium compounds, crystal structure, **1**: 9
Technetium-uranium compounds, fuel applications, **2**: 9
Thermal insulators (irradiated), effects, **1**: 58
Thorium, corrosion, **3**: 2–3
ductility, **4**: 5
heat of sublimation, **1**: 9
hot hardness, **1**: 10
H effects, **4**: 5
plating with Ni, **3**: 58
silver brazing, **4**: 55
soldering, **4**: 55
tensile elongation, **1**: 10
vapor pressure, **1**: 9
Thorium (Al-clad), hot pressing, **1**: 67
Thorium (irradiated), annealing effects, **1**: 10
effects, **1**: 10
hardness, **3**: 6
tensile elongation, **1**: 10
Thorium (Ni-Cr plated), corrosion, **2**: 60
Thorium aluminide (Th_2Al), hardness, **4**: 5
Thorium beryllide ($ThBe_{13}$), corrosion and hardness, **4**: 5
Thorium boride (ThB_4), hardness, **4**: 5
Thorium carbide, temperature effects on electron and ion emission, **2**: 9
Thorium carbide–uranium carbide systems, corrosion, **2**: 5
density, **2**: 5
oxidation, **3**: 6

Thorium compounds, corrosion, **4**: 5
preparation of cubic perovskite type, **3**: 13
properties, **4**: 5
refractory properties, **3**: 6
Thorium dicarbide, corrosion, **3**: 13
oxidation, **1**: 15
vapor pressure, **4**: 13
Thorium dicarbide–uranium dicarbide system, oxidation, **1**: 15; **3**: 6
solubility, **1**: 15
Thorium dioxide, compaction, **3**: 14
density, **1**: 15
oxidation-reduction, **1**: 15
physical properties, **3**: 13
sintering, **3**: 15
thermal expansion, **4**: 10, 12
vapor pressure, **4**: 13
Thorium dioxide (Al-clad), hot pressing, **1**: 67
Thorium dioxide compacts, sinterability, **4**: 15
Thorium dioxide pellets, production, **3**: 14–15
Thorium dioxide powder, explosive compaction, **4**: 58
Thorium dioxide–uranium dioxide, compaction, **3**: 14
thermal expansion, **4**: 10
Thorium dioxide–uranium dioxide (Al-clad), hot pressing, **1**: 67
Thorium dioxide–uranium dioxide (clad)(irradiated), fission-gas release, **1**: 13
Thorium dioxide–uranium dioxide (irradiated), effects, **1**: 12
metal-fiber effects on thermal conductivity, **2**: 7
Thorium dioxide–uranium dioxide (sintered), oxidation, **3**: 9–10
Thorium monocarbide, corrosion, **3**: 13
Thorium nitride, corrosion, **3**: 13
Thorium nitride–uranium nitride system, corrosion, **1**: 10
Thorium silicides, corrosion, **3**: 13
hardness, **4**: 5
Thorium sulfide, corrosion, **3**: 13
crystal structure, **1**: 9
physical properties, **3**: 13
sintering, **2**: 9; **4**: 15
Thorium-uranium alloys, compatibility with stainless steel, **1**: 10
corrosion, **1**: 9
creep strength, **1**: 9–10
recrystallization, **1**: 9
strength, **1**: 10
Thorium-uranium alloys (irradiated), effects, **1**: 10; **3**: 6
stability, **4**: 5
Thorium uranium aluminide $[(Th_3U)_2Al]$, hardness, **4**: 5
Thorium uranium beryllide $[(Th_3U)Be_{13}]$, hardness, **4**: 5
Thorium uranium boride $[(Th_3U)B_4]$, hardness, **4**: 5
Thorium-uranium compounds, refractory properties, **3**: 6
Thorium-uranium couples, galvanic effects, **3**: 3
Thorium uranium dicarbide particles (coated), preparation, **2**: 59; **4**: 7, 9
Thorium uranium monocarbide (C-coated), properties, **1**: 67
Thorium uranium silicide $[(Th_3U)_3Si_2]$, hardness, **4**: 5
Thorium-yttrium alloys, **2**: 5
Thorium-zinc alloys, structure, **3**: 5
Thorium-zirconium alloys, hardness and recrystallization, **4**: 5
Timken 16-15-6, corrosion, **1**: 42
Tin, diffusion, **2**: 45
self-diffusion, **2**: 45
Tin (irradiated), effects, **2**: 35–6
Tin-yttrium alloys, phase studies, **3**: 41
Tin-zirconium alloys, creep properties, **3**: 46
Sn and Zr diffusion, **2**: 45
Titanium, brazing with, **4**: 56
coating with complex fluorides, **3**: 60
compatibility with UN, **2**: 10
diffusion with fissium-Pu-U alloys, **2**: 5; **4**: 4
hardness, **1**: 39
interdiffusion with U, **2**: 45
plating, **3**: 37
Sn^{113} diffusion, **2**: 45
U diffusion, **1**: 52
Titanium (irradiated), anisotropic growth and sputtering, **4**: 38
Titanium alloy coating, **3**: 60
Titanium alloys (BC 120 VCA), explosive welding, **1**: 70
Titanium dioxide–uranium dioxide powder, explosive compaction, **4**: 58
sinterability, **3**: 12
Titanium dioxide–uranium dioxide powder (irradiated), fission-gas release, **3**: 11–12
Titanium dioxide–uranium dioxide powder (sintered), strength, **3**: 12
Titanium hydride, solubility in molten Li hydride, **1**: 33
Titanium monocarbide coatings, preparation on steel, **2**: 58
Titanium monocarbide–uranium nitride powder, explosive compaction, **3**: 62
Titanium nitride coating, vapor deposition on graphite, **3**: 57
Titanium powder, explosive compaction, **3**: 62; **4**: 56–7
Titanium-vanadium alloys, beta-phase stability, **2**: 44
Titanium-vanadium-zirconium alloys, yield strength, **1**: 51
Titanium-yttrium alloys, phase studies, **1**: 51; **3**: 41
Titanium-zirconium alloys, creep properties, **3**: 46–7
Transition metals
See Metals (transition)
Tubing, nondestructive testing, **2**: 60; **3**: 65

Tungsten, bibliography, **4**: 44
brazing, **4**: 56
C solubility, **1**: 52
casting, **2**: 51; **4**: 51
coating, **1**: 67; **2**: 58; **4**: 54
compatibility with UO_2, **2**: 6; **4**: 11
compatibility with UN, **2**: 10
diffusion barriers for, **4**: 45
diffusion in Mo, **2**: 45
explosive forming, **1**: 68; **3**: 63
H solubility, **1**: 52
joining, **4**: 55–6
melting, **2**: 51; **4**: 51
N solubility, **1**: 52
oxidation, **1**: 42–3
O solubility, **1**: 52
plating, **1**: 68
reactions with UC and UO_2, **4**: 45
self-diffusion, **3**: 44
vacancy annealing, **3**: 31–2
welding, **4**: 56
Tungsten (glass and zircon-coated), preparation, **2**: 60
Tungsten (Hf carbide-coated), preparation, **2**: 57
Tungsten (irradiated), damage and recovery, **3**: 34
density, **4**: 38
effects, **2**: 36
energy dependence of damage, **3**: 31
sputtering, **4**: 38
vacancy annealing, **3**: 31–2
X-ray lattice parameter and line breadth, **4**: 38
Tungsten alloys, bibliography, **4**: 44
ductility, **2**: 42
hardness, **2**: 42
mechanical properties, **4**: 51
melting, **4**: 51
phase studies, **4**: 45
strength, **1**: 48–9
strength-weight ratios, **1**: 48–9
twinning, **2**: 42
welding, **4**: 56
Tungsten carbides, bibliography, **4**: 44
coatings, **4**: 35
Tungsten compounds, bibliography, **4**: 44
Tungsten powder, explosive compaction, **3**: 62
Tungsten sheet, development, **1**: 63
Tungsten–uranium dioxide dispersion fuels, development, **1**: 12
Tungsten–uranium dioxide powder, explosive compaction, **3**: 62

U

Ultrasonic testing, evaluation, **4**: 59
transducer properties, **2**: 62
Uranium, alpha-beta cycling, **2**: 1
Al diffusion, **1**: 53; **3**: 2
annealing, **1**: 64; **3**: 1–2, 53
brazing, **4**: 55
casting, **3**: 52
Cr diffusion, **1**: 52
cladding, **4**: 3
coating, **1**: 16
compatibility, **4**: 2
Cu diffusion, **1**: 52–3
corrosion, **1**: 5, 16; **2**: 11; **3**: 2–3; **4**: 1–2
creep rate, **3**: 1
cross-rolling effects, **3**: 2
deformation, **3**: 2
diffusion in graphite, **4**: 46
dilatometry, **1**: 1
dimensional stability, **1**: 16
economics of fuels, **2**: 52
electrolytic production, **3**: 59
enthalpy, **2**: 1
entropy, **2**: 1
extraction, **4**: 2
extrusion, **3**: 1–2, 53
fabrication, **2**: 52; **3**: 53; **4**: 2
formability, **2**: 52
free-energy function, **2**: 1
furnace-charge-material effects, **4**: 51
Au diffusion, **3**: 2
grain refinement, **3**: 1
heat capacity, **2**: 1
heat-treatment, **3**: 53
hydriding, **2**: 11
H diffusion, **3**: 1
interdiffusion with Fe and Ti, **2**: 45
internal friction, **3**: 2
Fe diffusion, **1**: 52
La diffusion, **2**: 45
mechanical properties, **4**: 2
metallurgy, **4**: 1
Mo diffusion, **1**: 52
Ni diffusion, **1**: 52–3
Nb diffusion, **1**: 53
occurrence, **4**: 2
orientation effects, **3**: 2
outgassing, **3**: 53
oxidation, **2**: 11; **4**: 2, 16
physical properties, **4**: 2
plating, **3**: 58–9
preferred orientation, **3**: 2
preparation, **4**: 2
rare-gas solution in, **1**: 16
reaction with steam, **1**: 18
reaction with water, **1**: 17
recrystallization, **2**: 1; **3**: 1
self-diffusion, **1**: 16; **3**: 2
Si diffusion, **1**: 52
Sr diffusion, **2**: 45
structure, **3**: 1–2
temperature effects, **3**: 2
thermal analysis, **1**: 1
thermal-cycling effects, **3**: 1
thermal expansion, **3**: 2
Ti diffusion, **1**: 52
transformation, **1**: 1; **3**: 2

Uranium (Continued)
ultrasonic grain-size testing, 2: 61
Zr diffusion, 1: 52
Uranium (Al-clad), burnup, 1: 2–3
canning, 3: 56
corrosion, 2: 11
Uranium (Al-coated), corrosion, 3: 3
Uranium (Al-plated), preparation, 2: 60
Uranium (Be-clad), coextrusion, 1: 23, 66
Uranium (Cr-plated), coating, 4: 54
Uranium (clad), interactions, 2: 45
Uranium (Cu-plated), development, 1: 68
Uranium (dingot), stress-rupture properties, 1: 2–3
tensile properties, 1: 2
Uranium (Fe-plated), preparation and cladding, 1: 68
Uranium (irradiated), bubble formation, 3: 15
dimensional changes, 3: 15
effects, 1: 3–4, 16, 56; 3: 35; 4: 2, 17
fission-product ranges, 3: 32
growth, 2: 13; 3: 15; 4: 1, 17
heating effects on fission-gas resolution, 3: 15–16
Kr release, 3: 15
lattice defects, 2: 13
point-defect effects, 4: 17
reactions with air, CO_2, and steam, 1: 17–18
stresses, 3: 15
structural changes, 4: 16–17
swelling, 1: 3–4, 16; 2: 12; 3: 3, 15; 4: 17
thermal expansion, 4: 16–17
Uranium (Mg-clad), extrusion, 1: 64
Uranium (metal-coated), corrosion, 1: 68
Uranium (molten), interaction with Zr, 2: 45
reaction with water, 3: 30; 4: 36
Zr diffusion, 2: 45
Uranium (Ni-plated), preparation and properties, 1: 68
Uranium (Ni-plated)(Al-clad), corrosion of bonds, 3: 4
Uranium (single-crystal), adiabatic elastic moduli, 2: 1
Uranium (S.S.-clad), extrusion, 1: 64
Uranium (S.S.-clad)(irradiated), interface effects, 3: 35
Uranium (vinyl-coated), corrosion, 3: 3
Uranium (Zircaloy-clad), corrosion, 4: 1
rupture, 4: 1
swaging, 4: 52
Uranium (Zircaloy-2-clad), defect-test behavior, 4: 1
Uranium (Zircaloy-2-clad)(irradiated), bond damage, 3: 35
Uranium (Zr-clad), canning, 3: 56
casting, 4: 53
corrosion, 2: 11
Uranium (Zr-coated), vapor deposition, 3: 57
Uranium alloys, beta-phase metastability and retention, 1: 2
casting, 3: 52
corrosion, 1: 5; 3: 3
Uranium alloys (clad), Na bonding, 1: 66
Uranium alloys (cubic)(irradiated), effects, 2: 12
Uranium alloys (irradiated), effects on beta phase, 1: 2
swelling, 2: 12–13
Uranium alloys (Ni-plated), preparation, 2: 59–60
Uranium alloys (Ni-plated)(Al-clad), testing, 2: 59–60
Uranium blanket rods [S.S.(304)-clad], canning and Na bonding, 2: 57
Uranium carbide (C-coated) matrix fuels, fabrication, 4: 9
Uranium carbide powder, explosive compaction, 4: 58
fabrication and preparation, 2: 9
Uranium carbide–vanadium dispersion fuels, development, 2: 10
Uranium carbide–zirconium carbide system, creep strength, 1: 15
reactive hot pressing, 4: 14
Uranium carbide–zirconium dispersion fuels, development, 2: 10
Uranium carbides, casting, 1: 16; 3: 13–14; 4: 13; 4: 13–14
cladding materials, 2: 8
coatings, 1: 15
corrosion, 1: 15
deformation, 4: 12
density, 1: 15; 4: 14
electrical resistivity, 1: 15; 4: 12
evaluation, 3: 13
fabrication, 1: 16; 3: 13
flexure strength, 1: 15
fuel development, 4: 13
grain growth, 4: 12
hardness, 1: 5, 15; 3: 13
hot hardness, 3: 13; 4: 12
isostatic hot pressing, 3: 14
lattice parameters, 3: 13; 4: 12
melting, 1: 16; 4: 13
microhardness, 3: 13
microstructure, 1: 15
Poisson's ratio, 3: 13
powder metallurgy, 3: 13
preparation, 1: 16; 3: 14
production, 4: 14
properties, 1: 14; 3 13
reactions with cladding materials, 4: 45
self-diffusion, 2: 8
sintering, 3: 14
slip casting, 3: 14
temperature effects, 4: 12
thermal conductivity, 1: 14–15; 3: 13
thermal-cycling effects, 3: 13
thermal expansion, 1: 14–15; 3: 13
thermal properties, 4: 12
transient heating effects, 2: 8–9
Xe diffusion, 3: 16
Uranium carbides (Be-clad), coextrusion, 1: 23
Uranium carbides (clad), pressure bonding, 2: 54

Uranium carbides (irradiated), compatibility with Ta, 4: 12
effects, 1: 15; 2: 8; 3: 13
fission-gas release, 4: 12
Uranium carbides (Nb-Zr alloy-clad), swaging, 3: 54
Uranium carbides (Si-SiC-canned), fabrication, 4: 53
Uranium crystals, thermal expansion, 3: 2
Uranium crystals (irradiated), effects, 4: 17
Uranium dicarbide, cubic modification, 2: 9
dissociation pressure, 1: 15
hot hardness, 3: 13
oxidation, 1: 15
vapor pressure, 4: 13
Uranium dicarbide (C-coated), development, 1: 67
production, 4: 9
Uranium dioxide, bibliography, 3: 9
compatibility with metals and alloys, 2: 6; 4: 11, 23–4, 26
data, 3: 9
decomposition, 1: 13
electrical conductivity, 4: 10
Kr^{88} diffusion in, 3: 10
oxidation, 3: 9, 12
oxidation-reduction cycling, 3: 12
O self-diffusion, 4: 10
physical properties, 3: 13
reaction with Be, 3: 55
reaction with cladding materials, 4: 45
reaction with graphite, 2: 17–18
reaction with Zr, 3: 55
rod rolling, 2: 53
sintering, 3: 12
stabilization against oxidation, 3: 12
Sr diffusion in, 1: 53
swaged density, 2: 52–3
temperature profile, 1: 13
thermal conductivity, 2: 6; 3: 9; 4: 10
thermal expansion, 1: 13; 2: 6; 3: 12; 4: 10
thermal stress, 1: 13
U self-diffusion, 4: 10
vibratory compaction, 3: 54
Xe diffusion, 3: 11, 16
Zr diffusion, 1: 53
Uranium dioxide (Al alloy-clad), coextrusion, 2: 56
Uranium dioxide (Al-clad), swaged density, 2: 52–3
Uranium dioxide (Al-Fe alloy-clad), pressure bonding, 2: 53
Uranium dioxide (Al_2O_3-coated), development, 1: 67–8
Uranium dioxide (Be-coated), preparation, 4: 6
Uranium dioxide (BeO-coated), development, 4: 6
Uranium dioxide (ceramic-clad), development, 4: 55
Uranium dioxide (Cr-coated), preparation, 1: 67; 4: 6
Uranium dioxide (Cr-Ni alloy-clad), cold drawing, 3: 54
Uranium dioxide (Cr-plated), development, 1: 68
Uranium dioxide (clad), pressure bonding, 2: 53–4; 4: 53
Uranium dioxide (clad)(irradiated), fission-gas release, 1: 13
Uranium dioxide (Cu-plated), development, 1: 68
Uranium dioxide (Fansteel-80 and -82 clad), swaging, 4: 52
Uranium dioxide (Hastelloy-F-clad), swaging, 4: 52
Uranium dioxide (Inconel-X-clad), swaging, 4: 52
Uranium dioxide (irradiated), activation energy, 4: 9
effects, 1: 12–14, 16–17, 56; 2: 6; 4: 11
electrical conductivity, 4: 9–10
fission-gas diffusion, 1: 17
fission-gas release, 1: 13, 17; 2: 13–14; 3: 10–12; 4: 10–11
fission tracks, 2: 13, 37
fracture, 2: 13
Kr^{85m} and Kr^{88} diffusion, 4: 10–11
melting point, 2: 13; 4: 10
oxidation in water, 2: 6
structure, 3: 11
thermal conductivity, 1: 13; 2: 6
Xe^{133} and Xe^{135} diffusion, 4: 10
Uranium dioxide (mild-steel-clad), swaged density, 2: 52–3
Uranium dioxide (molten), compatibility with Ta, 4: 11
Uranium dioxide (Mo-clad), extrusion, 1: 64
Uranium dioxide (Mo-coated), preparation, 4: 6
Uranium dioxide (Mo-plated), development, 1: 68
Uranium dioxide (Ni-coated), preparation, 4: 6
Uranium dioxide (Ni-plated), development, 1: 68
Uranium dioxide (Nb-coated), preparation, 4: 6
pressure bonding, 2: 53
Uranium dioxide (Nb-plated), development, 1: 68
Uranium dioxide (Nb-V alloy-coated), preparation, 4: 6
Uranium dioxide (pressure-bonded), density, 3: 54
Uranium dioxide (pyrolytic C-coated), development and properties, 1: 68
Uranium dioxide (Si-coated), preparation, 1: 67; 4: 6
Uranium dioxide (sintered), grain growth and surface area, 3: 9
Uranium dioxide (S.S.-clad), coextrusion, 1: 66
extrusion, 1: 64
pressure bonding, 2: 53; 3: 54–5
swaged density, 2: 52–3
swaging, 1: 65
vibratory compaction, 1: 65
Uranium dioxide [S.S.(304)-clad], density and stoichiometry of coextruded, 1: 66
swaged density, 2: 52–3
Uranium dioxide (W-plated), development, 1: 68
Uranium dioxide (V-coated), preparation, 4: 6
Uranium dioxide (Zircaloy-clad), coextrusion, 1: 66
fabrication, 2: 8
swaging, 4: 52

Uranium dioxide (Zircaloy-2-clad), pressure bonding, **1**: 68; **2**: 54
swaged density, **2**: 52–3
swaging, **1**: 64
Uranium dioxide (Zircaloy-2-clad)(irradiated), failure, **4**: 12
interface effects, **3**: 35
Uranium dioxide (Zircaloy-4-clad), swaged density, **2**: 52–3
Uranium dioxide ceramics, economics, **4**: 12
Uranium dioxide ceramics (irradiated), annealing, **4**: 17–18
dislocations, **4**: 17
effects, **1**: 12
fission-fragment trajectories, **4**: 17
Uranium dioxide ceramics (Zircaloy-clad), diffusion bonding, **2**: 55
Uranium dioxide cermets, **3**: 7–8
Uranium dioxide cermets (clad), pressure bonding, **2**: 53–4
Uranium dioxide cermets (irradiated), effects, **1**: 12
Uranium dioxide crystals, explosive compaction, **4**: 58
orientation, **3**: 9
Uranium dioxide dispersion fuels (clad), fabrication, **4**: 5–6
pressure bonding, **2**: 53–4
Uranium dioxide dispersion fuels (clad)(irradiated), effects, **4**: 5–6
Uranium dioxide films (irradiated), microstructure, **1**: 13
Uranium dioxide materials, fabrication, **1**: 14
Uranium dioxide–oxide mixtures, melting points, **1**: 13
Uranium dioxide particles (Al_2O_3-coated), development, **4**: 6
preparation, **2**: 59
properties, **2**: 59; **3**: 57–8
Uranium dioxide particles (Cr-coated), preparation and properties, **2**: 59
Uranium dioxide pellets, fabrication, **3**: 12
Uranium dioxide plates, fabrication, **2**: 8
Uranium dioxide powder, consolidation, **2**: 53
explosive compaction, **3**: 63–4; **4**: 57
preparation, **2**: 7–8
sinterability, **2**: 7–8
Uranium dioxide powder (Al_2O_3-coated), development, **2**: 59
preparation, **4**: 6
pressure bonding, **2**: 54
properties, **2**: 59
Uranium dioxide powder (clad), pressure bonding, **2**: 53–4
Uranium dioxide powder (V-coated), preparation, **1**: 67
Uranium dioxide spheres (Mo-coated), preparation, **2**: 58–9
Uranium dioxide spheres (Nb-V alloy, Cr-coated), preparation, **2**: 58
Uranium dioxide–thorium dioxide particles (BeO-coated), production, **4**: 6
Uranium dioxide–yttrium oxide solid solutions, stability, **2**: 6
Uranium dioxide–yttrium oxide system (irradiated), phase studies, **3**: 11
Uranium dioxide–yttrium oxide system (sintered), structure, **3**: 11
Uranium dioxide–zirconium dioxide system, corrosion, **2**: 6–7
lattice parameters, **2**: 6
phase studies, **2**: 6; **3**: 11; **4**: 12
structure, **3**: 11
thermal expansion, **2**: 6
Xe^{133} diffusion, **3**: 11
Uranium dioxide–zirconium dioxide system (irradiated), effects, **1**: 56
structure, **3**: 11
Xe^{133} diffusion, **2**: 7
Uranium hydride, oxidation, **2**: 11
Uranium ingots, furnace atmosphere effects, **1**: 63
Uranium-molybdenum alloy–uranium carbide dispersion fuels, development, **1**: 11
Uranium-molybdenum alloy–uranium dioxide dispersion fuels, development, **1**: 11
Uranium nitride, compatibility with metals, **2**: 10
deformation, **4**: 12
densification, **2**: 11
fabrication, **2**: 9
isostatic hot pressing, **3**: 14
modulus of rupture, **3**: 13
modulus of shear, **3**: 13
Poisson's ratio, **3**: 13
preparation, **2**: 9
production, **4**: 14–15
sintering, **3**: 14
thermal expansion, **2**: 9; **3**: 13; **4**: 10, 12
Uranium nitride (clad), pressure bonding, **2**: 54
Uranium nitride (irradiated), fabrication, **3**: 14
Uranium nitride [S.S.(304)-clad], cold swaging, **3**: 54
Uranium nitride cermet fuels, fabrication, **1**: 12
gas-pressure bonding, **2**: 10
sintering, **2**: 10
Uranium nitride dispersion fuels [S.S.(347)-clad], fabrication, **4**: 5–6
Uranium nitride dispersion fuels [S.S.(347)-clad] (irradiated), effects, **4**: 5–6
Uranium oxides, cathodic deposition, **3**: 59
plating, **3**: 59
pressure bonding, **3**: 55
thermal conductivity, **2**: 6
Uranium oxides (irradiated), effects, **1**: 55
Uranium oxides (metal-coated), corrosion, **1**: 68
Uranium oxides (Zircaloy-2-clad), failure, **3**: 30
Uranium selenide, corrosion, **3**: 13
density, **3**: 13
development, **2**: 9
Uranium silicide, behavior, **2**: 2
chemical properties, **1**: 15; **3**: 13

Uranium silicide (Continued)
deformation, **4**: 12
disintegration, **1**: 15
mechanical properties, **3**: 13
modulus of rupture, **3**: 13
modulus of shear, **3**: 13
oxidation, **1**: 15
physical properties, **1**: 15; **3**: 13
Poisson's ratio, **3**: 13
properties, **2**: 2
thermal expansion, **1**: 15–16; **2**: 9; **3**: 13
weight gain, **1**: 15
Young's modulus, **1**: 16
Uranium silicide (irradiated), effects, **3**: 13
Uranium sulfide, development, **2**: 9
heat of dissociation, **2**: 9
lattice parameter, **2**: 9
melting point, **2**: 9
physical properties, **3**: 13
resistivity, **2**: 9
sintering, **3**: 15
vapor species, **2**: 9
Uranium sulfide powder, production, **4**: 14
sintering, **2**: 9
Uranium sulfide–vanadium dispersion fuels, development, **2**: 10
Uranium sulfide–zirconium dispersion fuels, development, **2**: 10
Uranium telluride fuels, development, **2**: 9
Uranium tubing, **1**: 63–4
Uranium–uranium carbide fuels, **3**: 13; **4**: 12
Uranium–uranium carbide fuels (Be-clad), coextrusion, **2**: 56
rolling, **3**: 53
Uranium–uranium dioxide dispersion fuels, isotopic interchange, **3**: 8–9
Uranium-vanadium alloys (irradiated), swelling, **1**: 3–4
Uranium wire, **1**: 63–4
Uranium-yttrium alloys (irradiated), swelling, **1**: 3–4
Uranium-yttrium dispersions, mechanical strength and powder metallurgy, **2**: 10
Uranium-zinc alloys, structure, **3**: 5
Uranium-Zircaloy-2 alloys, phase studies and structure, **3**: 40
Uranium-zirconium alloy cladding, **4**: 3
Uranium-zirconium alloy fuels, phase transformation, **1**: 6
Uranium-zirconium alloy fuels (Be-clad), extrusion, **1**: 23
Uranium-zirconium alloy fuels (irradiated), effects, **1**: 16; **3**: 3
Uranium-zirconium alloy fuels [S.S.(304)-clad](irradiated), effects, **2**: 1–2
Uranium-zirconium alloy fuels [S.S.(347)-clad], hot drawing and swaging, **3**: 54
Uranium-zirconium alloy fuels (Zircaloy-2-clad), **1**: 1–2
Uranium–zirconium hydride dispersion fuels, fabrication, **1**: 34
properties, **2**: 25

V

Vanadium, cladding applications, **4**: 53
coating, **1**: 67
diffusion barrier for W, **4**: 45
diffusion with fissium-Pu-U alloys, **2**: 5; **4**: 4
solubility of C, H, N, and O, **1**: 52
Vanadium (irradiated), sputtering and thermal conductivity, **4**: 38
Vanadium alloys, diffusion with fissium-Pu-U alloys, **2**: 5; **4**: 4
mechanical properties, **4**: 51
melting, **4**: 51
Vanadium crystals, elastic constants, **3**: 39
Vanadium-yttrium alloys, phase studies, **3**: 41
Vanadium-zirconium compounds, hydriding, **4**: 28
Vinyl coating corrosion, **3**: 3

W

Welding, bibliographies, **4**: 56
ultrasonic testing, **1**: 72

X

Xenon, diffusion, **2**: 45–6; **3**: 16
Xenon-133, diffusion, **3**: 11; **4**: 10
Xenon-135, diffusion, **2**: 46; **4**: 10

Y

Yttrium, diffusion with fissium-Pu-U alloys, **2**: 5; **4**: 4
oxidation, **1**: 43–4; **3**: 29
Yttrium hexaboride, reaction with stainless steel (304B), **1**: 36
Yttrium oxide, diffusion in graphite, **2**: 46
Yttrium-zirconium alloys, H heat of transport and phase studies, **3**: 41

Z

Zinc (irradiated), anisotropic growth, **4**: 38
Zircaloy, coating, **3**: 59
Cu diffusion, **1**: 53
corrosion, **1**: 47
diffusion bonding, **1**: 66
plating, **4**: 54–5

Zircaloy (Continued)
ultrasonic testing, 1: 72
welding, 2: 60
Zircaloy (Cr-plated), preparation and properties, 2: 60
Zircaloy (Cu-plated), preparation, 2: 60
Zircaloy-2, cold-roll joining to stainless steel (410), 3: 53–4
compatibility with UO_2, 4: 11
contamination, 2: 46
corrosion, 1: 40, 46; 2: 32; 4: 51–2
creep properties, 1: 46–7; 2: 46–7; 3: 46; 4: 43
diffusion with fissium-Pu-U alloys, 2: 5; 4: 4
eddy-current testing, 1: 73
explosive joining to stainless-steel (410) tubing, 3: 63
fabrication, 2: 46; 4: 51–2
heat-treatment effects, 3: 44
hydriding, 1: 33–4, 40–1; 2: 32; 3: 46; 4: 33
H solubility, 3: 40–1
H thermal diffusion, 3: 42, 44
impact properties, 1: 46; 3: 44
mechanical properties, 2: 46; 3: 45–6
melting, 4: 51–2
notch sensitivity, 3: 44
oxidation, 2: 32
physical properties, 3: 45–6
powder metallurgy, 2: 10
properties, 2: 10, 46
reaction with Al-Pu alloys, 3: 5
reaction with UC, 4: 45
reaction with UO_2, 4: 45
reaction with water, 3: 30
self-diffusion, 4: 46
stress relaxation, 2: 46
stringer content, 4: 51–2
tensile properties, 1: 46–7; 2: 46; 3: 44
welding, 3: 60; 4: 52–3
Zircaloy-2 (Cr-plated), properties, 1: 67
Zircaloy-2 (cold-worked), annealing effects, 3: 46
Zircaloy-2 (irradiated), effects, 1: 57–8
rupture life, 2: 40
tensile properties, 3: 35, 37
Zircaloy-2 cladding (irradiated), strength, 3: 35
Zircaloy-2 powder, explosive compaction, 3: 62
sintering, 4: 46
Zircaloy-2 sheaths (swaged), burst and tensile properties, 3: 44–5
Zircaloy-2 sheet, spinning, 2: 52
Zircaloy-2 tubing, cold extrusion, 4: 52
properties, 2: 46–7; 3: 35
testing, 1: 72–3; 3: 65
Zircaloy-2 tubing (irradiated), burst strength, 3: 35; 4: 42–3
Zircaloy-4, hydriding, 2: 32; 4: 52
properties, 1: 46; 3: 44
swaging, 4: 52
Zircon
See Glass and zircon coatings
Zirconium, coating, 3: 60; 4: 35
compatibility with UN, 2: 10
corrosion, 1: 40–1; 3: 29
diffusion, 1: 53; 2: 45
diffusion barrier for Ta, 4: 45
elastic constants, 1: 72
fissium-Pu-U alloy diffusion, 4: 4
grain growth, 1: 51
hardness, 3: 40
H diffusion, 2: 45; 3: 42
H solubility, 3: 40–1
interaction with molten U, 2: 45
lattice constants, 3: 40
N effects, 3: 40
oxidation, 1: 44–5
reaction with UO_2, 3: 55
reaction with water, 1: 17; 3: 30
self-diffusion, 1: 52; 2: 45; 3: 44; 4: 46
Sr diffusion, 1: 53
Ta diffusion, 2: 45
unit cell volume, 3: 40
U diffusion, 1: 52
Zirconium (irradiated), anisotropic growth, 4: 38
density, 4: 38
effects, 2: 36; 4: 41
X-ray lattice parameter and line breadth, 4: 38–9
Zirconium (molten), reaction with water, 1: 17; 3: 30; 4: 36
Zirconium alloys, beta-phase decay, 1: 51
coating with complex fluorides, 3: 60
corrosion, 1: 40; 2: 32; 4: 33
hardness, 4: 45
oxidation, 1: 40, 44–5
properties, 2: 46
Zr diffusion, 2: 45
Zirconium alloys (irradiated), effects, 4: 41
Zirconium carbide, coatings, 4: 35
oxidation, 3: 6
thermal expansion, 4: 44
Zirconium crystals, ultrasonic testing, 2: 60; 3: 65
Zirconium dioxide, diffusion in graphite, 2: 46
reaction with PuO_2, 1: 15
stability, 1: 15
Zirconium dioxide (irradiated), effects, 1: 55
fission tracks, 2: 37
structure, 3: 11
Zirconium hydride, creep-rupture properties, 1: 32
density, 1: 31
electrical resistivity, 1: 32–3; 2: 25
formation on Zircaloy-2, 1: 33–4
hardness, 1: 31
heat capacity, 4: 27–8
H thermal diffusion, 1: 31
mechanical properties, 1: 31
metallographic structure, 1: 30–1
O effects, 2: 24–5
phase studies, 1: 30–1; 2: 24
physical properties, 1: 31
solubility, 1: 33; 2: 24–5

Zirconium hydride (Continued)
specific heat, 1: 32–3
stress relaxation, 2: 25
thermal conductivity, 1: 32–3; 3: 42
thermal expansion, 1: 32; 3: 24
thermodynamic functions, 4: 28
twinning, 2: 25
ultimate tensile strength, 1: 31
Zirconium silicon oxide (irradiated), effects, 1: 55
Zirconium tubing, production and testing, 1: 64

LEGAL NOTICE

This document was prepared under the sponsorship of the U. S. Atomic Energy Commission. Neither the United States, nor the Commission, nor any person acting on behalf of the Commission:

A. Makes any warranty or representation, expressed or implied, with respect to the accuracy, completeness, or usefulness of the information contained in this report, or that the use of any information, apparatus, method, or process disclosed in this report may not infringe privately owned rights; or

B. Assumes any liabilities with respect to the use of, or for damages resulting from the use of any information, apparatus, method, or process disclosed in this report.

As used in the above, "person acting on behalf of the Commission" includes any employee or contractor of the Commission, or employee of such contractor, to the extent that such employee or contractor of the Commission, or employee of such contractor prepares, disseminates, or provides access to, any information pursuant to his employment or contract with the Commission, or his employment with such contractor.

NUCLEAR SCIENCE ABSTRACTS

The U. S. Atomic Energy Commission, Division of Technical Information, publishes *Nuclear Science Abstracts (NSA)*, a semimonthly journal containing abstracts of the literature of nuclear science and engineering.

NSA covers (1) research reports of the U. S. Atomic Energy Commission and its contractors; (2) research reports of government agencies, universities, and industrial research organizations on a world-wide basis; and (3) translations, patents, books, and articles appearing in technical and scientific journals.

Complete indexes covering subject, author, source, and report number are included in each issue. These are cumulated quarterly, semiannually, and annually providing a detailed and convenient key to the literature.

Availability of *NSA*

SALE *NSA* is available on subscription from the Superintendent of Documents, U. S. Government Printing Office, Washington 25, D. C., at $22.00 per year for the semimonthly abstract issues and $15.00 per year for the four cumulated-index issues. Subscriptions are postpaid within the United States, Canada, Mexico, and all Central and South American countries, except Argentina, Brazil, British and French Guiana, Surinam, and British Honduras. Subscribers in these Central and South American countries, and in all other countries throughout the world, should remit $27.50 per year for subscriptions to semimonthly abstract issues and $17.50 per year for the four cumulated-index issues.

EXCHANGE *NSA* is also available on an exchange basis to universities, research institutions, industrial firms, and publishers of scientific information. Inquiries should be directed to the Division of Technical Information Extension, U. S. Atomic Energy Commission, P. O. Box 62, Oak Ridge, Tennessee.

TECHNICAL PROGRESS REVIEWS may be purchased from Superintendent of Documents, U. S. Government Printing Office, Washington 25, D. C. for $2.00 per year for each subscription or for $0.55 per issue. The use of the coupon below will facilitate the handling of your order.

POSTAGE AND REMITTANCE: Postpaid within the United States, Canada, Mexico, and all Central and South American countries except as hereinafter noted. Add $0.50 per year, or $0.15 per single issue, for postage to all other countries, including Argentina, Brazil, British and French Guiana, Surinam, and British Honduras. Payment should be by check, money order, or document coupons, and MUST accompany order. Remittances from foreign countries should be made by international money order, or draft on an American bank, payable to the Superintendent of Documents, or by UNESCO book coupons.

order form

SUPERINTENDENT OF DOCUMENTS
U. S. GOVERNMENT PRINTING OFFICE
WASHINGTON 25, D. C.

Enclosed:
document coupons ☐ check ☐ money order ☐

Charge to Superintendent of Documents No. _____

Please send a one-year subscription to

☐ REACTOR CORE MATERIALS
☐ POWER REACTOR TECHNOLOGY
☐ NUCLEAR SAFETY
☐ REACTOR FUEL PROCESSING

(Each subscription $2.00 a year; $0.55 per issue.)

SUPERINTENDENT OF DOCUMENTS
U. S. GOVERNMENT PRINTING OFFICE
WASHINGTON 25, D. C.

(Print clearly)

Name _____

Street _____
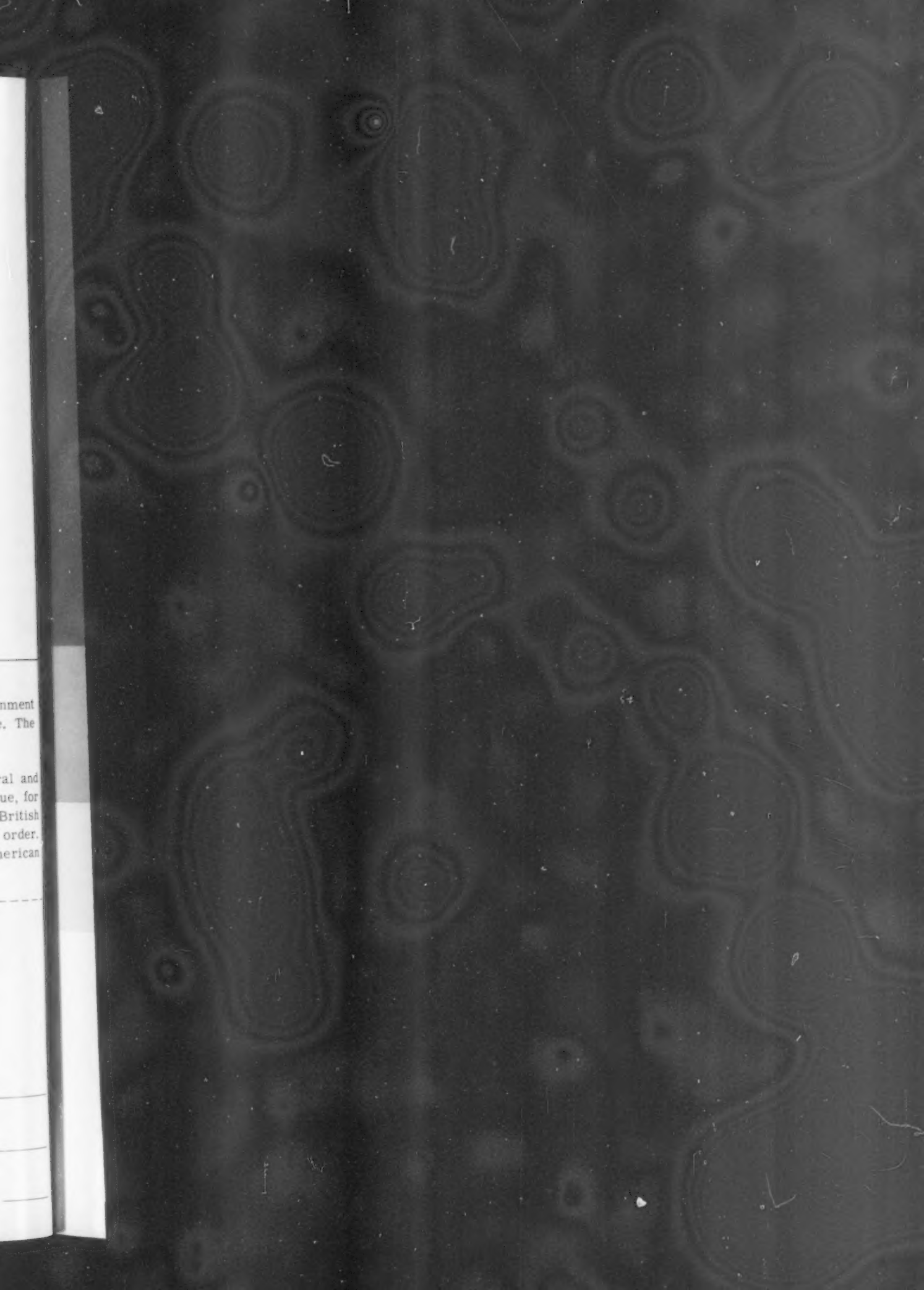
City _____ Zone ____ State _____